**INAUGURAL-DISSERTATION**
**zur**
**Erlangung der Doktorwürde**
**der**
**Naturwissenschaftlich-Mathematischen Gesamtfakultät**
**der**
**Ruprecht-Karls-Universität Heidelberg**

**vorgelegt von**
**Dipl.-Phys. Markus Demleitner**
**aus Erlangen**

**Tag der mündlichen Prüfung: 17. Mai 2000**

# Über einen neuen Zugang zum Problem von Moden in Mestelscheiben

**Gutachter: Prof. Dr. Burkhard Fuchs**
**Prof. Dr. Josef Fried**

Dissertation
Submitted to the
Combined Faculties for the Sciences and Mathematics
of Ruperto Carola University, Heidelberg, Germany
for the Degree of
Doctor of Sciences

# A New Approach to the Problem of Modes in Mestel Disks

presented by
Markus Demleitner, born in Erlangen

Heidelberg, May 17, 2000

Gutachter: Prof. Dr. Burkhard Fuchs
Prof. Dr. Josef Fried

## Über einen neuen Zugang zum Problem von Moden in Mestelscheiben

Diese Arbeit untersucht, wann Scheiben mit global flacher Rotationskurve (Mestelscheiben) stationäre, harmonische Störungen (Normalmoden) zulassen und wie diese beschaffen sind. Während die existierenden Analysen dieses Problems (Zang 1976, Read 1997) die Orbits in diesen Scheiben seminumerisch bestimmen, werden hier von vorneherein genäherte Orbits verwendet. Dies erlaubt eine Bestimmung des Kerns der das Problem beschreibenden Integralgleichung in fast geschlossener Form.

Zusätzlich zur selbstkonsistenten Scheibe wird der Fall einer Scheibe, in der ein Teil der Matrie immobilisiert wird (*cut-out disk*, gekappte Scheibe), untersucht. Die gekappte Scheibe hat eine finite aktive Masse und ist nicht mehr selbstähnlich, was zu einem qualitativ anderen Verhalten führt. Im selbstkonsistenten Fall ist der Kern relativ überschaubar, wenn auch immer noch zu kompliziert, um auf analytische Lösungen hoffen zu können. Die Terme für die gekappte Scheibe hingegen sind ausgesprochen unhandlich.

Im Wesentlichen reproduziert die Näherung die Ergebnisse der vorangehenden Analysen bemerkenswert gut. Im Fall der selbstkonsistenten Scheibe ermöglicht der geschlossene Ausdruck des Kerns ein verbessertes Verständnis des Eigenschaften der neutralen (nichtrotierenden, nichtwachsenden) Moden. Zusätzlich bietet er einen Zugang zu der nach den Arbeiten von Zang und Read noch offenen Frage der nichtaxialsymmetrischen wachsenden Moden. Solche Moden können nicht über der Stabilitätsgrenze der neutralen Moden existieren, und unterhalb dieser Grenze können sie keine beschränkte Mellintransformierte besitzen. Die Existenz solcher Moden konnte nicht gezeigt werden.

## A New Approach to the Modes in Mestel Disks

In this work I examine the modes admitted by the Mestel disk, a disk with a globally flat rotation curve. In contrast to previous analyses of this problem by Zang (1976) and Read (1997), I approximate the orbits to obtain almost closed expressions for the kernel of the integral equation governing the behaviour of the modes.

I investigate the modes admitted by both the self-consistent and a cut-out Mestel disk, the difference being that in the latter case a part of the matter in the disk is immobilized. This breaks the self-similarity and produces a pronouncedly different picture. While the expressions for the kernel in the self-consistent disk are quite managable (though still beyond the reach of analytic techniques), the kernels for cut-out disks tends to rather complicated indeed.

In general, my approximation reproduces the results of the previous works remarkably well. Due to the sheer size of the terms, examining the solution behaviour in the approximation does not save computing time compared to Zang's method at least for the cut-out disks. The more handy expressions in the self-consistent disk, on the other hand, allow an intuitive understanding of most of the properties of neutral (nonrotating, nongrowing) modes there. Also, non-axisymmetric modes of finite growth rate and pattern speed in the self-consistent disk become almost treatable. I can prove that there are no such modes above the velocity dispersions at which the neutral modes appear, and that any modes that exist below these thresholds cannot possess a bounded Mellin transform. Unfortunately, I still cannot prove the existence of such modes.

**Contents**

# 1. Introduction

## *1.1. Closing in on Modes*

The riddle why some of the nebular patches seen on the sky appear to have a clearly discernable spiral structure puzzles astronomers ever since this spirality was first noticed in by Lord Rosse (1852).

The first serious attempt at a theory of spiral structure was undertaken by Bertil Lindblad (1926, 1940). Although his theories were badly flawed, his basic assumption still is the predominant explanation of spiral structure: A spiral arm is a density wave in which the spiral is not material as, e.g., the spiral formed by milk being poured into a cup of tea. Instead, the stars and in particular the interstellar medium (ISM) are slowed down while passing through the density wave but finally manage to leave it again, so that the constituent stars and clouds of a spiral arm constantly change. For most density wave theories, a convenient model is a traffic jam that slowly moves but is made up of different cars at different times since vehicles slow down at the rear of the congestion and leave it at its head.

It should be noted that there are theories of spiral structure without a density wave, the most prominent of which probably is stochastic self-propagating star formation (e.g., Jungwiert and Palouš 1994). However, kinematical studies and investigation of the older populations within spiral galaxies (supposed to be dominating the infrared $K$-band) show that even in flocculent galaxies without much global structure some dynamical processes usually are at work (Thornley and Mundy 1997, Kuno et al 1997), so that while SSPSF might provide a framework to understand what is going on in irregular galaxies, bona fide spirals are most likely linked to density waves.

Despite the empirical evidence in favour density waves as the driving agent for spiral structure and the relatively long time astrophysicists have been developing their theory, dynamical theories about them are still a muddy ground in which progress is slow and hard. Lindblad's original ideas were quickly superseded by the density wave theory connected with the names of Lin and Shu (Lin and Shu 1964, for a review see Rohlfs 1977 or Bertin and Shu 1996). Lin, Shu, and their followers simply inserted a density wave into a disk and tried to find conditions under which this spiral would rigidly rotate, thereby deriving a dispersion relation linking angular frequency and wave length of a spiral wave.

Although the Lin-Shu theory appeared to explain quite a few observations (Burton 1971, Rots 1975), its rather phenomenological approach kept the astrophysicists looking for deeper insight, even more so since gradually more and more shortcomings of the theory surfaced. Probably the most severe of them was that due to the non-constant dispersion relation a pure Lin-Shu mode moves inwards or outwards (Toomre 1969). Also, it was found out that

such modes are absorbed at the Lindblad resonances, i.e., the radii within a disk at which the angular frequency of the mode is in resonance with the epicyclic frequency (Lynden-Bell and Kalnajs 1972).

These problems indicated that the global structure of a galaxy, largely disregarded in the first inceptions of the Lin-Shu theory, plays a significant role in the formation of spiral arms. During the seventies and the eighties, several theories were worked out that strived to enrich the Lin-Shu theory with such global features (Bertin et al 1989). A common trait of those "modal" theories is a feedback loop, in which incoming waves are reflected at the inner border of the disk or some other feature near the centre. This might be facilitated by the increasing velocity dispersion near the bulge. By the dispersion relation of Lin-Shu density waves, they will bend back outwards quite analogous to the bending of short radio waves in the ionosphere of the earth. This inner reflecting zone is commonly referred to as the $Q$-barrier, where the letter $Q$ refers to Toomre's stability parameter $Q$ (Toomre 1964), the variation of which plays the central role in the reflection process.

To close the feedback loop, an outer reflector is required. The most popular candidate suggested for this outer reflector is the corotation resonance, i.e., the radius at which the pattern speed of the mode is equal to the angular frequency of a star on a circular orbit. At corotation, one can reflect (and even amplify) density waves back inwards by a mechanism dubbed overreflection by the proponents of this model (Mark 1976), or by swing amplification (Julian and Toomre 1966).

While modal theories do indeed give a framework for the interpretation of observations, they frequently lack analytic tractability, particularly when the spiral patterns are rather open and the WKBJ approximation they usually employ breaks down. In the introduction to their 1996 book, Bertin and Shu describe their approach as "semiempirical, that is, our dynamical studies will always attempt to address issues directly raised by empirical facts [...] We shall avoid too much speculation on dynamical mechanisms and physical scenarios that do not have sufficient empirical basis."

It was felt by many, however, that daring some "speculation" might nevertheless pay off. Pioneering works attempting stability analyses "from first principles" include the local analyses by Toomre (1964), Goldreich and Lynden-Bell (1965) and Julian and Toomre (1966), and the global analyses in a series of papers by Kalnajs (1971, 1976a, 1976b, 1977) and in Zang's Ph.D. thesis (1976).

The hope of these works was that by simply considering the stability properties of the set of equations given by the Poisson equation and either the Jeans equations or the Boltzmann equation one would find that disks develop spiral structure as a part of their nature, as it were, at least when certain conditions are met, most notable the absence of too much unordered motion, or, in gas-dynamical terms, pressure support.

The first of the works listed above, Toomre (1964), focused on the axisymmetric stability of disks in a local analysis, i.e., just looking at a patch of a larger disk, thus developing a variant of Jeans' (1919) analysis for a rotating disk, or, more precisely, a shearing sheet. It was this work that introduced the concept of the stability parameter $Q$ as the ratio between the velocity dispersion of the disk $\sigma$ and a critical velocity dispersion $\sigma_{\rm crit}$ below which the disk becomes susceptible to growing axisymmetric (ringlike) disturbances.

Goldreich and Lynden-Bell (1965) also restricted themselves to a local analysis but examined non-axisymmetric perturbations. They described their patch by the Jeans equations ("gas-dynamically") and found that violent albeit transient instabilities occur in this shearing medium even when it is stable to axisymmetric perturbations, whereas quasistationary modes in the sense of Lin and Shu are absent. Julian and Toomre (1966) chose to investigate the same problem using the Boltzmann equation ("stellar-dynamically") and found a rather similar behaviour.

Later, Toomre (1981) coined the term "swing amplification" for this sort of instability and speculated that at least flocculent galaxies might be shaped by a recurrence of swing amplification events. As a matter of fact, Fuchs (1991) showed that by nonlinear coupling instabilities might trigger new instabilities themselves, thus producing some sort of feedback loop again. Models along these lines got additional credibility form simulations like those of Sellwood and Carlberg (1984), who also found the "swirling hotch-potch" of perpetual growth and decay of spiral fragments.

However, there *are* galaxies with a beautiful spiral structure that appears to be "global" and thus cannot be expected to turn up in the local analysis. In particular, disk models based on plastering the disk with copies of a patch do not possess any borders like the $Q$-barrier that appeared so central in the modal picture. Although it was found that some of the most beautiful spirals can be explained without regarding their internal dynamics as simply being the result of interactions (Toomre and Toomre, 1972), it still appears that the local analyses miss important ingredients to a real disk. As Toomre (1977) wrote, it appears likely that "even in M51 the main *spiral* structure is in essence just a badly-dented version of what would have been there anyway."

At this point the global analyses mentioned above come into play. After the rather abstract work of Kalnajs mentioned above, Zang (1976) was the first to succeed in a complete stability analysis of a galactic disk using the Boltzmann equation. Zang chose the Mestel disk (Mestel 1963) as basic state, a disk the rotation curve of which is flat from the centre out to infinity. While this certainly is a grossly unrealistic model because of its infinite mass and a density singularity in the centre, it is simple enough to allow detailed calculations that require only moderate numerical effort. What is more, the part of real galaxies in which spiral structure is prominent is frequently characterised by a flat rotation curve, so that Zang could indeed hope that at least some of his results should be readily generalisable to more realistic galaxy models. One of the remarkable results of Zang was that he could not find "interesting"—in a sense that will be clarified below—modes in the Mestel disk unless he immobilised a part of the disk matter in such a way that he essentially introduced a $Q$-barrier in the disk.

The axisymmetric stability of the self-consistent disk was later reconsidered by Lemos, Kalnajs and Lynden-Bell (1991) for a gaseous disk. They basically reproduced Zang's findings, except that the gaseous disk may also admit breathing modes (i.e., modes with no radial node) if the adiabatic exponent is larger than 3/2, which is impossible for a stellar disk.

One drawback of Zang's work was that it was never published in generally accessible literature and that the presentation of the material is not always as clear as one might wish. Furthermore, it made heavy use of the fact that the Mestel disk is self-similar, i.e., that the orbits near the centre of the disk are just scaled copies of those further out. Those were the reasons to embark on this research: To find an easily apprehensible, conceptually and

computational simple and possibly readily generalisable way to reproduce Zang's results and to follow the behaviour of the Mestel disk even further than Zang without having to take recourse to numerical integration.

While I was working on this project, the accessibility of Zang's results was greatly enhanced by Read's (1997) Ph.D. Thesis and the papers by Evans and Read (1998a, 1998b) based on it. Read generalised Zang's method to power law disks of almost arbitrary exponent. The following chapter is intended to supply the reader with enough background from those works to see the parallels and differences between their and my approach.

## 1.2. Modes in the Mestel disks according to Read

In her PhD thesis, Read (1997—henceforth referred to as Read) investigates the stability of power law disks (her results are also published in Evans and Read (1998a, 1998b)), of which the Mestel disk studied here and earlier by Zang (1976 – henceforth referred to as Zang) is a special case. Since Read's work is published and much more readable than Zang's, I will usually refer to her work instead of Zang's, although most of the results on Mestel disks were already present in the earlier work. Since these previous results provide the framework in which to judge mine, it seems appropriate to shortly summarise them here.

Quite as I will do in the present work, Read starts out with computing the orbits of mass points in her disks. Read extended her investigation to the entire family of physically feasible power law disks with a surface density $\Sigma(r) = \Sigma_0(r/r_0)^{\beta-1}$, of which the Mestel disk is the $\beta = 0$ special case. In contrast to the present work, she chooses to keep exact expressions. This forces her to introduce an auxiliary integral not reducible to well-known functions. Using this integral, all the orbit parameters can be expressed in rather short terms. From this analysis, Read picks the maximum radial velocity of the orbit, $U$, and the home radius $R_H$ as the integrals of motion in which to perform the calculation.

The distribution function used by Read in the Mestel disk case is the classical one also employed here, and she investigates "cut-outs" by letting only a part of the matter participate in the perturbations. Two cases are worked out: (a) the "inner cut out", where active matter is removed only in the centre, and (b) the "double cut-out", where active matter is removed both in the centre and in the outer parts of the disk. When used in this work, the term "cut-out disk" is usually supposed to mean doubly cut out disks with inner and outer cut-out indices $N = M = 2$ (see chapter 4.1 for the meaning of these parameters and the shape of the cut-out).

Read goes on to derive the equation that governs the evolution of the power law disks using the projection method suggested by Kalnajs (1971). Starting out at the Poisson and the linearised Boltzmann equations, she finds expressions for the response of a disk to an imposed perturbation. By projection of both an imposed perturbation and the response to it onto the basis of logarithmic spirals, she arrives at one integral equation for each azimuthal harmonic $m$, where different harmonics are decoupled due to the linearity of the problem.

The kernel of this integral equation, called the transfer function $\mathcal{S}_m(\alpha, \alpha')$ by Read (Eq. 3.80), decomposes into an integral over the angular momentum $L_z$, into which the dependence on the size of the orbit is condensed, and a sum over Fourier components of a given orbit with

respect to the logarithmic spirals that control to what extent a given orbit is susceptible to the perturbation. This decomposition is possible because of the self-similarity of the disk and is particularly convenient because the integral over $L_z$ can be carried out analytically for the distribution functions chosen by Read.

To compute the kernel, one still has to perform an integration over the eccentric velocity $U$ and determine the Fourier coefficients. Read does this numerically and finds, as the most striking feature, that the kernel exhibits a strong trailing bias, i.e., $\mathcal{S}_m(\alpha, \alpha')$ is much larger for $\alpha > \alpha'$ than on the other side of the $\alpha = \alpha'$ diagonal. This means that power flows almost exclusively from leading to trailing spiral components in these disks.

The solutions of those integral equations can be found by transforming the equation $A(\alpha) = \int \mathcal{S}_m(\alpha, \alpha')A(\alpha')\,d\alpha'$ to $\lambda A(\alpha) = \int \mathcal{S}_m(\alpha, \alpha')A(\alpha')\,d\alpha'$, thus writing the problem as an eigenvalue problem (note that $\alpha$ and $\alpha'$ will be used with their roles exchanged in the rest of this work, and Read's $S_m$ is $\mathcal{K}$ or $\bar{\mathcal{K}}$ here; I apologise for the confusion). In that formulation, one has found solutions to the original equations when $\lambda$, the"mathematical eigenvalue" in Zang's nomenclature, is unity. By discretizing $\mathcal{S}_m$, one can use standard numerical software to obtain those eigenvalues.

At this point Read can examine the stability properties of her disks, starting with the axisymmetric perturbations. She finds that the Mestel disk becomes unstable at $\sigma_u = 0.378069\,v_c$ with the rotation speed of the disk $v_c$, in close agreement with the local analysis (Toomre 1964). For the doubly cut-out disk with $N = M = 2$, axisymmetric instabilities set in at $\sigma_u = 0.377\,v_c$. As expected, in no case breathing modes are found.

Since the most beautiful galaxies feature prominent two-armed patterns, the first non-axisymmetric modes one will look for are the bisymmetric ones. For the self-consistent disk (i.e., the one with no cut-out applied), Read can only find neutral bisymmetric modes with zero pattern speed. Due to the lack of a time scale in the Mestel disk, the existence of one growing mode would lead to the expectation that Mestel disks should be unstable to modes of every pattern speed and growth rate at a time when their temperature was low enough. However, Read cannot conclusively rule out such a continuum of modes since the integral equation describing this problem is very hard to treat numerically. In the Mestel disk, neutral bisymmetric modes set in at $\sigma_u = 0.17\,v_c$.

By introducing the cut-out, a power-law disk attains a length-, and therfore a time scale. Thus isolated modes are possible and are indeed found. But like Zang before her, Read finds that disks in which the density of the active matter declines only slowly are surprisingly stable against bisymmetric modes. In the doubly cut-out Mestel disk, they set in at $\sigma_u = 0.205\,v_c$ which is far less than the velocity dispersion needed to stabilise the disk against axisymmetric perturbations. This changes only when the inner cut-out is made significantly steeper, thus allowing bisymmetric modes in axisymmetrically stable disks at the expense of probably unrealistically sharp inner edges.

The dependence of the minimum velocity dispersion on the steepness of the cut-out is consistent with qualitative reasoning based on the Lin-Shu theory. The cut-out acts as a Q-barrier shielding waves travelling towards the galactic centre from the inner Lindblad resonance (ILR) that would otherwise absorb them and additionally reflects the waves back, thus opening the possibility for a feedback loop. Indeed, for the modes found by Read, the ILR always lies safely within the cut-out (i.e., in zones with little active matter).

Zang (1976) had already found that Mestel disks strongly favour $m = 1$-modes over their $m = 2$ counterparts. Indeed, $m = 1$-modes are already growing when axisymmetric modes are just marginally stable. Unfortunately, however, the marginal stability is quite problematic in Read's $m = 1$ analysis, since the mathematical eigenvalues appear to follow the real axis in the plane of complex eigenvalues when the growth rate vanishes and the pattern speed tends to zero. Thus, growing one-armed modes seem to exist at any temperature. This suggestion is also backed by results for the self-consistent disk.

A concern for $m = 1$-modes is that they might shift the barycentre of the disk. However, Read finds that at least for the Mestel disk, this is not the case, since in cut-out disks the density profile of the mode tends to cancel out the drags to the barycentre. Even the logarithmic spiral in the self-consistent case has no effect on the barycentre since the perturbation falls off faster than the unperturbed surface density.

Read also investigates three- and four-armed modes. As a rule, these are even move difficult to maintain than the two-armed modes. However, the stability behaviour of the $m = 4$ mode in the cut-out Mestel disk has mathematical eigenvalues at very low pattern speeds and vanishing growth rate along the positive real axis. For $m = 3$, this does not occur. Analogously, the self-consistent Mestel disk has neutral modes for $m = 4$ even at high velocity dispersions. Based on analogous behaviour for varying disk index $\beta$, Read speculates that this phenomenon is linked to the emergence of closed orbits with $m = 3$ symmetry which are not present in the $m = 4$ case and which might somehow damp the modes.

## 1.3. This work

This work set out as an attempt to reproduce Zang's (1976) results in a more straightforward way. Even if they have become far more accessible in the meantime due to Evan's and Read's efforts, it is still worthwhile to try and get analytic approximations for the kernel of the integral equation describing the modes in Mestel disks, not the least in the hope of trying to unravel sume of the vexating properties of the Mestel disk.

After briefly laying out the basic physics of the problem, I will derive analytic approximations for the orbits in the Mestel disk and further simplify them in order to find convenient action-angle coordinates in which I will express the equations. The derivation of the kernel then requires a few quadratures, the most involved of which is the one over the angular momentum. Still, all of these quadratures can be carried out analytically.

Having established the kernels for the self-consistent and the cut-out disks, I will show that the results obtained using this simplified theory are in satisfying accord with the previous results Zang and Read obtained,where I will go from axisymmetric to four-armed perturbations. Finally, I tackle the problem Read could not conclusively solve, the issue of growing modes in the self-consistent disk.

# 2. The Matrix Equation

In this section I will state the basic assumptions of the model, derive an approximated Hamiltonian and combine it with the Boltzmann equation to arrive at an integro-differential equation. Instead of writing this equation down, I will immediately convert it into what Kalnajs (1971) calls a matrix equation by projection onto the space spanned by the logarithmic spirals.

## 2.1. The Physics of the Problem

### 2.1.1. The Mestel Disk

The Mestel disk is named after Leon Mestel, who in a work published in 1963 investigated the gravitational collapse of a spherical cloud of gas, back then being mainly concerned with star formation. He found that under appropriate assumptions the collapse will lead to a disk with a surface density profile

$$\Sigma(r) = \Sigma_0 r_0 / r, \tag{1}$$

where $r_0$ is a normalising length, at which, obviously, $\Sigma(r_0) = \Sigma_0$, and $r$ is the radial coordinate with the centre of the disk at $r = 0$. Using the Poisson equation for a razor-thin disk, this can immediately be integrated to yield the potential

$$\Phi(r) = 2\pi \mathrm{G} \Sigma_0 r_0 \ln r \tag{2}$$

with the gravitational constant G.

As can be seen from (1), $r_0$ is not really a free parameter of the disk, since disks with different $r_0$ can also be viewed as having identical $r_0$ but different $\Sigma_0$. I exploit this liberty to choose $r_0$ to one unit length.

This type of disk is interesting for the investigation of spiral structure not only because of its analytic simplicity, but also because it has a flat rotation curve, i.e. the circular velocity $v_c$ of a mass point a Mestel disk is independent from its distance to the disk's centre. At least nearly flat rotation curves are fairly universal for the off-centre regions of giant spiral galaxies (e.g., Rubin et al. 1985 or Persic and Salucci 1991 and references therein), with indeed flatter rotation curves apparently associated with a more dominant global mode (Biviano et al. 1991).

In this work, I choose the unit velocity such that this circular velocity

$$v_c = 2\pi \mathrm{G} \Sigma_0 = 1. \tag{3}$$

In this way, the equations of motion in the Mestel disk in polar coordinates $(r, \vartheta)$ are

$$\ddot{r} = r\dot{\vartheta}^2 - 1/r \tag{4a}$$
$$L_z = r^2\dot{\vartheta} = \text{const}, \tag{4b}$$

where $L_z$ denotes the angular momentum per unit mass and the dot signifies the temporal derivative.

### 2.1.2. Derivation of the Hamiltonian in Action-Angle Coordinates

In my programme of solving the Boltzmann and Poisson equations of the perturbed Mestel disk, I will start with the Boltzmann equation. This equation takes its simplest form when it is formulated in the action-angle coordinates of the problem. Therefore, it is favourable to start out with deriving a Hamiltonian of the perturbed Mestel disk in action-angle coordinates.

The most straightforward way to find the transformation equations between the (non-canonical sets of coordinates $(r, \vartheta, \dot{r}, \dot{\vartheta})$ and the yet-to-be-determined action-angle coordinates $(w_1, w_2, L_z, J)$ is to solve the equations of motion. Unfortunately, an exact closed solution of (4) does not exist in elementary functions.

The path most frequently taken to get approximate solutions, the epicyclic approximation, yields a Hamiltonian that does not contain any terms originating from non-circular motions and thus is useless for the investigation of perturbations. I therefore employ a different approximation based on the method of harmonic balance. The method of harmonic balance belongs to the large family of asymptotic methods, where nonlinear differential equations are solved by expanding the nonlinearity into a series and dropping higher terms. The choice of the basis functions for this expansion is crucial for the quality of the solutions.

In the case of primarily oscillatory motion the most straightforward basis functions are sines and cosines, and thus the coefficients of the series are just the Fourier coefficients of the nonlinearity. Keeping only the constant and the two lowest order terms (those proportional to $\sin(x)$ and $\cos(x)$), one is left with a linear differential equation that can readily be solved. More on asymptotic expansions can be found in Bogoliubov and Mitropolski (1961), Kuypers (1990) gives a very nice and concise treatment of the method of harmonic balance itself.

Inserting (4b) into (4a) yields

$$\ddot{r} = L_z^2/r^3 - 1/r. \tag{5}$$

In order to perform the development of the nonlinearity in (5), I substitute

$$r(t) = R_0\big(1 + \zeta\cos(\kappa t)\big) \tag{6}$$

with an epicyclic frequency $\kappa$ and a parameter $\zeta$ that gives the ellipticity of an orbit such that $\zeta = 0$ indicates a circular orbit. $R_0$ is the orbit's reference radius. The parameter $\zeta$ is the small parameter of this asymptotic expansion, so $\zeta$ should not exceed 0.1, say, for the majority of the constituents of the model galaxy. I will return to the issue how much of a restriction this is in a moment.

The first Fourier terms of the right hand side of (5) with respect to $t$ are

$$\begin{aligned} a_0 &= \frac{L_z^2\left(1+\zeta^2/2\right) - R_0^2\left(1-\zeta^2\right)^2}{R_0^3\left(1-\zeta^2\right)^{5/2}} \\ a_1 &= -\frac{2R_0^2\left(1-\zeta^2\right)^2\left(\sqrt{1-\zeta^2}-1\right) + 3L_z^2\zeta^2}{\zeta R_0^3\left(1-\zeta^2\right)^{5/2}} \\ b_1 &= 0, \end{aligned} \tag{7}$$

where $a_i$ and $b_i$ denote the cosine and sine coefficients, respectively. Dropping all higher Fourier terms Eq. (5) now reads

$$\ddot{r} = a_0 + \frac{a_1}{\zeta}\left(\frac{r}{R_0} - 1\right). \tag{8}$$

I parametrise the orbits by $R_0$ and $\zeta$. Inserting (6) and comparing the terms independent of $t$ one immediately obtains

$$L_z = \frac{\sqrt{2}R_0(1-\zeta^2)}{\sqrt{\zeta^2+2}}. \tag{9}$$

By comparing the terms with $\cos(\kappa t)$ the epicyclic frequency $\kappa$ is found to be

$$\kappa = \frac{\sqrt{2}}{\zeta R_0}\sqrt{1 - 2\frac{\sqrt{1-\zeta^2}}{\zeta^2+2}}. \tag{10}$$

To determine the circular frequency of the guiding centre $\Omega$ in this approximation one inserts (6) and (9) into Eq. (4b) and Fourier analyses with respect to $t$ again. This yields

$$\Omega = \frac{L_z}{R_0^2\left(1-\zeta^2\right)^{3/2}}. \tag{11}$$

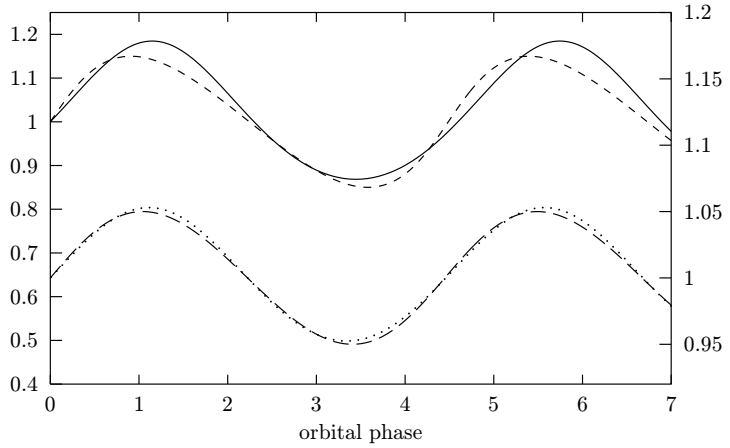


*Fig. 1: A comparison of numerically integrated and approximated orbits. The upper pair is for $\zeta = 0.15$ and has to be read with the left scale, the lower one for $\zeta = 0.05$ and corresponds to the right scale. In both cases, $R_0 = 1$.*

This completely determines the orbits. For what kind of orbit parameters will those approximated orbits be useful? The temporal derivative of (6) shows that the maximal radial velocity attained on a given orbit (the eccentric velocity in Zang's nomenclature) is $U = R_0\zeta\kappa$. In the epicyclic approximation of the Mestel disk, $\kappa = \sqrt{2}\Omega$, so that $U = \sqrt{2}\zeta v_c$ for small $\zeta$.

As can be seen in Fig. 1, the method of harmonic balance gives at least useful estimates of both $\kappa$ and the radial extent of the orbits up to $\zeta \approx 0.15$. However, the shape of the real orbits is quite different from a sine already when $\zeta$ is that high. If our Galaxy were a Mestel disk, in the solar neighbourhood ($v_c = 200 \cdots 250\,\mathrm{km\,s^{-1}}$) that would correspond to an eccentric velocity of roughly $U = 50\,\mathrm{km\,s^{-1}}$, which again means that its orbit should be confined to a torus roughly 2 kpc wide. It is probably justified to assume that most of the stars that significantly participate in a spiral instability will more or less meet this criterion. Of course, this does not decide the question whether the quite severe distortion of the shape of the orbits will greatly degrade the results, and it is hard to do this *a priori*. Still, the fact that the times spent within and out of the reference radius are quite comparable for the approximated and the true orbits may restore some confidence shaken by the optical appearance of the $\zeta = 0.15$ orbit.

However, even this approximation is not enough to make the problem of the transformation to action-angle coordinates tractable, since unfortunately determining the Hamiltonian in action coordinates from Eqs. (10) and (11) results in rather messy expressions. In particular, solving (10) for $\zeta$ gets quite involved. However, for small $\zeta$ one may linearise (10) and (11) to

$$\kappa = \sqrt{2}/R_0 \qquad \Omega = 1/R_0 \tag{12}$$

(this is identical to the result of classic epicyclic theory) and finds on developing the Hamiltonian to the second order and dropping higher Fourier coefficients

$$H_0(J, L_z) = \frac{1}{2} + \ln(L_z) + \frac{\sqrt{2}J}{L_z}, \tag{13}$$

where $J = \kappa\zeta^2 R_0^2/2$. This $J$ simply is the energy in the epicyclic motion divided by $\kappa$, which, in an epicyclic approximation, is the second integral and thus the second action besides $L_z$.

Clearly, this Hamiltonian is the simplest one that could possibly be related to the Mestel disk. The justification of the rather brutal simplifications I was forced to adopt can (and will) only be given *a posteriori* by showing that the disks described by the Hamiltonian (13) do indeed behave quite like the "true" Mestel disks studied by Zang and Read.

The action variables $J$ and $L_z$ are conjugate to the angle variables

$$\begin{aligned} w_1 &= \kappa t \qquad & \frac{\partial H_0}{\partial J} &= \dot{w}_1 = \kappa \\ w_2 &= \Omega t \qquad & \frac{\partial H_0}{\partial L_z} &= \dot{w}_2 = \Omega \end{aligned} \tag{14}$$

Although the Hamiltonian (13) is of order $\zeta^2$ due to the presence of a term with $J/L_z$, the canonical equations (14) are not correct to $\zeta^2$; in fact, while $\partial H_0/\partial L_z = 1/L_z - \sqrt{2}J/L_z^2$, one has $\Omega = 1/L_z - (3/2)J/L_z^2$ to second order in $\zeta$, a 5% difference in the second-order

coefficient (the corresponding relations for $w_1$ and $J$ are correct to second order). However, the term with $J$ is important for the derivation of the Boltzmann equation, and terms of order $J/L_z = O(\zeta^2)$ will be disregarded after its derivation.

Now, if I had derived the exact action-angle coordinates, the transformation from Cartesian coordinates and their canonically conjugate momenta into the space of action-angle coordinates $(w_1, w_2, J, L_z)$ would be a canonic transformation. Since (6) and (12) are approximations, it is almost certainly not. However, if the "non-canonicity" caused by the approximations is small enough, i.e., of order $O(\zeta^2)$, the error made by treating this transformation as canonic is negligible. I will now check that this indeed the case by computing the Jacobian of the transformation from the set of action-angle coordinates $(w_1, w_2, L_z, J)$ to the Cartesian coordinates $(x, y)$ and the momenta per unit mass $(\dot{x}, \dot{y})$.

The transformation from the action-angle coordinates to the set of polar coordinates and their temporal derivatives is

$$\begin{aligned}
r &= L_z + \sqrt{\sqrt{2}JL_z}\cos(w_1) \\
\dot{r} &= -\sqrt{2}\sqrt{\frac{\sqrt{2}J}{L_z}}\sin(w_1) \\
\vartheta &= w_2 - \sqrt{2}\sqrt{\frac{\sqrt{2}J}{L_z}}\sin(w_1) \\
\dot{\vartheta} &= -\frac{1}{L_z} + 2\frac{\sqrt{\sqrt{2}JL_z}}{L_z^2}\cos(w_1).
\end{aligned}$$

Inserting this into the transformation form polar to Cartesian coordinates yields

$$\begin{aligned}
x =& L_z\left(1+\zeta\cos(w_1)\right)\cos\Big(w_2 - \sqrt{2}\zeta\sin(w_1)\Big) \\
y =& \left(L_z+\zeta\cos(w_1)\right)\sin\Big(w_2 - \sqrt{2}\zeta\sin(w_1)\Big) \\
\dot{x} =& -\sqrt{2}\zeta\sin(w_1)\cos\Big(w_2 - \sqrt{2}\zeta\sin(w_1)\Big) \\
& -\left(1+\zeta\cos(w_1)\right)\Big(1-2\zeta\cos(w_1)\Big)\sin\Big(w_2 - \sqrt{2}\zeta\sin(w_1)\Big) \\
\dot{y} =& -\sqrt{2}\zeta\sin(w_1)\sin\Big(w_2 - \sqrt{2}\zeta\sin(w_1)\Big) \\
& -\left(1+\zeta\cos(w_1)\right)\Big(1-2\zeta\cos(w_1)\Big)\cos\Big(w_2 - \sqrt{2}\zeta\sin(w_1)\Big),
\end{aligned} \tag{16}$$

where I have kept $\zeta = \sqrt{\sqrt{2}J/L_z}$ to save space.

The Jacobian $\partial(x, y, \dot{x}, \dot{y})/\partial(w_1, w_2, J, L_z)$ of this transformation turns out to be

$$\mathcal{J} = 1 + 6\sqrt{\frac{\sqrt{2}J}{L_z}}\cos(w_1) + 9\frac{\sqrt{2}J}{L_z}\cos^2(w_1) + 4\sqrt{\frac{\sqrt{2}J}{L_z}}^3\cos^3(w_1). \tag{17}$$

Developing this into a series in $\zeta$, one finds

$$\mathcal{J} = 1 + 6\zeta\cos(w_1) + 9\zeta^2\cos^2(w_1) + O(\zeta^3). \tag{18}$$

Thus, only after averaging over one epicyclic period is the Jacobian really of the desired $1+O(\zeta^2)$ order. This should not be a major issue in limiting the accuracy of my calculations, though, in particular because the kernel I will calculate is a quantity averaged over both periodic motions.

### 2.1.3. The Distribution Function

Binney and Tremaine (1987) give a distribution function of the Mestel disk (without counter-rotating stars) as

$$f_0(\mathcal{E}, L_z) = \begin{cases} F_{\mathrm{BT}} L_z^q \mathrm{e}^{\mathcal{E}/\sigma^2}, & L_z > 0 \\ 0, & L_z < 0 \end{cases} \tag{19}$$

with the relative energy $\mathcal{E} = \Psi - v^2/2$, the relative potential $\Psi$, and

$$F_{\mathrm{BT}} = \frac{\Sigma_0 \tilde{r}_0}{2^{q/2}\sqrt{\pi}\left(\frac{q-1}{2}\right)!\,\sigma^{q+2}}, \qquad q = \sigma^{-2} - 1. \tag{20}$$

Noting that $\mathcal{E}$ is just the negative of the Hamiltonian, I can express the distribution function in $J$ and $L_z$ as

$$f_0(L_z, J) = \frac{F}{L_z}\exp\left(-\frac{\sqrt{2}J}{\sigma^2 L_z}\right), \tag{21}$$

where I have collected the terms not dependent on the actions in

$$F = \frac{\mathrm{e}^{-1/2\sigma^2}\Sigma_0 \tilde{r}_0}{2^{q/2}\sqrt{\pi}\left(\frac{q-1}{2}\right)!\,\sigma^{q+2}}. \tag{22}$$

The equilibrium distribution function $f$ only depends on actions, as it should by the Jeans theorem. Again, this is not much of a test for the approximated transformation equations, but it provides some reassurance.

The parameter $q$ usually is the range $10\cdots100$ in disks responsive to spiral perturbations, corresponding to $\sigma \approx (0.1\cdots0.3)v_c$ or $(20\cdots70)\mathrm{km\,s^{-1}}$ for a disk like our own Galaxy's in the regions that show spiral structure. Thus, an application of Stirling's formula in $F$ is well justified and significantly reduces later numerical hassles. The result is

$$F = \frac{\sqrt{2}\sqrt{1-2\sigma^2}^{1-1/\sigma^2}}{4\mathrm{e}\pi^2\sigma^2\mathrm{G}} \tag{23}$$

where (3) has been used to eliminate $\Sigma_0$ and I have set $r_0 = \tilde{r}_0$.

### 2.1.4. The Potential Basis

Following Kalnajs (1971), I use logarithmic spirals

$$\varphi_{\alpha,m}(r,\vartheta) = \frac{\mathrm{e}^{\mathrm{i}\alpha\ln(r)+\mathrm{i}m\vartheta-\mathrm{i}\omega t}}{\sqrt{r}} \tag{24}$$

as the basis into which the potential is developed. The factor $r^{-1/2}$ has been added to ensure definiteness of the $L_z$-integration in the matrix equation and will silently be replaced by a $L_z^{-1/2}$ when linearising in the actions. This is not exact for a linearisation in $\zeta$ and has in that sense to be justified *a posteriori*. However, the potential basis is just that, a set of basis functions, and thus slightly changing the shape of the basis functions while retaining their central features (orthogonality, span) should not be critical anyway and would only influence the expansion coefficients but not the expansion itself.

The sign of the term with $\omega$ has been chosen so that spirals with $\omega$, $m$, and $\alpha$ all positive are trailing. While the main impetus of this work is the study of marginal (i.e., neither growing nor decaying) modes, it should be noted that growing modes correspond to an $\omega$ with positive imaginary part with this distribution of signs. This will be of particular importance in the application of Landau's rule further below.

The quantity $\alpha$, appearing here as the tangent of the inclination of a spiral arm, can also be viewed as something like a radial wave number. Indeed, the larger $|\alpha|$, the tighter wrapped the spirals are. However, since $\alpha$ is multiplied with $\ln(r)$ instead of $r$ in (24), it is not true that the spiral pattern is periodic with period $2\pi/\alpha$ in $r$. Instead, $2\pi/\alpha$ is the period of $\ln r$, and thus $\alpha$ should be called logarithmic wave number. I will nevertheless talk about wave numbers in this text.

It should be noted that with this definition the pattern speed of the wave is $\Omega_p = \omega/m$, since at a given point in the galaxy a potential trough has to pass $m$ times for the spiral pattern to complete an entire rotation around the centre.

The expression (24) has to be reduced to order $O(\zeta^2)$. Some care is required in doing this since I want to keep terms like $\sin(\zeta\sin(w_1))$, in accord with my programme of keeping oscillatory terms of order $\exp(\mathrm{i}\zeta)$. This is done by linearising just the exponent to order $\zeta$, not the entire exponential.

After the linearisation the potential basis has the form

$$\varphi_{\alpha,m}(w_1,w_2,J,Lz) = L_z^{\mathrm{i}\alpha-1/2}\exp\left(\mathrm{i}\,mw_2 + \mathrm{i}\sqrt{\frac{\sqrt{2}J}{L_z}}\Big(\alpha\cos(w_1) - \sqrt{2}m\sin(w_1)\Big) - \mathrm{i}\,\omega t\right). \tag{25}$$

In this work, I assume all possible potential perturbations have an expansion like

$$\sum_{m=0}^{\infty}\int_{-\infty}^{\infty}\Phi_{\alpha,m}\varphi_{\alpha,m}(w_1,w_2,J,L_z)\,d\alpha. \tag{26}$$

This is certainly true for all continuous (and therefore bounded for finite $r$) perturbations that vanish quickly enough as $r\to\infty$ to be acceptable in a linear perturbation analysis.

## 2.2. Derivation of the Matrix Equation

### 2.2.1. The Linearised Boltzmann Equation

The response of the Mestel disk to a perturbation of the type (25) can be computed using the Boltzmann equation,

$$\frac{df}{dt} = \frac{\partial f}{\partial t} + [f, H] = 0, \tag{27}$$

where the symbol $[\,.\,,.\,]$ denotes Poisson brackets, $H$ is the total Hamiltonian of the system, and $f$ its total distribution function. For brevity, I do not indicate the dependence on the angles and actions in the distribution function and the potential (and their perturbations) except where it seems necessary for reasons of clarity.

Since I am only interested in small deviations from the equilibrium, I may significantly simplify this equation by linearising it. To this end, I write $H = H_0 + \Phi_1$ and $f = f_0 + f_1$, where $H_0$ and $f_0$ are given by (13) and (21), respectively. I immediately specialise on the case of a perturbation potential $\Phi_1$ of the form (25). I furthermore demand that $\Phi_1 \ll H_0$ and $f_1 \ll f_0$. Using the linearity of the Poisson brackets, (27) then becomes

$$\frac{\partial f_1}{\partial t} + [f_0, H_0] + [f_1, H_0] + [f_0, \Phi_1] + [f_1, \Phi_1] = 0 \tag{28}$$

The second summand on the left side of this equation is zero by definition of the equilibrium, whereas the last summand is neglected since it is quadratic in the small quantities $f_1$ and $\Phi_1$. Hence the linearised Boltzmann equation reads

$$\frac{\partial f_1}{\partial t} + [f_1, H] = -[f_0, \Phi_1]. \tag{29}$$

After inserting the canonical equations and (12), the left hand side of (29) becomes

$$\begin{aligned} \text{l.h.s.} =& \frac{\partial f_1}{\partial t} + \frac{\partial f_1}{\partial w_1}\dot{w}_1 + \frac{\partial f_1}{\partial w_2}\dot{w}_2 \\ =& \frac{\partial f_1}{\partial t} + \frac{\sqrt{2}}{L_z}\frac{\partial f_1}{\partial w_1} + \frac{1}{L_z}\frac{\partial f_1}{\partial w_2}. \end{aligned} \tag{30}$$

The right hand side of (29) is somewhat more involved. Evaluating at first only the derivatives of $f_0$ one gets

$$\text{r.h.s.} = \frac{f_0}{(\sigma L_z)^2}\left(\sqrt{2}L_z\frac{\partial \Phi_1}{\partial w_1} + \left(\sigma^2 L_z - \sqrt{2}J\right)\frac{\partial \Phi_1}{\partial w_2}\right). \tag{31}$$

In this expression the term with $J$ is of order $\zeta^2$ and is therefore discarded.

Before inserting the potential basis (25), I have to decide on the sign of $\varphi_{\alpha,m}$ in the Hamilton function. Since I want to save me the trouble of maintaining a sign in the Poisson equation (where it enters with the opposite sign), I use $\Phi_1 = -\Phi_{\alpha,m}\varphi_{\alpha,m}$ here, where $\Phi_{\alpha,m}$ is a complex

number and corresponds to the coefficients of the series (26). Carrying out the remaining derivatives, one arrives at

$$\begin{aligned}\text{r.h.s.} = -\mathrm{i}\,\Phi_{\alpha,m}\frac{FL_z^{\mathrm{i}\alpha-3}}{\sigma^2}\left(\sqrt{2\sqrt{2}J}\Big(\alpha\sin(w_1)+\sqrt{2}\,m\cos(w_1)\Big)-m\sigma^2\sqrt{L_z}\right)\\ \exp\left(\mathrm{i}mw_2+\mathrm{i}\sqrt{\frac{\sqrt{2}J}{L_z}}\Big(\alpha\cos(w_1)-\sqrt{2}m\sin(w_1)\Big)-\frac{\sqrt{2}J}{\sigma^2L_z}-\mathrm{i}\omega t\right).\end{aligned} \tag{32}$$

### 2.2.2. Computation of the Response

The solution of the inhomogeneous linear partial differential equation (30)=(32) gives the response $f_1(J, L_z, w_1, w_2, t)$ of the disk to an elementary forcing (25) in the limit of vanishing perturbation amplitude. To find a solution, I first convert the Boltzmann equation to an ordinary differential equation which, due to the linearity of the equation, is easily solved.
The structure of (32) invites a separation of variables by

$$f_1(w_1, w_2, t) = g_1(w_1)\mathrm{e}^{\mathrm{i}mw_2-\mathrm{i}\omega t}, \tag{33}$$

which results in the inhomogeneous ordinary linear differential equation

$$\begin{aligned}g_1'(w_1)+\mathrm{i}\frac{(\omega L_z+m)}{\sqrt{2}}g_1(w_1) = C\left(\alpha\sin(w_1)+\sqrt{2}m\cos(w_1)-m\sigma^2\sqrt{\frac{L_z}{2\sqrt{2}J}}\right)\\ \exp\left(\mathrm{i}\sqrt{\sqrt{2}J/L_z}\Big(\alpha\cos(w_1)-\sqrt{2}m\sin(w_1)\Big)-\frac{\sqrt{2}J}{\sigma^2L_z}\right).\end{aligned} \tag{34}$$

Here, the prime denotes the derivative with respect to $w_1$ and

$$C = -\mathrm{i}\,\Phi_{\alpha,m}\sqrt{2\sqrt{2}J}\frac{FL_z^{\mathrm{i}\,\alpha-3}}{\sigma^2}. \tag{35}$$

This inhomogeneous equation is solved in the usual way by finding the solution of the homogenous equation and then applying the method of variation of constants. The solution of the homogenous equation is

$$\tilde{g}_1(w_1) = \mathrm{e}^{\mathrm{i}(\omega L_z-m)w_1/\sqrt{2}}. \tag{36}$$

By variation of constants one immediately has

$$g_1(w_1) = \mathrm{e}^{\mathrm{i}\eta w_1}\left(D+\int_0^{w_1}S(w_1')\,dw_1'\right), \tag{37}$$

where I have abbreviated $\eta = (\omega L_z - m)/\sqrt{2}$ and $D$ is an integration constant. The lower integration bound is arbitrary, but the choice of 0 is quite convenient for the calculations below. The integrand $S(w_1')$ is given by

$$\begin{aligned}S(w_1') =& C\left(\alpha\sin(w_1)+\sqrt{2}m\cos(w_1)-m\sigma^2\sqrt{\frac{L_z}{2\sqrt{2}J}}\right)\\ &\exp\left(-\mathrm{i}\eta w_1'+\mathrm{i}\sqrt{\sqrt{2}J/L_z}\Big(\alpha\cos(w_1')-\sqrt{2}m\sin(w_1')\Big)-\frac{\sqrt{2}J}{\sigma^2L_z}\right)\end{aligned} \tag{38}$$

and has the property that $S(w_1' + 2\pi) = \mathrm{e}^{2\pi\mathrm{i}\eta} S(w_1')$. Therefore,

$$\int_0^{2\pi+w_1} S(w_1')\,dw_1' = \int_0^{2\pi} S(w_1')\,dw_1' + \mathrm{e}^{2\pi\mathrm{i}\eta} \int_0^{w_1} S(w_1')\,dw_1'. \tag{39}$$

I now have to find the particular solution appropriate to my problem, i.e., fix $D$. Because (34) is a first-order differential equation, I only need one condition that in this case is generated from a periodicity requirement: $f$ has to be uniquely defined and thus $2\pi$-periodic in $w_1$. Hence $f$ must satisfy $f(w_1) = f(w_1 + 2\pi)$, which in turn implies $g(w_1) = g(w_1 + 2\pi)$. Inserting (37) and applying (39) one arrives at

$$D = \frac{1}{\mathrm{e}^{-2\pi\mathrm{i}\eta} - 1} \int_0^{2\pi} S(w_1')\,dw_1'. \tag{40}$$

Note that, in contrast to the usual theory of linear differential equations with initial or boundary conditions, this requirement does not necessarily cut down the solution space to a single point. For example, requiring $f(w_1) = f(w_1 + \pi)$ will lead to different functions that also satisfy $f(w_1) = f(w_1 + 2\pi)$. It might be a worthwhile exercise to investigate such solutions.

The integral in (37) can also be somewhat simplified—at least as far as computability is concerned—by using periodicity arguments. Here one uses

$$\int_0^{w_1} S(w_1')\,dw_1' = \int_0^{2\pi} S(w_1')\,dw_1' + \mathrm{e}^{2\pi\mathrm{i}\eta} \int_0^{w_1} S(w_1')\,dw_1' - \int_0^{2\pi} S(w_1' + w_1)\,dw_1',$$

implying $\int_0^{w_1} S(w_1')\,dw_1' = \left(\int_0^{2\pi} S(w_1')\,dw_1' - \int_0^{2\pi} S(w_1' + w_1)\,dw_1'\right)/\left(1 - \mathrm{e}^{2\pi\mathrm{i}\eta}\right)$ and finds on inserting (40)

$$g_1(w_1) = \frac{\mathrm{e}^{\mathrm{i}\eta w_1}}{\mathrm{e}^{-2\pi\mathrm{i}\eta} - 1} \int_0^{2\pi} S(w_1' + w_1)\,dw_1' \tag{42}$$

This integral can be further simplified by noting that the trigonometric functions of $w_1$ in the coefficient appear in the same linear combination as those in the exponent derived w.r.t. $w_1$, which is hardly surprising, since they came into the coefficient by a derivation of the exponent. This invites partial integration in order to get rid of the trigonometric terms outside the exponential. Setting

$$\begin{aligned} u &= -\frac{\mathrm{i}}{C}\sqrt{\frac{\sqrt{2}J}{L_z}}\exp\left(\mathrm{i}\,(w_1 + w_1')\left(\frac{m\sigma^2}{\sqrt{2}} + \eta\right)\right) \\ v &= \exp\left(\mathrm{i}\frac{m\sigma^2}{\sqrt{2}}(w_1 + w_1') + \mathrm{i}\sqrt{\frac{\sqrt{2}J}{L_z}}\left(\alpha\cos(w_1 + w_1') - \sqrt{2}m\sin(w_1 + w_1')\right) - \frac{\sqrt{2}J}{\sigma^2 L_z}\right) \end{aligned} \tag{43}$$

one may write $S = v'/u$ (the prime now denotes derivation w.r.t. $w_1'$).

Assembling the result one is left with

$$g_1(w_1) = C\sqrt{\frac{L_z}{\sqrt{2}J}}\exp\left(-\frac{\sqrt{2}J}{\sigma^2 L_z}\right)\left(\mathrm{i}\,\exp\left(\mathrm{i}\sqrt{\frac{\sqrt{2}J}{L_z}}\big(\alpha\cos(w_1)-\sqrt{2}m\sin(w_1)\big)\right)\right.$$
$$-\frac{1}{\mathrm{e}^{-2\pi\mathrm{i}\eta}-1}\left(\sqrt{2}\eta+m\sigma^2\right) \tag{44}$$
$$\left.\int_0^{2\pi}\exp\left(\mathrm{i}\sqrt{\frac{\sqrt{2}J}{L_z}}\big(\alpha\cos(w_1+w_1')-\sqrt{2}m\sin(w_1+w_1')\big)-\mathrm{i}\eta w_1'\right)dw_1'\right).$$

Substituting this equation into (33) gives the desired response of the disk.

### 2.2.3. The Poisson Equation

After I have computed the response to an elementary forcing, I proceed to ask when this response is self-consistent, i.e., for which parameters the density perturbation resulting from the change in the distribution function causes just the potential perturbation that I started with. To answer this question, the Poisson equation linking the potential $\Phi$ and the density $\rho$

$$\triangle\Phi = -4\pi\mathrm{G}\rho$$

with Newton's gravitational constant G must be solved simultaneously to the Boltzmann equation. Since the equation is linear, it is immediately valid for the perturbation quantities just like for the total potential and density.

Intuitively, one expects that the elementary forcing (25) will as a rule have a rather different shape after having been mangled through the Boltzmann and Poisson equations, i.e., the response to (25) in potential space contains many contributions of the form (25) and has the form (26).

Indeed, the Laplace operator in the Poisson equation does not commute with the operator in the Boltzmann equation, and thus they will not possess common eigenfunctions. What is more, the Laplacian expressed in action-angle coordinates is quite cumbersome. Thus, the integro-differential equation resulting from a simple insertion of the Boltzmann into the Poisson equation would be very hard to handle. To overcome this difficulty, I follow Kalnajs (1971) in avoiding this integro-differential equation by converting the equation system into a matrix equation. This can be done by projecting the potential perturbation and the density response onto a set of suitable basis functions.

The basis functions in potential space have been chosen above to the be the logarithmic spirals (24). To find the corresponding basis in density space, I employ Toomre's device (Clutton-Brock 1972). One has

$$\triangle\mathrm{e}^{-k|z|} = k^2\mathrm{e}^{-k|z|} - 2k\delta(z), \tag{46}$$

and, by definition of the Bessel function,

$$\triangle\Big(J_m(kr)\mathrm{e}^{\mathrm{i}m\vartheta}\Big) = -k^2 J_m(kr)\mathrm{e}^{\mathrm{i}m\vartheta}. \tag{47}$$

Since the Laplace operator in cylinder coordinates,

$$\triangle = \frac{1}{r}\frac{\partial}{\partial r}\left(r\frac{\partial}{\partial r}\right) + \frac{1}{r^2}\frac{\partial^2}{\partial \vartheta^2} + \frac{\partial^2}{\partial z^2}, \tag{48}$$

decomposes into independent operators in $(r, \vartheta)$ and $z$, using (46) and (47) one can easily verify that the functions $\Phi_k$ and $\rho_k$ defined by

$$\Phi_k(r, \vartheta, z) = J_m(kr)e^{\mathrm{i}m\vartheta}e^{-k|z|} \qquad \rho_k(r, \vartheta, z) = \frac{k}{2\pi \mathrm{G}}J_m(kr)e^{\mathrm{i}m\vartheta}\delta(z) \tag{49}$$

form a potential-density pair. Multiplying by a suitable function $g(k)$—it is completely unrelated to the function $g_1(w_1)$ introduced in the last chapter—and integrating over $k$ one sees that

$$\begin{aligned} \rho(r, \vartheta, z) &= \frac{\mathrm{e}^{\mathrm{i}m\vartheta}}{2\pi G}\int_0^\infty J_m(kr)g(k)k\delta(z)\,dk \\ \Phi(r, \vartheta, z) &= e^{\mathrm{i}m\vartheta}\int_0^\infty J_m(kr)g(k)e^{-k|z|}\,dk \end{aligned} \tag{50}$$

form a potential-density pair as well.

Multiplying the second line of (50) with $rJ_m(k'r)$, integrating over $r$ and applying the Fourier-Bessel-Theorem

$$\int_0^\infty J_m(k'r)J_m(kr)r\,dr = \frac{\delta(k'-k)}{k} \tag{51}$$

yields

$$g(k) = ke^{k|z|-\mathrm{i}m\vartheta}\int_0^\infty \Phi(r, \vartheta, z)J_m(kr)r\,dr \tag{52}$$

($k'$ has been renamed $k$ here).

The resulting $g(k)$ can now be inserted into the first line of (50). After an integration over $z$ one has

$$\mu(r, \vartheta) = \frac{1}{2\pi G}\int k^2 J_m(kr)\int \Phi(r', \vartheta, 0)J_m(kr')r'\,dr'\,dk, \tag{53}$$

where $\mu$ denotes a surface density. Inserting (24), for the moment omitting the dependence on $t$, one has integrals of the type $\int_0^\infty x^\mu J_\nu(ax)$. The integrals can be carried out using Gradshteyn and Ryzhik (1979), 6.561.14,

$$\int_0^\infty x^\mu J_\nu(ax)\,dx = 2^\mu a^{-\mu-1}\frac{\Gamma\Big((1+\nu+\mu)/2\Big)}{\Gamma\Big((1+\nu-\mu)/2\Big)}, \tag{54}$$

where Gradshteyn and Ryzhik require that $-(\mathrm{Re}\,\nu + 1) < \mathrm{Re}\,\mu < \frac{1}{2}$ and $a > 0$, which given the asymptotics of the Bessel function is of course necessary for the definiteness of the integral. In the present context, however, it is permissable to carry this formula to the limits $\mathrm{Re}\,\mu \to 1/2$ and $a \to 0$.

For the $r'$-integration, one sets

$$x = r' \qquad \nu = m \qquad \mu = \frac{1}{2} + \mathrm{i}\,\alpha \qquad a = k,$$

and for the integration over $k$

$$x = k \qquad \nu = m \qquad \mu = \frac{1}{2} - \mathrm{i}\,\alpha \qquad a = r.$$

This gives the basis functions in surface density,

$$\mu_{\alpha,m}(r,\vartheta) = K_m(\alpha)\mathrm{e}^{\mathrm{i}m\vartheta} r^{-3/2+\mathrm{i}\alpha}, \tag{55}$$

where

$$K_m(\alpha) = \frac{\left|\Gamma\left(\frac{3}{4} + \frac{1}{2}m + \frac{1}{2}\mathrm{i}\alpha\right)\right|^2}{\pi \mathrm{G}\left|\Gamma\left(\frac{1}{4} + \frac{1}{2}m + \frac{1}{2}\mathrm{i}\alpha\right)\right|^2} \tag{56}$$

is related to the Kalnajs gravity factor as used by Read, $K(\alpha, m)$, through $K_m(\alpha) = \left(2\pi G K(\alpha,m)\right)^{-1}$. In writing down $K_m(\alpha)$ in terms of moduli, I have already exploited the fact that $\Gamma(\bar{z}) = \overline{\Gamma(z)}$.

The two sets of functions $\mu_{\alpha,m}$ and $\varphi_{\alpha,m}$ both form a basis for two function spaces. If both a potential perturbation $\Phi(r,\vartheta)$ and the density response computed by projection of the distribution function resulting from the Boltzmann equation into the $(r,\vartheta)$-space are elements of those spaces, they can be expanded into two series,

$$\begin{aligned} \Phi(r,\vartheta) &= \sum_m \int \Phi_{\alpha,m}\varphi_{\alpha,m}(r,\vartheta)\,d\alpha \\ \mu(r,\vartheta) &= \sum_m \int M_{\alpha,m}\mu_{\alpha,m}(r,\vartheta)\,d\alpha. \end{aligned} \tag{57}$$

By definition of $\varphi_{\alpha,m}$ and $\mu_{\alpha,m}$ as an orthonormal potential density pair, the Poisson equation for the coefficients of the series (57) takes the simple form

$$\Phi_{\alpha,m} = M_{\alpha,m}. \tag{58}$$

For later reference, it should be noted that the scalar product of two corresponding basis functions is

$$\int_0^{2\pi}\int_0^{\infty} \varphi^*_{\alpha,m}\mu_{\alpha,m} r\,dr\,d\vartheta = 4\pi^2 K_m(\alpha)\delta_{m,m'}\delta(\alpha-\alpha'). \tag{59}$$

### 2.2.4. The Matrix Equation

I am now ready to write down the matrix equation. To this end (42) can be written as

$$f_1^{\text{response}} = \mathcal{L}\Phi^{\text{imposed}} \tag{60}$$

with a linear operator $\mathcal{L}$. Assuming for the moment that this equation is formulated in Cartesian coordinates, the perturbation of the distribution function $f_1$ can be transformed into a density perturbation $\mu_1$ by integration over the momenta per unit mass $\dot{x}$ and $\dot{y}$. Inserting the expansions for $\mu^{\text{response}}$ and $\Phi^{\text{imposed}}$, for the moment assumed to be expressed in Cartesian coordinates as well, one finds

$$\sum_m \int d\alpha\, \mu_{\alpha,m}(x,y) M_{\alpha,m}^{\text{response}} = \int dp_x\, dp_y \sum_m \int d\alpha\, \Phi_{\alpha,m}^{\text{imposed}} \mathcal{L}\varphi_{\alpha,m}(x,y). \tag{61}$$

In this chapter only, I write the differentials directly behind their integral signs to improve the readability of the expressions.

A projection of this equation onto $\varphi_{\alpha',m'}$ yields

$$4\pi^2 K_{m'}(\alpha') M_{\alpha',m'}^{\text{response}} = \int dx\, dy \int dp_x\, dp_y \sum_m \int d\alpha\, \Phi_{\alpha,m}^{\text{imposed}} (\mathcal{L}\varphi_{\alpha,m}) \varphi_{\alpha',m'}^*. \tag{62}$$

One advantage of Kalnajs' method is that the projection can be carried out in any set of coordinates. Since canonical transformations have a unity Jacobian, I may directly replace the impulse-space coordinates with the action-angle coordinates derived above.

Inserting the Poisson equation (58) yields

$$\begin{aligned} 4\pi^2 K_{m'}(\alpha') \Phi_{\alpha',m'}^{\text{response}} = \int_{-\infty}^{\infty} d\alpha \int_0^{\infty} dL_z \int_0^{\infty} dJ \int_0^{2\pi} dw_1 \\ \sum_{m=0}^{\infty} \int_0^{2\pi} dw_2 \Phi_{\alpha,m}^{\text{imposed}} (\mathcal{L}\varphi_{\alpha,m}) \varphi_{\alpha',m'}^* \end{aligned}. \tag{63}$$

I have silently swapped the order of integrations into something convenient for me. The integration limits on $L_z$ would be $-\infty$ and $\infty$ in the general case. Here, however, I demanded that the distribution function was identically zero for $L_z < 0$, hence the smaller integration interval.

I am looking for self-consistent solutions, and thus the stability problem is solved when $\Phi^{\text{imposed}} = \Phi^{\text{response}}$. Before looking for such solutions, I first carry out the integrals over the action and angle coordinates. The structure of the integrand in (63) invites a separation of this task into the integration of a part independent of $w_1'$ and one containing the integral over the auxiliary angle $w_1'$. After solving (63) for $\Phi_{\alpha',m'}$, these integrands take the forms

$$\begin{aligned} I_1 =& \Phi_{\alpha,m} \frac{F L_z^{\mathrm{i}(\alpha-\alpha')-2}}{4\pi^2\sigma^2 K_{m'}(\alpha')} \\ & \exp\left( \mathrm{i}\sqrt{\frac{\sqrt{2}J}{L_z}} \big( (\alpha-\alpha')\cos(w_1) - \sqrt{2}(m-m')\sin(w_1) \big) + \mathrm{i}(m-m')w_2 - \frac{\sqrt{2}J}{\sigma^2 L_z} \right), \end{aligned} \tag{64}$$

and

$$I_2 = \mathrm{i}\Phi_{\alpha,m}\frac{\sqrt{2}FL_z^{\mathrm{i}(\alpha-\alpha')-2}\left(m\sigma^2+\sqrt{2}\eta\right)}{8\pi^2\sigma^2K_{m'}(\alpha')(\mathrm{e}^{-2\pi\mathrm{i}\eta}-1)}\exp\Bigg(\mathrm{i}(m-m')w_2-\mathrm{i}\eta w_1'-\frac{\sqrt{2}J}{\sigma^2L_z}$$
$$+\mathrm{i}\sqrt{\frac{\sqrt{2}J}{L_z}}\Big(\alpha\cos(w_1'+w_1)-\alpha'\cos(w_1)-\sqrt{2}\,m\sin(w_1'+w_1)+\sqrt{2}\,m'\sin(w_1)\Big)\Bigg), \tag{65}$$

respectively. Here, I have written the complete right-hand sides, not indicating for the four (or, in the case of $I_2$, five) quadratures and the one summation required to compute the matrix elements of the kernel. I will use this convention throughout the following and call the right-hand sides emerging after the integration over the variable $x$ as $I_{1,2}^{(x)}$, not writing down the remaining integral and summation signs.

Again adopting a sloppy stance towards exchanging integration orders, the complete integral equation now is

$$\Phi_{\alpha',m'} = \int_{-\infty}^{\infty}d\alpha\sum_{m=0}^{\infty}\int_0^{\infty}dL_z\int_0^{2\pi}dw_1'\int_0^{\infty}dJ\int_0^{2\pi}dw_1\int_0^{2\pi}dw_2\,(I_1+I_2). \tag{66}$$

# 3. Simplifying the Kernel

In this section I will carry out the quadratures in (66). This will result in an integral-free expression for the kernel in elementary and special functions. One series introduced in this process will not be representable in well-known functions. Concluding this section, I will discuss some general features of the kernel.

## 3.1. Integration Over the Azimuthal Angle

The first integration, $\int_0^{2\pi} dw_2$, is straightforward. In both $I_1$ and $I_2$, the only term dependent on $w_2$ is

$$\int_0^{2\pi} \mathrm{e}^{\mathrm{i}(m-m')w_2}\, dw_2 = 2\pi\delta_{m,m'}. \tag{67}$$

The Kronecker delta decouples modes of different $m$, which was to be expected in a linear analysis. I will, however, postpone the summation over $m$ and thus its elimination until all integrations have been carried out, since keeping $m$ does not overly complicate the computations and might give some hints what should happen in the mildly nonlinear regime when modes of different $m$ start to couple.

## 3.2. Integration Over the Epicyclic Angle

The next step is the integration over $w_1$. The integrals to be computed are

$$\int_0^{2\pi} \exp\left(\mathrm{i}\sqrt{\sqrt{2}J/L_z}\left((\alpha-\alpha')\cos(w_1) - \sqrt{2}\,(m-m')\sin(w_1)\right)\right) dw_1 \tag{68}$$

for $I_1$ and

$$\begin{aligned}\int_0^{2\pi} \exp\Bigg(\mathrm{i}\sqrt{\sqrt{2}J/L_z}\Bigg(&\left(\alpha\cos(w_1') - \sqrt{2}\,m\sin(w_1') - \alpha'\right)\cos(w_1)\\ &-\left(\alpha\sin(w_1') + \sqrt{2}\,m\cos(w_1') - \sqrt{2}\,m'\right)\sin(w_1)\Bigg)\Bigg)\, dw_1\end{aligned} \tag{68}$$

for $I_2$.

This type of integral can be carried out by noting that the integrands can be rewritten

$$\begin{aligned}\mathrm{e}^{A\sin(w_1)+B\cos(w_1)} &= \exp\left(\sqrt{A^2+B^2}\left(\frac{A}{\sqrt{A^2+B^2}}\sin(w_1)+\frac{B}{\sqrt{A^2+B^2}}\cos(w_1)\right)\right)\\ &= \exp\Big(\sqrt{A^2+B^2}\big(\cos(v)\sin(w_1)+\sin(v)\cos(w_1)\big)\Big)\\ &= \exp\Big(\sqrt{A^2+B^2}\sin(w_1+v)\Big),\end{aligned} \tag{70}$$

where $A$ and $B$ are arbitrary coefficients and $v$ has to be chosen such that $\sin(v) = B/\sqrt{A^2+B^2}$ and $\cos(v) = A/\sqrt{A^2+B^2}$. Since

$$\begin{aligned}\int_0^{2\pi}\mathrm{e}^{\sin(w_1+v)}\,dw_1 &= \int_v^{2\pi}\mathrm{e}^{\sin(w_1)}\,dw_1+\int_{2\pi}^{2\pi+v}\mathrm{e}^{\sin(w_1)}\,dw_1\\ &= \int_v^{2\pi}\mathrm{e}^{\sin(w_1)}\,dw_1+\int_0^{v}\mathrm{e}^{\sin(w_1)}\,dw_1\\ &= \int_0^{2\pi}\mathrm{e}^{\sin(w_1)}\,dw_1,\end{aligned} \tag{71}$$

one may drop the $v$ from the argument of the sine in (70). By expansion into Bessel functions and using the fact that $\int_0^{2\pi}\sin(\sin(w_1))\,dw_1$ vanishes for symmetry reasons one finds

$$\int_0^{2\pi}\mathrm{e}^{\mathrm{i}A\sin(w_1)}\,dw_1 = 2\pi\mathrm{J}_0(A). \tag{72}$$

Actually, this result is readily found in any integral table; however, since I am going to apply the very same technique for more complex terms later, a broader presentation in this simple case seemed justified.

An application of (70), (71), and (72) to (68) and (69) yields

$$I_1^{(w_1)} = \Phi_{\alpha,m}\frac{F\delta_{m,m'}L_z^{\mathrm{i}(\alpha-\alpha')-2}}{\sigma^2 K_{m'}(\alpha')}\mathrm{J}_0\left(\sqrt{\frac{\sqrt{2}J}{L_z}}\sqrt{(\alpha-\alpha')^2+2(m-m')^2}\right)\exp\left(-\frac{\sqrt{2}J}{\sigma^2 L_z}\right) \tag{73}$$

and

$$\begin{aligned}I_2^{(w_1)} =& \mathrm{i}\Phi_{\alpha,m}\frac{F\delta_{m,m'}L_z^{\mathrm{i}(\alpha-\alpha')-2}\big(\omega L_z - m(1-\sigma^2)\big)}{\sqrt{2}\,\sigma^2 K_{m'}(\alpha')}\frac{\mathrm{e}^{\mathrm{i}w_1'(\omega L_z-m)/\sqrt{2}}}{(\mathrm{e}^{-\sqrt{2}\pi\mathrm{i}(\omega L_z-m)}-1)}\\ &\exp\left(-\frac{\sqrt{2}J}{\sigma^2 L_z}\right)\mathrm{J}_0\Bigg(\sqrt{\frac{\sqrt{2}J}{L_z}}\Big(\alpha^2+\alpha'^2+2(m^2+m'^2)+2\sqrt{2}\sin(w_1')(m\alpha'-m'\alpha)-\\ &2\cos(w_1')(\alpha\alpha'+2mm')\Big)^{1/2}\Bigg).\end{aligned} \tag{74}$$

## 3.3. Integration Over the Second Integral

I next perform the integration over $J$. The terms in question are

$$\int_0^\infty \mathrm{J}_0\Big(\sqrt{\sqrt{2}J/L_z}\sqrt{(\alpha-\alpha')^2+2(m-m')^2}\Big)\exp\left(-\frac{\sqrt{2}J}{\sigma^2 L_z}\right)\,dJ \tag{75}$$

for $I_1$ and

$$\begin{aligned}\int_0^\infty \mathrm{J}_0\Bigg(\sqrt{\sqrt{2}J/L_z}\Big(\alpha^2+\alpha'^2+2(m^2+m'^2)+2\sqrt{2}\sin(w_1')(m\alpha'-m'\alpha)\\ -2\cos(w_1)(\alpha\alpha'+2mm')\Big)^{1/2}\Bigg)\exp\left(-\frac{\sqrt{2}J}{\sigma^2 L_z}\right)\,dJ.\end{aligned} \tag{76}$$

for $I_2$.

Again, the two integrals are structurally equivalent and can be computed using

$$\int_0^\infty x^{\nu+1}\mathrm{e}^{-\alpha x^2}\mathrm{J}_\nu(\beta x)\,dx = \beta^\nu\frac{\mathrm{e}^{-\beta^2/(4\alpha)}}{(2\alpha)^{\nu+1}} \tag{77}$$

(Gradshteyn and Ryzhik 1979, 6.631.4) by letting $x=\sqrt{J}$ and $\nu=0$. The results are

$$I_1^{(J)} = \Phi_{\alpha,m}\frac{F\delta_{m,m'}L_z^{\mathrm{i}(\alpha-\alpha')-1}}{\sqrt{2}K_{m'}(\alpha')}\exp\left(-\frac{\sigma^2}{4}\Big((\alpha-\alpha')^2+2(m-m')^2\Big)\right) \tag{78}$$

and

$$\begin{aligned}I_2^{(J)} =&\mathrm{i}\Phi_{\alpha,m}\frac{F\delta_{m,m'}L_z^{\mathrm{i}(\alpha-\alpha')-1}\Big(\omega L_z - m(1-\sigma^2)\Big)}{2K_m(\alpha)\,\mathrm{e}^{(\sigma^2/4\left((\alpha^2+\alpha'^2)+2(m^2+m'^2)\right)}}\frac{\mathrm{e}^{-\mathrm{i}w_1'(\omega L_z-m)/\sqrt{2}}}{\mathrm{e}^{-\sqrt{2}\pi\mathrm{i}(\omega L_z-m)}-1}\\ &\exp\left(-\frac{\sigma^2}{2}\Big(\sqrt{2}\sin(w_1')(m\alpha'-m'\alpha)-\cos(w_1')(\alpha\alpha'+2mm')\Big)\right).\end{aligned} \tag{79}$$

## 3.4. Integration Over the Auxiliary Angle

The integration over $w_1'$ is only necessary in $I_2$. The term in question is

$$\int_0^{2\pi} \exp\!\left(\frac{\sigma^2}{2}\big(\alpha\alpha'+2mm'\big)\cos(w_1')+\frac{\sigma^2}{\sqrt{2}}\big(m\alpha'-m'\alpha\big)\sin(w_1')+\mathrm{i}\,w_1'(\omega L_z-m)/\sqrt{2}\right) dw_1'. \quad (80)$$

This integrand resembles the one treated in the integration over $w_1$, where the case is more complicated here because of the presence of a linear term in the exponent that unfortunately breaks the periodicity of the integrand that could be exploited in (71). Applying the method outlined above, the integral attains the structure

$$\int_0^{2\pi} \cos(\tau w_1')\mathrm{e}^{\nu\cos(v-w_1')} + \mathrm{i}\sin(\tau w_1')\mathrm{e}^{\nu\cos(v-w_1')}\,dw_1'. \quad (81)$$

Here,

$$\begin{aligned} \tau &= -(\omega L_z - m)/\sqrt{2} \\ v &= \arctan\Big(\sqrt{2}(\alpha m' - \alpha' m), \alpha\alpha' + 2\,mm'\Big) \\ \nu &= -\frac{\sigma^2}{2}\sqrt{(\alpha^2+2m^2)(\alpha'^2+2m'^2)}. \end{aligned} \quad (82)$$

One has to use the two-argument arctan in the definition of $v$ since the parameters can put $v$ in any quadrant. To get rid of the arctan, I set

$$\Lambda = \frac{\alpha\alpha' + 2mm' + \sqrt{2}\,\mathrm{i}\,(\alpha m' - \alpha' m)}{\sqrt{(\alpha^2+2m^2)(\alpha'^2+2m'^2)},} \quad (83)$$

after which I can write $v = -\ln(\Lambda)$. The expansion of $\exp\big(\nu\cos(v-w_1')\big)$ into Bessel functions is (Abramowitz and Stegun 1968, 9.6.34)

$$\mathrm{e}^{\nu\cos(v-w_1')} = \mathrm{I}_0(\nu) + 2\sum_{k=1}^{\infty}\mathrm{I}_k(\nu)\cos\big(k(v-w_1')\big). \quad (84)$$

After expanding the cosine, one can again exchange the order of integration and summation, and using the usual symmetry arguments one finds

$$\begin{aligned} &\int_0^{2\pi} \cos(\tau w_1')\mathrm{e}^{\nu\cos(v-w_1')} + \mathrm{i}\sin(\tau w_1')\mathrm{e}^{\nu\cos(v-w_1')}\,dw_1' = \\ &\qquad = -\,\mathrm{i}\,\mathrm{I}_0(\nu)\frac{\mathrm{e}^{2\pi\mathrm{i}\,\tau}-1}{\tau} + 2\sum_{k=1}^{\infty}\mathrm{I}_k(\nu)\frac{\mathrm{e}^{2\pi\mathrm{i}\,\tau}-1}{\tau^2-k^2}\Big(k\sin(v)+\mathrm{i}\,\tau\cos(v)\Big). \end{aligned} \quad (85)$$

Using this, the integral over $w_1'$ computes to

$$I_2^{(w_1')} = -\Phi_{\alpha,m}\frac{F\delta_{m,m'}L_z^{\mathrm{i}(\alpha-\alpha')-1}\Big(\omega L_z - m(1-\sigma^2)\Big)}{\sqrt{2}K_{m'}(\alpha')\,\mathrm{e}^{(\sigma^2/4)\left((\alpha^2+\alpha'^2)+2(m^2+m'^2)\right)}}$$
$$\left(\mathrm{I}_0\left(\tfrac{\sigma^2}{2}\sqrt{(\alpha^2+2m^2)(\alpha'^2+2m'^2)}\right)\frac{1}{\omega L_z - m} + \right. \tag{86}$$
$$\left.\sum_{k=1}^{\infty}\mathrm{I}_k\left(\tfrac{\sigma^2}{2}\sqrt{(\alpha^2+2m^2)(\alpha'^2+2m'^2)}\right)\left(\frac{\Lambda^k}{\omega L_z - m + \sqrt{2}k} + \frac{\Lambda^{-k}}{\omega L_z - m - \sqrt{k}}\right)\right).$$

## 3.5. Integration Over the Angular Momentum

In addition to splitting the integration into $I_1^{(J)}$ and $I_2^{(w_1')}$, it is advantageous to carry out the $L_z$-quadrature of $I_2^{(w_1')}$ separate for the part without and the part with the sum.

### 3.5.1. Integration of $I_1^{(J)}$

For the integration over $L_z$ in $I_1^{(J)}$ one only has to compute $\int_0^\infty L_z^{\mathrm{i}(\alpha-\alpha')-1}\,dL_z$, which after the substitution $u = \ln(L_z)$ is

$$\int_{-\infty}^{\infty}\mathrm{e}^{I(\alpha-\alpha')u}\,du = 2\pi\delta(\alpha-\alpha'). \tag{87}$$

Thus,

$$I_1^{(L_z)} = \sqrt{2}\pi\Phi(\alpha,m)\frac{F\delta_{m,m'}\delta(\alpha-\alpha')}{K_{m'}(\alpha')}\exp\left(-\frac{\sigma^2}{4}\Big((\alpha-\alpha')^2 + 2(m-m')^2\Big)\right) \tag{88}$$

### 3.5.2. Integration of $I_2$, Part Without Sum

For the term not containing the sum in $I_2^{(w_1')}$, one has to compute

$$\int_0^\infty L_z^{\mathrm{i}\gamma-1}\frac{\omega L_z - m(1-\sigma^2)}{\omega L_z - m}\,dL_z, \tag{89}$$

where for brevity $\gamma = \alpha - \alpha'$. After a substitution $u = \ln(\omega L_z/m)$ this becomes

$$\left(\frac{m}{\omega}\right)^{\mathrm{i}\gamma}\int_{-\infty}^{\infty}\frac{\mathrm{e}^{\mathrm{i}\gamma u}}{\mathrm{e}^u - 1}\Big(\mathrm{e}^u - (1-\sigma^2)\Big)\,du \tag{90}$$

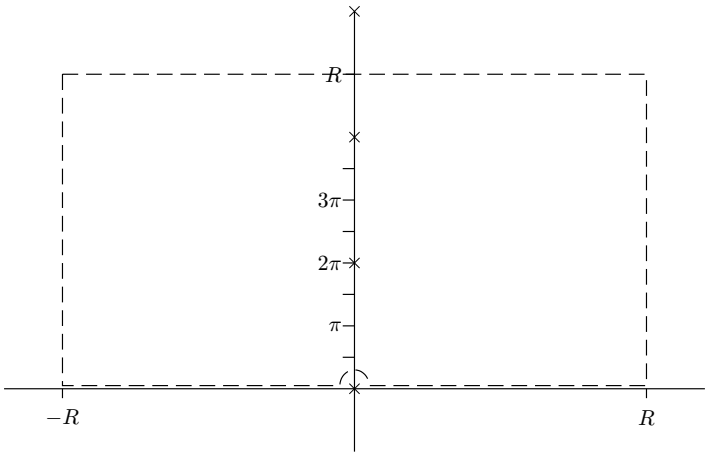


*Fig. 2: Integration path for the $L_z$-Integration over $I_1^{(J)}$. The crosses mark the poles relevant for the integration.*

when $\omega > 0$. Although this expression is not overly complex, it pays off to first analyse the simpler problem of computing

$$\int_{-\infty}^{\infty} \frac{\mathrm{e}^{(\mathrm{i}\gamma+\lambda)u}}{\mathrm{e}^u - 1}\, du \tag{91}$$

for $\lambda \in \{0, 1\}$, since (90) nicely decomposes into integrals of this type and later integrals, though more complex, can be evaluated along the same lines. I will perform this integration using the residue theorem.

The first thing to note about (91) is that the integral does not exist in a conventional sense, since the integrand does not vanish as $u \to \pm\infty$. However, (91) does exist as a distribution limit, i.e., it is meaningful to compute an integral over, say, $\gamma$ of a suitable function multiplied with (91). The distribution limit is well known from integrals like $\int_{-\infty}^{\infty} \exp(\mathrm{i}\omega t)\, dt$ frequently occurring in Fourier theory. For the moment, I will pretend that the integrand vanishes faster than $1/u$ for $u \to \infty$ and return to the question how to handle the tails later.

The second complication in the computation of (91) is that the integrand diverges at $u = 0$. The most straightforward way to handle this would be to take a Cauchy principal value, which, however, leads to nonphysical results. This was noted in a plasma-physical context by Landau (1946), who, in the same publication, also gave the correct prescription for handling this sort of situation. Landau's idea was that by requiring that in the very distant past the system was in equilibrium, one may conclude that any mode must have started out as a growing mode. If it has evolved continuously, any integration contours must also have been deformed continuously during the evolution of the system that has lead to the quasi-steady state characterised by a purely real $\omega$. Consequently, a real $\omega$ has to be seen as the limit of $\omega + \mathrm{i}\epsilon$ (for my sign convention in (24)) as $\epsilon \to 0$ and $\epsilon > 0$. This prescription is generally known as Landau's rule. A welcome side-effect of applying it is that the expressions to be derived shortly will also be valid for growing modes (complex $\omega$ with positive imaginary part).

Giving $\omega$ a minute positive imaginary part results in a shift of the poles of the integrand in (101) into the lower half plane, $L_z = m(\omega - \mathrm{i}\epsilon)/(\omega^2 + \epsilon^2)$. Equivalently, the substitution leading to (90) would put the integration path into the upper half plane if $\omega$ has a positive imaginary part. Thus, the correct application of Landau's rule here is to integrate around

the pole on the real axis into the upper half-plane. The resulting integration path for $\gamma > 0$ is shown in Fig. 2.

A third problem complicates the use of the residue theorem in the present case. On letting $R$ in Fig. 2 to infinity, the path should be continuously deformable. This is not the case here, where a pole is in the way every $2\pi\mathrm{i}$. However, the poles of the integrand get very sharp indeed, so that ignoring just "a few" points the contour sweeps over during the deformation, one can continuously deform the contour and still gets a rapid decay of the modulus of the integrand on the upper line of the path in Fig. 2. A bit more precisely put, one can show that for any $\epsilon > 0$ there is an $R_0$ such that the integral $\int_{-\infty+\mathrm{i}R}^{\infty+\mathrm{i}R}$ is smaller than $\epsilon$ for all $R > R_0$ and $|R - 2\pi\mathrm{i}j| > \epsilon$.

Another way to view this is to notice that the residues (93) rapidly decrease with growing $j$. Thus, even when one fixes the upper horizontal line in the integration path Fig. 2 and only lets the vertical parts move towards $\pm\infty$, the error one makes is quite small when the upper horizontal line is put far enough into the complex plane avoiding the poles, since both (1) the contribution from the contour integral along the upper horizontal line, and (2) the contribution from the residues above the line will be very small. Numerical checks show that this somewhat sloppy treatment delivers correct results. In these numerical checks, the periodic tails have to be taken care of. This can be done by damping the integrand with a Gaussian of width $a$ and then letting $a$ grow until the results converge. Usually, however, it works better to numerically compute a few (30, say) definite integrals with boundaries equally distributed over a period of the tail, where the boundaries should be far enough from zero to ensure they are in the region where the integrand is purely periodic for all practical purposes. The mean value of those definite integrals then is an approximation for the integral without the contribution form the periodic tail.

The denominator in (91) has poles of order 1 at

$$u_j^{(1)} = 2\pi\mathrm{i}\, j. \tag{92}$$

The residues at these points are easily computed using $\mathrm{res}(f, z) = \lim_{u\to z} f(u)(u - z)$. An application of de l'Hospial's rule yields

$$\mathrm{res}\left(\frac{\mathrm{e}^{(\mathrm{i}\gamma+\lambda)u}}{\mathrm{e}^u - 1}, u_j^{(1)}\right) = \mathrm{e}^{-2\pi\mathrm{i}j(\mathrm{i}\gamma+\lambda-1)}. \tag{93}$$

When $\gamma > 0$, the residues from (93) have to be summed up for $j = 1 \cdots \infty$ (starting at 1 ensures that Landau's rule is followed). Because the terms with $\lambda$ in the series evaluate to 1, this leads to a single geometric series,

$$\sum_{j=1}^{\infty} \mathrm{e}^{-2\pi\gamma j} = -1 + \sum_{j=0}^{\infty} \mathrm{e}^{-2\pi\gamma j} = \frac{1}{1 - \mathrm{e}^{-2\pi\gamma}} - 1 = \frac{1}{\mathrm{e}^{2\pi\gamma} - 1} \tag{94}$$

and one finds

$$\int_{-\infty}^{\infty} \frac{\mathrm{e}^{(\mathrm{i}\gamma+\lambda)u}}{\mathrm{e}^u - 1}\, du = \frac{2\pi\mathrm{i}}{\mathrm{e}^{2\pi\gamma} - 1} - \text{border terms}. \tag{95}$$

The same result is found for $\gamma < 0$, where this time the summation limits are $j = 0 \cdots -\infty$:

$$\sum_{j=0}^{-\infty} \mathrm{e}^{-2\pi\gamma j} = \sum_{j=0}^{\infty} \mathrm{e}^{2\pi\gamma j} = \frac{1}{1-\mathrm{e}^{2\pi\gamma}}. \tag{96}$$

The "border terms" in (95) arise from the harmonic tails of the integrand in (91), and they enter negatively since they contribute to the contour integral off the real axis. The harmonic tails of the integrand are

$$\frac{\mathrm{e}^{(\mathrm{i}\gamma+\lambda)u}}{\mathrm{e}^u - 1} \sim \begin{cases} -\mathrm{e}^{\mathrm{i}\gamma u}; & \lambda = 0 \text{ and } u \to -\infty \\ \mathrm{e}^{\mathrm{i}\gamma u}; & \lambda = 1 \text{ and } u \to \infty. \end{cases} \tag{97}$$

In the other two cases the integrand falls off exponentially.

Thus, the vertical parts of the integration contour in Fig. 2 contribute

$$\begin{aligned} \lim_{x\to-\infty} \int_{x+\mathrm{i}\infty}^{x} -\mathrm{e}^{\mathrm{i}\gamma u}\, du &= -\lim_{x\to\infty} \frac{\mathrm{i}\mathrm{e}^{\mathrm{i}\gamma x}}{\gamma} \quad \text{at } -\infty, \text{ and} \\ \lim_{x\to\infty} \int_{x}^{x+\mathrm{i}\infty} \mathrm{i}\mathrm{e}^{\mathrm{i}\gamma u}\, du &= \lim_{x\to\infty} \frac{\mathrm{i}\mathrm{e}^{\mathrm{i}\gamma x}}{\gamma} \quad \text{at } +\infty, \end{aligned} \tag{98}$$

where I have substituted $u = x + \mathrm{i}y$.

As briefly mentioned above, the limits in (98) have to be taken in the sense of a distribution with the following integration over $\alpha$ in mind. In the distribution limit,

$$\begin{aligned} \lim_{x\to-\infty} \frac{\mathrm{e}^{\mathrm{i}\gamma x}}{\gamma} &= -\mathrm{i}\pi\delta(\gamma) \\ \lim_{x\to\infty} \frac{\mathrm{e}^{\mathrm{i}\gamma x}}{\gamma} &= \mathrm{i}\pi\delta(\gamma). \end{aligned} \tag{99}$$

Expressions of this type have to be read as a shorthand for

$$\lim_{x\to\infty} \int_{-\infty}^{\infty} f(\gamma) \frac{\mathrm{e}^{\mathrm{i}\gamma x}}{\gamma}\, d\gamma = -\mathrm{i}\pi f(0), \tag{100}$$

say, as is customary in distribution theory. For a concise and not too technical treatment of distribution theory, see Wladimirow (1972).

Inserting this result and (95) into (90) finally yields

$$\int_0^{\infty} L_z^{\mathrm{i}\gamma-1} \frac{\omega L_z - m(1-\sigma^2)}{\omega L_z - m}\, dL_z = \pi \left(\frac{m}{\omega}\right)^{\mathrm{i}\gamma} \left(\frac{2\mathrm{i}\sigma^2}{\mathrm{e}^{2\pi\gamma}-1} + \delta(\gamma)(2-\sigma^2)\right). \tag{101}$$

### 3.5.3. Integration of $I_2$, Part With Sum

In the part of $I_2^{(w_1')}$ with the sum, one has to compute

$$\int_0^\infty L_z^{\mathrm{i}\gamma-1}\frac{\omega L_z - m(1-\sigma^2)}{\sqrt{2}}\left(\frac{\Lambda^{2k}}{\omega L_z - m + \sqrt{2}k} + \frac{1}{\omega L_z - m - \sqrt{2}k}\right) dL_z \tag{102}$$

Again substituting $u = \ln(\omega L_z/m)$, this takes the form

$$\left(\frac{m}{\omega}\right)^{\mathrm{i}\gamma}\int_{-\infty}^\infty \mathrm{e}^{\mathrm{i}\gamma u}\frac{\mathrm{e}^u + \sigma^2 - 1}{\sqrt{2}\left(2\xi^2 - (1-\mathrm{e}^u)^2\right)}\left(\Lambda^{2k}(1+\sqrt{2}\,\xi - \mathrm{e}^u) + 1 - \sqrt{2}\,\xi - \mathrm{e}^u\right) du, \tag{103}$$

where $\xi = k/m$. As above, I will first tackle the technically easier but conceptually equivalent problem of evaluating

$$\int_{-\infty}^\infty \frac{\mathrm{e}^{(\mathrm{i}\gamma+\lambda+1)u}}{2\left(2\xi^2 - (1-\mathrm{e}^u)^2\right)}\, du \tag{104}$$

for $\lambda \in \{-1, 0, 1\}$.

The integral (104) shares all the problems that were to be solved in the previous paragraph: it converges only in the sense of a distribution limit, it has a pole on the integration interval, and the integration contour is not continuously deformable to infinity. Luckily, the case is rather analogous, so the basic arguments and techniques remain the same.

I start out with an analysis of the poles, i.e., the zeroes of the denominator of the integrand of (104). These lie at

$$u_j^{(2)} = \ln(1+\sqrt{2}\xi) + 2\pi\mathrm{i}\,j \qquad \text{and} \qquad u_j^{(3)} = \ln(1-\sqrt{2}\xi) + 2\pi\mathrm{i}\,j. \tag{105}$$

Of course, when $\xi > 1/\sqrt{2}$, the poles at $u_j^{(3)}$ are no longer situated on the real axis but are at $\tilde{u}_j^{(3)} = \ln(1-\sqrt{2}\xi) + (2j+1)\pi\mathrm{i}$. I will handle this in a moment. The case $\xi = 1/\sqrt{2}$ cannot occur since $\xi$ by definition is a rational number. Note, however, that the $\sqrt{2}$ originates from the ratio of epicyclic and azimuthal frequency of the orbit. Had I kept the more exact expressions (9), (10), and (11), there could be values of $\zeta$ for which that ratio is rational which in turn could displace the poles at $u_j^{(3)}$ to $-\infty$ for some $k$ and $m$. In Read's formalism, this situation does occur; at least in her case, it did not require significant changes to the procedures to solve the integral equation. Quite possibly simply ignoring the problem of poles on the integration contour would be sufficient in a higher-order analysis with my formalism as well.

The residues at the poles $u_j^{(2)}$ and $u_j^{(3)}$ are again of order 1 and can be computed following the prescription given for $u_j^{(1)}$. The results are

$$\begin{aligned}
\operatorname{res}\left(\frac{\mathrm{e}^{(\mathrm{i}\gamma+\lambda+1)u}}{2\left(2\xi^2-(e^u-1)^2\right)}; u_j^{(2)}\right) &= -\mathrm{e}^{\ln(1+\sqrt{2}\xi)(\mathrm{i}\gamma+\lambda)}\frac{\mathrm{e}^{2\pi\mathrm{i}j(\mathrm{i}\gamma+\lambda)}}{4\sqrt{2}\xi} \\
\operatorname{res}\left(\frac{\mathrm{e}^{(\mathrm{i}\gamma+\lambda+1)u}}{2\left(2\xi^2-(e^u-1)^2\right)}; u_j^{(3)}\right) &= \mathrm{e}^{\ln(1-\sqrt{2}\xi)(\mathrm{i}\gamma+\lambda)}\frac{\mathrm{e}^{2\pi\mathrm{i}j(\mathrm{i}\gamma+\lambda)}}{4\sqrt{2}\xi}
\end{aligned} \tag{106}$$

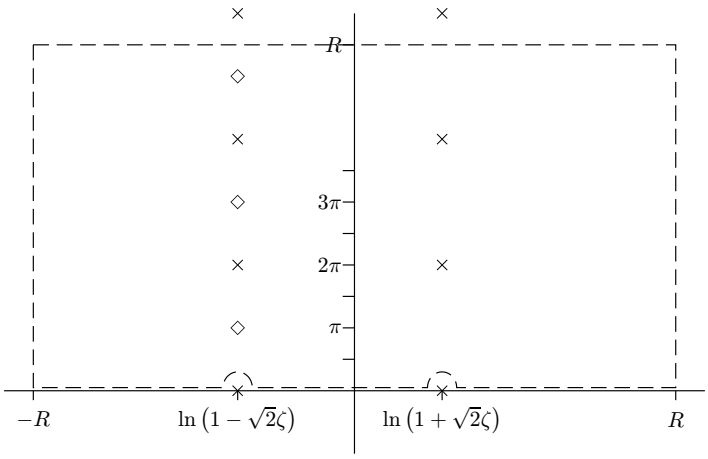


*Fig. 3: Integration path for the $L_z$-Integration over $I_2^{(w_1')}$. The crosses mark the poles relevant for the integration. The diamonds indicate where the poles lie in the case $\xi > 1/\sqrt{2}$. While it does not really matter, one could let the integration contour follow the real axis at $\ln(1-\sqrt{2}\xi)$ in this case.*

Both of those residues have to be summed up for $j = 1 \cdots \infty$ when $\gamma > 0$. This is straightforward and yields

$$\int_{-\infty}^{\infty} \frac{\mathrm{e}^{(\mathrm{i}\gamma+\lambda+1)u}}{2\big(2\xi^2-(e^u-1)^2\big)}\,du = \mathrm{i}\pi\frac{\mathrm{e}^{\ln(1-\sqrt{2}\xi)(\mathrm{i}\gamma+\lambda)} - \mathrm{e}^{\ln(1+\sqrt{2}\xi)(\mathrm{i}\gamma+\lambda)}}{2\sqrt{2}\xi(\mathrm{e}^{2\pi\gamma}-1)} + \text{border terms.} \quad (107)$$

Now, in the case $\xi > 1/\sqrt{2}$ the poles $u_j^{(3)}$ are replaced by poles at $\tilde{u}_j^{(3)}$. Here, for $\gamma > 0$ all residues at poles in the (open) upper half plane have to be added up. To carry over the results from above, one can set the branch cut of the logarithm in the definition of $u_j^{(3)}$ in (105) such that they "shift down" by $-\mathrm{i}\pi$ when going from $\xi < 1/\sqrt{2}$ to $\xi > 1/\sqrt{2}$. To do this, one sets $\ln(-1) = -\mathrm{i}\pi$, which, when $\ln(1) = 0$ is to be preserved, suggests a branch cut at the positive imaginary axis ($\frac{\pi}{2} \geq \ln(\mathrm{e}^{\mathrm{i}\varphi}) > -\frac{3\pi\mathrm{i}}{2}$). With this choice, (107) remains valid for all rational and positive $\xi$.

The border terms this time arise from the $\lambda = -1$ contribution at $u = -\infty$ and the $\lambda = 1$ contribution at $u = \infty$. The $\lambda = 0$ contribution is well behaved at both $u = \pm\infty$. An evaluation of the contributions following the path lined out in the treatment of $I_1$

$$\text{border terms} = \begin{cases} \dfrac{\pi\delta(\gamma)}{4\xi^2-2} & \lambda = -1 \\ \pi\delta(\gamma) & \lambda = +1 \end{cases} \quad (108)$$

Thus the contribution from the part with the series of $I_2$ is

$$\begin{aligned} &\int_0^{\infty} L_z^{\mathrm{i}\gamma-1}\Big(2m+\sqrt{2}\sigma^2(\omega L_z-\sqrt{2}m)\Big)\left(\frac{\Lambda^{2k}}{\omega L_z-\sqrt{2}m+k}+\frac{1}{\omega L_z-\sqrt{2}m-k}\right) = \\ &\qquad -\mathrm{i}\sqrt{2}\,\pi\frac{\omega^{-\mathrm{i}\gamma}}{\mathrm{e}^{2\pi\gamma}-1}\Big((\sqrt{2}k-m\sigma^2)\Lambda^{2k}\mathrm{e}^{(\mathrm{i}\gamma-1)\ln(m-\sqrt{2}k)} \\ &\qquad\qquad -(\sqrt{2}k+m\sigma^2)\mathrm{e}^{(\mathrm{i}\gamma-1)\ln(m+\sqrt{2}k)}\Big) \\ &+\frac{\pi\delta(\gamma)}{\sqrt{2}}\left(\frac{m}{\omega}\right)^{\mathrm{i}\gamma}\left(\frac{2\sqrt{2}\,k-m(1+\sigma^2)}{\sqrt{2}k-m}\Lambda^{2k}+\frac{2\sqrt{2}\,k+m(1+\sigma^2)}{\sqrt{2}k+m}\right). \end{aligned} \quad (109)$$

Since the $I_2^{(L_z)}$ is a rather lengthy expression and furthermore naturally decomposes into a part with and without the Dirac delta, I postpone assembling it until I write down the kernel in chapter 3.6.

### 3.5.4. The case $\omega = 0$

The reasoning in the previous three paragraphs breaks down when $\omega = 0$. Indeed, as Read (1997) has already noted, the $\omega = 0$ case cannot be obtained by taking the limit of the $\omega \neq 0$ expressions, mainly, of course, because this limit does not exist—$\exp\bigl(\mathrm{i}\gamma \ln(\omega)\bigr)$ has an essential singularity at $\omega = 0$ when $\gamma \notin \mathbb{Q}$, so according to Picard's theorem the image of an arbitrarily small neighbourhood of zero under the kernel as an analytic function of $\omega$ is at least dense in the complex plane.

To correctly evaluate the kernel when $\omega = 0$, one therefore has to go gack to an expression before the $\omega^{-\mathrm{i}\gamma}$ emerges and take the limit there; in the present problem the most convient choice for these expressions are $I_1^{(J)}$ and $I_2^{(w_1')}$. While $I_1^{(J)}$ does not depend on $\omega$, $I_2^{(w_1')}$ does. Setting $\omega = 0$ there leaves $L_z^{\mathrm{i}(\alpha-\beta)-1}$ as the integrand, and thus one has

$$I_2{}^{(L_z,\omega=0)} = -\sqrt{2}\pi\Phi_{\alpha,m}\delta(\alpha-\alpha')\frac{F\delta_{m,m'}m(1-\sigma^2)}{K_{m'}(\alpha')\,\mathrm{e}^{(\sigma^2/4)\left((\alpha^2+\alpha'^2)+2(m^2+m'^2)\right)}}$$
$$\left(\frac{\mathrm{I}_0\left(\frac{\sigma^2}{2}\sqrt{(\alpha^2+2m^2)(\alpha'^2+2m'^2)}\right)}{m}+\sum_{k=1}^{\infty}\mathrm{I}_k\left(\frac{\sigma^2}{2}\sqrt{(\alpha^2+2m^2)(\alpha'^2+2m'^2)}\right)\left(\frac{\Lambda^k}{m-\sqrt{2}k}+\frac{\Lambda^{-k}}{m+\sqrt{k}}\right)\right). \tag{110}$$

## 3.6. The Kernel of the Integral Equation

After having carried out the quadratures over the actions and angles in (64) and (65), I can now assemble the integral equation in the form I will use to examine it.

The first observation to make is that there are contributions proportional to $\delta(\alpha-\alpha')$ in $I_1^{(L_z)}$ as well as in $I_2^{(L_z)}$ coming from both the part without the series (101) and the part with the series (109). One can immediately integrate these contributions over $\alpha$, and thus the integral equation resulting will have the form

$$\Phi_{\alpha',m'} = \mathcal{F}(\alpha')\Phi_{\alpha',m'} + \int_{-\infty}^{\infty}\mathcal{K}(\alpha,\alpha')\Phi_{\alpha,m'}\,d\alpha, \tag{111}$$

where the summand with $\mathcal{F}$ originates from the terms proportional to $\delta(\alpha-\alpha')$.

If $\mathcal{K}$ was a compact operator, this would be a homogenous Fredholm equation of the second kind. According to the Fredholm Alternative, this would imply that solutions exist unconditionally, unless one happens to hit an eigenfunction of $\mathcal{K}$. In that case, additional solvability conditions would have to be satisfied. However, the Fredholm Alternative is only valid for integral equations with compact integral operators. Now, because of the infinite integration region the operator in (111) certainly is not compact. What is worse, it will shortly be seen

that $\mathcal{K}$ has a Cauchy-type singularity on the $\alpha = \alpha'$ diagonal, i.e. $\mathcal{K}(\alpha, \alpha') \sim \frac{1}{\alpha - \alpha'}$ as $\alpha \to \alpha'$ Under those circumstances, the solution theory of integral equations is significantly different. I will return to this issue in chapter 6.

Carrying out the sum over $m$ and the integral over $\alpha$ in $I_1^{(J)}$, one arrives at

$$\mathcal{F}_1 = \sqrt{2}\pi \frac{F}{K_{m'}(\alpha')}. \tag{112}$$

A similar procedure for the parts of (101) and (109) after a substitution into $I_2^{(w_1')}$ yields

$$\begin{aligned} \mathcal{F}_2 &= \pi \frac{F(2-\sigma^2)}{\sqrt{2}K_{m'}(\alpha')} \mathrm{I}_0\left(\tfrac{\sigma^2}{2}(\alpha'^2 + 2m'^2)\right) \mathrm{e}^{-\sigma^2(\alpha'^2+2m'^2)/2} \\ \mathcal{F}_3 &= \sqrt{2}\pi \frac{F}{K_{m'}(\alpha')} \mathrm{e}^{-\sigma^2(\alpha'^2+2m'^2)/2} \sum_{k=1}^{\infty} \left(\frac{m'^2(\sigma^2-1)}{2k^2 - m'^2} + 1\right) \mathrm{I}_k\left(\tfrac{\sigma^2}{2}(\alpha'^2 + 2m'^2)\right) . \end{aligned} \tag{113}$$

In $\mathcal{F}_3$, one can evaluate a part of the series (that converges absolutely because of the $\mathrm{I}_k$) using (84) written as $2\sum_{k=1}^{\infty} \mathrm{I}_k(z) = \mathrm{e}^z - \mathrm{I}_0(z)$. This leads to

$$\begin{aligned} \mathcal{F}_3 =& \sqrt{2}\pi \frac{F}{K_{m'}(\alpha')} \Bigg( -1 + \mathrm{e}^{-\sigma^2(\alpha'^2+2m'^2)/2} \\ & \left(\mathrm{I}_0\left(\tfrac{\sigma^2}{2}(\alpha'^2 + 2m'^2)\right) + \sum_{k=1}^{\infty} \left(\frac{m'^2(\sigma^2-1)}{2k^2 - m'^2}\right) \mathrm{I}_k\left(\tfrac{\sigma^2}{2}(\alpha'^2 + 2m'^2)\right)\right)\Bigg). \end{aligned} \tag{114}$$

In the parts of (101) and (109) without the Dirac delta, one can sum over $m'$ and has

$$\mathcal{K}_1 = -\left(\frac{m'}{\omega}\right)^{\mathrm{i}(\alpha-\alpha')} \frac{\mathrm{i}\sqrt{2}\,\pi\sigma^2 F}{K_{m'}(\alpha')(\mathrm{e}^{2\pi(\alpha-\alpha')} - 1)} \mathrm{I}_0\left(\tfrac{\sigma^2}{2}\sqrt{(\alpha^2+2m'^2)(\alpha'^2+2m'^2)}\right) \mathrm{e}^{-\frac{\sigma^2}{4}(\alpha^2+\alpha'^2+4m'^2)} \tag{115}$$

from (101) and

$$\begin{aligned} \mathcal{K}_2 =& \frac{\mathrm{i}\sqrt{2}\,\pi\omega^{-\mathrm{i}(\alpha-\alpha')}F}{K_{m'}(\alpha')(\mathrm{e}^{2\pi(\alpha-\alpha')} - 1)} \mathrm{e}^{-\sigma^2(\alpha^2+\alpha'^2+4m'^2)/4} \sum_{k=1}^{\infty} \mathrm{I}_k\left(\tfrac{\sigma^2}{2}\sqrt{(\alpha^2+2m'^2)(\alpha'^2+2m'^2)}\right) \\ & \left((\sqrt{2}k - m'\sigma^2)\Lambda^k \mathrm{e}^{(\mathrm{i}(\alpha-\alpha')-1)\ln(m'-\sqrt{2}k)} - (\sqrt{2}k + m'\sigma^2)\Lambda^{-k}\mathrm{e}^{(\mathrm{i}(\alpha-\alpha')-1)\ln(m'+\sqrt{2}k)}\right) \end{aligned} \tag{116}$$

from (109).

Collecting (112), (113), and (114) and substituting (23) and (56), one is left with

$$\begin{aligned} \mathcal{F} =& \frac{\sqrt{1-2\sigma^2}^{1-1/\sigma^2}}{2\sigma^2 \mathrm{e}^{\sigma^2(\alpha'^2+2m'^2)/2+1}} \frac{\left|\Gamma\left(\frac{1}{4} + \frac{1}{2}m' + \frac{1}{2}\mathrm{i}\alpha'\right)\right|^2}{\left|\Gamma\left(\frac{3}{4} + \frac{1}{2}m' + \frac{1}{2}\mathrm{i}\alpha'\right)\right|^2} \\ & \left(\frac{4-\sigma^2}{2}\mathrm{I}_0\left(\tfrac{\sigma^2}{2}(\alpha'^2 + 2m'^2)\right) + \sum_{k=1}^{\infty} \left(\frac{m'^2(\sigma^2-1)}{2k^2 - m'^2}\right) \mathrm{I}_k\left(\tfrac{\sigma^2}{2}(\alpha'^2 + 2m'^2)\right)\right). \end{aligned} \tag{117}$$

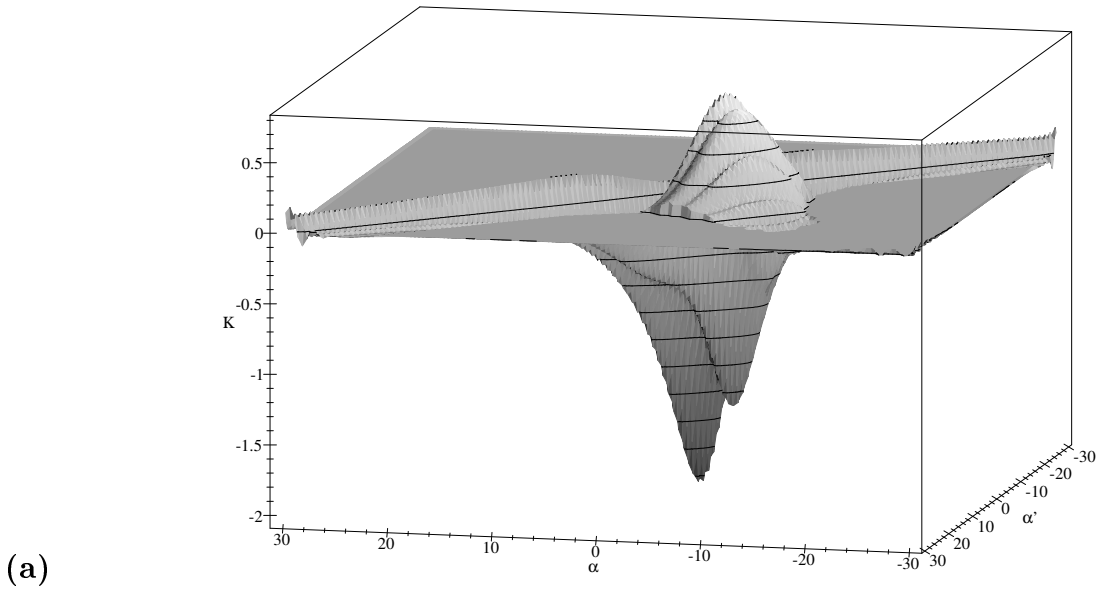


**(a)**

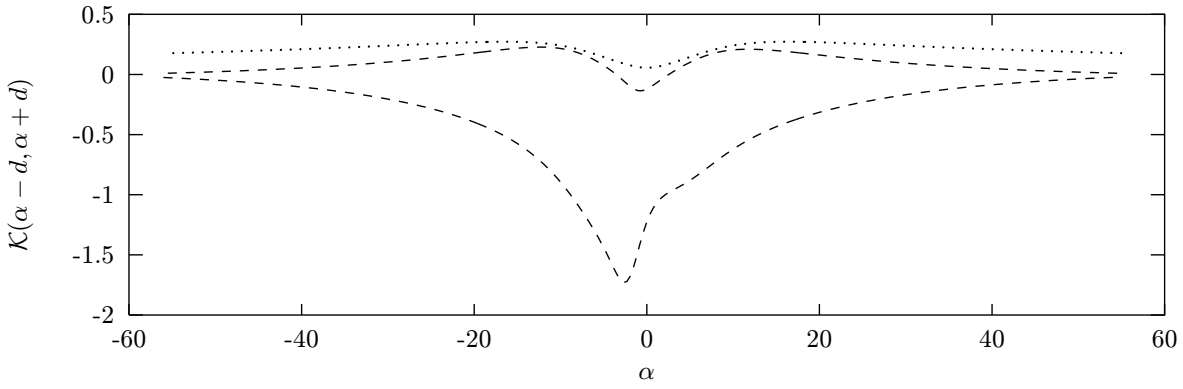


**(b)**

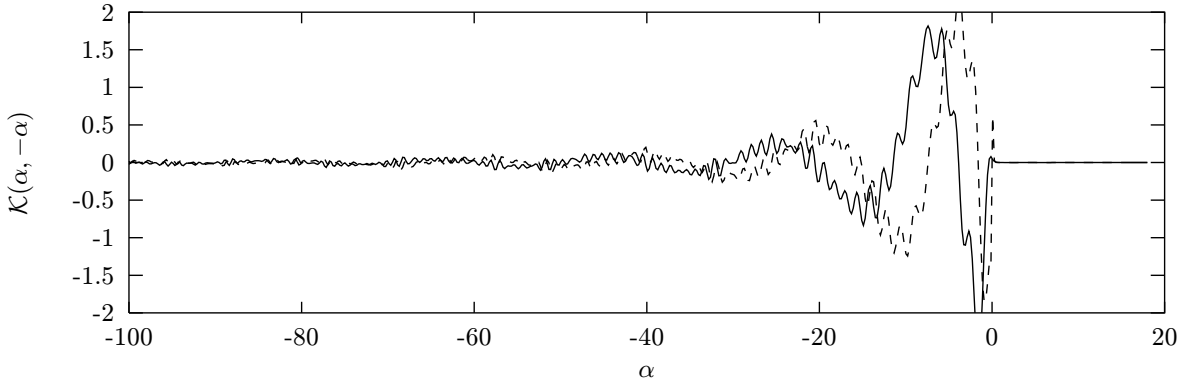


**(c)**

*Fig. 4: The kernel of the self-consistent disk. (a) shows the real part of the kernel $\mathcal{K}(\alpha, \alpha')$ in (111) of an $\omega = 0.5$, $\sigma = 0.2$, and $m = 2$-disk; (b) is the real part of the same kernel along the main diagonal (black line) and along parallels $\mathcal{K}(\alpha - d, \alpha' + d)$ with $d = 0.5$ (upper dotted line) and $d = 1$ (lower dotted line); (c) is the same kernel along the secondary diagonal $\alpha = -\alpha'$, this time with the imaginary part drawn as a dashed line. This is the "spur" visible in (a).*

The kernel itself computes to

$$\mathcal{K} = -\mathrm{i}\frac{\omega^{-\mathrm{i}(\alpha-\alpha')}\sqrt{1-2\sigma^2}^{1-1/\sigma^2}}{2\sigma^2\mathrm{e}^{\sigma^2(\alpha^2+\alpha'^2+4m'^2)/4+1}\left(\mathrm{e}^{2\pi(\alpha-\alpha')}-1\right)}\frac{\left|\Gamma\left(\frac{1}{4}+\frac{1}{2}m+\frac{1}{2}\mathrm{i}\alpha'\right)\right|^2}{\left|\Gamma\left(\frac{3}{4}+\frac{1}{2}m+\frac{1}{2}\mathrm{i}\alpha'\right)\right|^2}$$
$$\left(m'^{\mathrm{i}(\alpha-\alpha')}\sigma^2\mathrm{I}_0\left(\tfrac{\sigma^2}{2}\sqrt{(\alpha^2+2m'^2)(\alpha'^2+2m'^2)}\right)-\sum_{k=1}^{\infty}\mathrm{I}_k\left(\tfrac{\sigma^2}{2}\sqrt{(\alpha^2+2m'^2)(\alpha'^2+2m'^2)}\right)\right.$$
$$\left.\left((\sqrt{2}k-m'\sigma^2)\Lambda^k\mathrm{e}^{(\mathrm{i}(\alpha-\alpha')-1)\ln(m'-\sqrt{2}k)}-(\sqrt{2}k+m'\sigma^2)\Lambda^{-k}\mathrm{e}^{(\mathrm{i}(\alpha-\alpha')-1)\ln(m'+\sqrt{2}k)}\right)\right), \tag{118}$$

where, from (83),

$$\Lambda = \frac{\alpha\alpha'+\sqrt{2}m'(\sqrt{2}m'+\mathrm{i}\left(\alpha-\alpha'\right))}{\sqrt{(2m'^2+\alpha^2)(2m'^2+\alpha'^2)}}. \tag{119}$$

Interestingly, the only term in (118) dependent on $\omega$, i.e., $\omega^{\mathrm{i}(\alpha-\alpha')}$, can be factored out of the kernel, and $\mathcal{F}$ is entirely independent of $\omega$. Under these circumstances, the value of $\omega$ is completely irrelevant for the solvability of the integral equation. This means that as long as this kernel is valid, one will have either no solution at all or a two-dimensional continuum of solutions (corresponding to the real and imaginary parts of $\omega$). Of course, the case $\omega = 0$ handled below is an exception here, since the kernel (118) is not valid for $\omega = 0$. Actually, by considering the physics, this result is not too surprising and is required by the scale-freeness of the disk. Without a time scale to 'cling to' a disk has no way to know what growth rate or pattern speed it should prefer. However, see chapter 6.1 for a more thorough discussion.

The kernel $\mathcal{K}$ links the input spectrum of a perturbation with respect to the potential basis, $\Phi_{m'}(\alpha)$, to the output spectrum, $\Phi_{m'}(\alpha')$, which is why Zang called it the "transfer function". This interpretation is useful when one wants to attain some qualitative understanding of the various features of $\mathcal{K}$. In the case of the self-consistent disk, this interpretation is not literally correct, since the coefficient of $\Phi_{m'}(\alpha')$ depends on $\alpha'$. Still, to gain some qualitative insight a consideration of the kernel is valuable, and in the cut-out case the kernel does indeed directly link the input and the output spectrum of the perturbation. Since the real parts of the kernels are not qualitatively different for the cut-out and self-consistent disks (at some distance from the diagonal, this statement is true for the imaginary part as well), much of what is said here helps in understanding the cut-out disks.

By just looking at a picture of $\mathcal{K}$ like the one in Fig. 4a, one immediately notices the strong asymmetry in the kernel: Where $\alpha > \alpha'$, the kernel practically vanishes, except very close to the diagonal, whereas on the other side of the diagonal, quite a few features are visible. The interpretation is evident when one recalls that for $\omega > 0$ a spiral is more trailing when $\alpha$ is larger. Now, the kernel for $\alpha > \alpha'$ gives the power flow from more trailing to more leading spirals—which is minute. For this reason, this asymmetry is known as the trailing bias.

Going from $\alpha > \alpha'$ towards the diagonal, one next encounters an extended contribution streching out along the $\alpha = \alpha'$ line. In the real part of the kernel shown in Fig. 4a, this diagonal is rather inconspicuous; still, the large extent of the diagonal makes it one of the dominant features of the kernel. Kernels for axisymmetric ($m = 0$) perturbations basically

consist only of the diagonal. The imaginary part of the self-consistent kernel, on the other hand, has a singularity on the diagonal which severely influences the entire character of the eigenvalue problem (111). The diagonal roughly gives the feedback of a given logarithmic spiral onto itself.

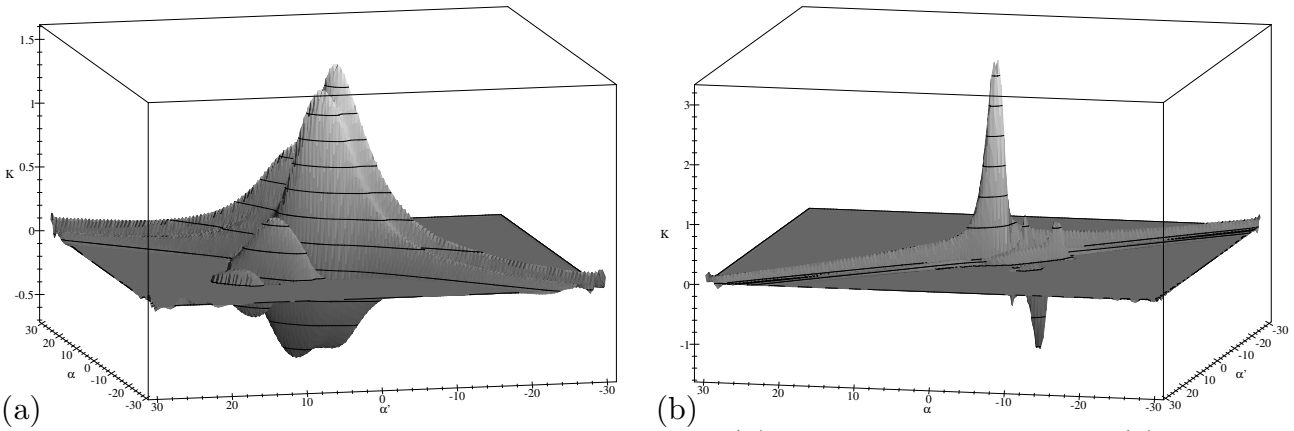


*Fig. 6: The kernel of the self-consistent disk for (a) $m = 2$, $\sigma = 0.12$ and (b) $m = 1$, $\sigma = 0.2$. Again, $\omega = 0.5$.*

Right behind the diagonal on its trailing side, one or a few major peaks dominate the visual appearance. A comparison between Fig. 4a and Fig. 6a suggests that these peaks widen when the velocity dispersion decreases, and comparing Fig. 4a and Fig. 6b, one suspects that lower $m$ correspond to more concentrated peaks. A closer investigation reveals that this is a definite trend.

In Fig. 6b one sees that while the $m = 1$-kernel is of course still symmetric on the diagonal, it quickly becomes almost antisymmetric with respect to the secondary diagonal, which sets it apart from the approximate symmetry of the $m = 2$ kernels (and these for the other azimuthal harmonics). This, and a quite pronounced peak on the diagonal, is special to the one-armed case and does not occur for other azimuthal harmonics.

The peaks are the main means of transport of power between spirals of different wave number $\alpha$. The first peak on the secondary diagonal transports power from leading to trailing waves around $\alpha = 0$, which suggests a relation to the well-known swing amplifier, in that the latter is most effective when the wave pattern is almost radial.

Finally, a "spur" continues down the secondary diagonal, with small ripples on top of an oscillation that is only slowly damped. This spur, reaching farther out for smaller $\sigma$, transports power from strongly leading to strongly trailing spiral components and might be related to either reflection at the centre or possibly waves travelling through the centre along the lines of the scheme hinted at in Binney and Tremaine (1987), Fig. 6-20. However, compared to this scheme, an explanation of the spur would require the signs to be reversed, and of course it is not obvious how these schemes should work in the presence of an inner Lindblad resonance, when the centre becomes unreachable for density waves. Still, the fact that the coupling mediated by the spur prefers waves of comparable wave numbers but different sign strongly suggests some mechanism along these lines.

Also note that in the kernel, there is little sign of a feedback loop that would transport power from trailing to leading waves. There is, however, a nonzero contribution on the trailing-to-leading side of the diagonal close to it. Taking a look forward, it should be noted that the kernels of the cut-out disk do indeed have a small peak around the secondary diagonal on the leading side of the main diagonal. It is tempting to connect this feature with the reflection at the $Q$-barrier, even more so since it is the only qualitative difference between the cut-out and the self-consistent kernels except for the singularity of the latter on the main diagonal.

### 3.6.1. The case $\omega = 0$

As pointed out above, the case $\omega = 0$ requires a special treatment. Fortunately, the expressions become much more compact in this case.

Adding together (86) and (88), one has

$$\begin{aligned}\mathcal{K} =& \frac{\sqrt{1-2\sigma^2}^{1-1/\sigma^2}}{\sqrt{2}\sigma^2} \frac{\left|\Gamma\left(\frac{1}{4}+\frac{1}{2}m+\frac{1}{2}\mathrm{i}\alpha'\right)\right|^2}{\left|\Gamma\left(\frac{3}{4}+\frac{1}{2}m+\frac{1}{2}\mathrm{i}\alpha'\right)\right|^2} \Bigg(1-(1+\sigma^2)\mathrm{e}^{-\sigma^2(\alpha'^2+2m'^2)/2} \\ & \left(\mathrm{I}_0\left(\frac{\sigma^2}{2}(\alpha'^2+2m'^2)\right)+\sum_{k=1}^{\infty}\frac{2m'^2}{m'^2-2k^2}\,\mathrm{I}_k\left(\frac{\sigma^2}{2}(\alpha'^2+2m'^2)\right)\right)\Bigg).\end{aligned} \tag{120}$$

Remarkably, the Dirac and Kronecker deltas in the kernel have collapsed the integral operator $\Phi(\alpha) \to \int \mathcal{K}(\alpha,\alpha')\Phi(\alpha)\,d\alpha$ to a simple multiplicative operator, and the integral equation becomes an ordinary nonlinear equation,

$$\Phi_{m'}(\alpha') = \mathcal{K}(\alpha')\Phi_{m'}(\alpha'), \quad \text{or} \quad \mathcal{K}(\alpha') - 1 = 0. \tag{121}$$

The solutions of (121) will always be marginal modes, since $\omega = 0$ of course implies a vanishing growth rate. To find these modes, one has to solve (121) as a nonlinear equation in the two variables $\alpha'$ and $\sigma$. Since the kernel is quickly evaluated and I will not mass-produce such results, bisection works well as a solution finder.

# 4. The Cut-Out-Disk

## 4.1. The Cut-Out Distribution Function

Two unphysical properties of the Mestel disk are the singularity of the density in the centre of the disk and its infinite total mass. Those features are responsible for the "border terms" in the $L_z$ integration above, and they cause the singularity on the diagonal. What is more, the perfectly self-similar Mestel disk has no length or time scales, which leads to the weird phenomenon that either a continuum of modes should be unstable or the disk is entirely stable, with the possible exception of neutral modes with $\omega = 0$ that do not need a time scale.

A catch-all for those problems is the introduction of a cut-out. The idea, already promoted by Zang (1976) is that a part of the matter in the disk is immobilised, i.e., it is only visible in the rotation curve but not in the distribution function used in the Boltzmann equation. Physically, this could mean that a stellar component with high velocity dispersion is present—like bulges near the centre of a spiral galaxy—, or that a gravitationally unresponsive dark matter halo strongly contributes to the rotation curve. Both possibilities appear to occur in nature, and so immobilising a part of the mass is not an entirely unphysical procedure.

Mathematically, the immobilisation is effected by multiplying the distribution function with another function $H(L_z)$ with the properties that $0 \leq H(L_z) \leq 1$ and preferably $H(L_z) = 0$ for $L_z \to 0, \infty$ strongly enough to ensure that the contributions proportional to $\delta(\alpha - \alpha')$ in $I_{1,2}^{(L_z)}$ are suppressed. Additionally, one drops the requirement of having a self-consistent model, i.e., the potential remains the same as before. Thus, while some of the matter remains dynamically important, it no longer takes part in a perturbation.

In the choice of the cut-out I do not strive to mimic any realistic models of haloes, disks, or bulges. My primary concern is analytic simplicity of the resulting expressions. A cut-out that leads to relatively compact expressions would be

$$H(L_z) = \frac{2L_z L_0}{L_0^2 + L_z^2}. \tag{122}$$

with a positive $L_0$. While I would recommend this functions for further analytic exploration of a cut-out Mestel disk, my primary motive here is to check my approximation by comparing my results to those of Read (1997), and therefore I will follow her choice of cut-out functions.

To damp down both harmonic tails in (90) and (103), I need to immobilise matter both at the centre and in the outer regions. Therefore, I will use Read's doubly cut-out function

$$H(L_z) = \frac{L_z^N L_c^M}{(L_z^N + L_0^N)(L_z^M + L_c^M)}. \tag{123}$$

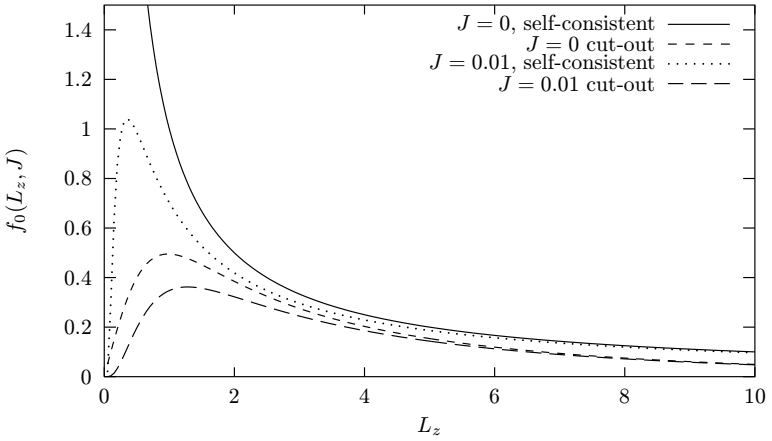


*Fig. 7: Effect of the cut out in a $\sigma = 0.2$ disk for two values of $J$. Note that the distribution function of the self-consistent disk really diverges as $J = 0$ and $L_z \to 0$.*

Since $M$ and $N$ will occur as the orders of poles and the computation of high-order residues leads to really messy expressions, I will only investigate the $M = N = 2$ case here. I do not expect the dependence of the behaviour of the disk on $M$ and $N$ to be very different from what Read found.

## 4.2. The Boltzmann Equation for the Cut-Out Disk

The modified distribution function does only introduce changes into the right hand side of the linearised Boltzmann equation (29). The equivalent of (31) now reads

$$\text{r.h.s.} = f_0 \left( \left( \frac{\sigma^2 L_z - \sqrt{2} J}{\sigma^2 L_z^2} + 2 \frac{L_z^4 - L_0^2 L_c^2}{L_z (L_z^2 + L_0^2)(L_z^2 + L_c^2)} \right) \frac{\partial \Phi_1}{\partial w_1} + \frac{\sqrt{2}}{\sigma^2 L_z} \frac{\partial \Phi_1}{\partial w_2} \right). \tag{124}$$

Again, the term with $J$ is of order $\zeta^2$ and is therefore discarded. Inserting the linearised potential basis (25) now yields

$$\begin{aligned} \text{r.h.s.} = &- \frac{\mathrm{i}\sqrt{2}\,\Phi_{\alpha,m} F L_z^{\mathrm{i}\alpha - 1}}{\sigma^2 (L_z^2 + L_0^2)(L_z^2 + L_c^2)} \mathrm{e}^{\mathrm{i}mw_2 + \mathrm{i}\sqrt{\frac{\sqrt{2}J}{L_z}}\left(\alpha\cos(w_1) - \sqrt{2}m\sin(w_1)\right) - \frac{\sqrt{2}J}{\sigma^2 L_z} - \mathrm{i}\omega t} \\ &\left( \sqrt{\sqrt{2} J} \Big( \alpha \sin(w_1) + \sqrt{2}\, m \cos(w_1) \Big) - \frac{\sigma^2 m \sqrt{L_z}}{\sqrt{2}} \left( 1 + \frac{2L_z^4 - 2L_0^2 L_c^2}{(L_z^2 + L_0^2)(L_z^2 + L_c^2)} \right) \right) \end{aligned} \tag{125}$$

## 4.3. The Matrix Equation for the Cut-Out Disk

Just as the cut-out influences Read's equations only via the angular momentum function, the changes from (32) to (125) only involve $L_z$. Thus, all derivations up to the integration over $L_z$ may be carried out for the cut-out disk following the path outlined for the self-consistent disk above. The two contributions to the kernel of the integral equation describing asymptotic modes in the cut-out disk are, with no quadratures yet carried out,

$$\begin{aligned}\bar{I}_1 =&\Phi_{\alpha,m}\frac{FL_z^{\mathrm{i}(\alpha-\beta)-2}}{4\pi^2\sigma^2K_{m'}(\alpha')}\frac{L_z^2L_c^2}{(L_z^2+L_0^2)(L_z^2+L_c^2)}\\ &\exp\left(\mathrm{i}\sqrt{\frac{\sqrt{2}J}{L_z}}\Big((\alpha-\alpha')\cos(w_1)-\sqrt{2}(m-m')\sin(w_1)\Big)\right)\\ &\exp\left(\mathrm{i}(m-m')w_2-\frac{\sqrt{2}J}{\sigma^2L_z}\right)\end{aligned} \tag{126}$$

and

$$\begin{aligned}\bar{I}_2 =&\mathrm{i}\Phi_{\alpha,m}\frac{FL_z^{\mathrm{i}(\alpha-\beta)-2}\big(m\sigma^2+\sqrt{2}\eta\big)}{8\pi^2\sigma^2K_{m'}(\alpha')(\mathrm{e}^{2\pi\mathrm{i}\eta}-1)}\frac{L_z^2L_c^2}{(L_z^2+L_0^2)(L_z^2+L_c^2)}\\ &\left(1+\frac{2m\sigma^2(L_z^4-L_0^2L_c^2)}{(m\sigma^2+\sqrt{2}\eta)(L_z^2+L_0^2)(L_z^2+L_c^2)}\right)\exp\Bigg(\mathrm{i}(m-m')w_2+\mathrm{i}\eta w_1'-\frac{\sqrt{2}J}{\sigma^2L_z}\\ &+\mathrm{i}\sqrt{\frac{\sqrt{2}J}{L_z}}\Big(\alpha\cos(w_1'+w_1)-\alpha'\cos(w_1)-\sqrt{2}\,m\sin(w_1'+w_1)+\sqrt{2}\,m'\sin(w_1)\Big)\Bigg).\end{aligned} \tag{127}$$

The conventions stated for the notation of (64) and (65) apply here, too, with the difference that I denote the integrands for the cut-out disks with $\bar{I}_{1,2}$.

To highlight the terms that are added in going from the equivalent expressions for the self-consistent disk, (64) and (65), the contributions already present in the self-consistent disk are grayed out.

The black factors in $\bar{I}_{1,2}$ just pull through all the quadratures I performed in the self-consistent disk up until the $L_z$ integration. There, matters get significantly more complicated than before.

# 4.4. Integration Over the Angular Momentum in the Cut-Out Disk

### 4.4.1. Integration of $\bar{I}_1^{(J)}$

The integrand of $\bar{I}_1^{(J)}$ is the black term in (126) times the $L_z^{\mathrm{i}(\alpha-\alpha')-1}$ from the self-consistent disk, which on transferring an $L_c^2$ to the rest of the term, leaves

$$\int_0^\infty \frac{L_z^{\mathrm{i}(\alpha-\alpha')+1}}{(L_z^2+L_0^2)(L_z^2+L_c^2)}\,dL_z \tag{128}$$

as the integral to evaluate. On substituting $u=\ln(L_z)$, one gets

$$\int_{-\infty}^\infty \frac{\mathrm{e}^{\mathrm{i}u\gamma+2}}{\left(\mathrm{e}^{2u}+L_0^2\right)^2\left(\mathrm{e}^{2u}+L_c^2\right)^2}\,du, \tag{129}$$

where again I abbreviate $\gamma=\alpha-\alpha'$.

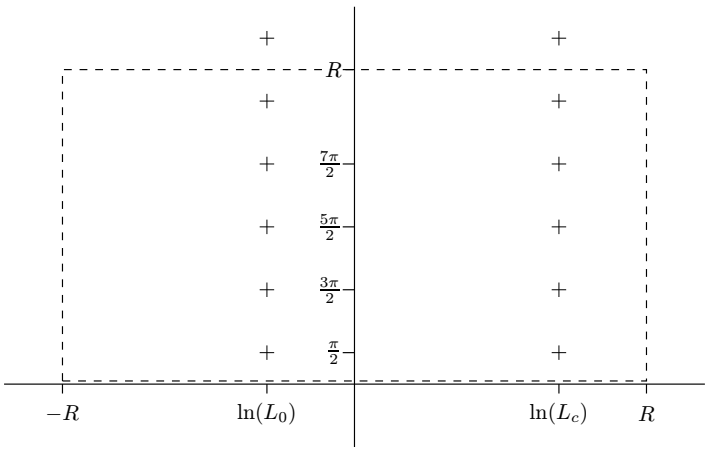


*Fig. 8: Integration path for the first integration of $\bar{I}_1^{(J)}$. The crosses mark the poles relevant for the integration.*

The integrand has poles of order 2 at

$$\bar{u}_j^{(1)} = \ln(L_0)+\mathrm{i}\pi(j+1/2)$$
$$\bar{u}_j^{(2)} = \ln(L_c)+\mathrm{i}\pi(j+1/2)$$

Assuming $\gamma>0$ again, one can use the integration path sketched in Fig. 8. Of the three problems noted with the integration of (91), only one is present here: Going towards $+\mathrm{i}\infty$, the poles of the integrand go all the way up, so that a continuous deformation of the integration path as we go to infinity is not possible. However, the remarks given above about why the residue theorem may still be applied hold for the present integration as well.

Otherwise, the integrand is much tamer than the one I considered in the self-consistent case, since it falls off exponentially as $u \to \pm\infty$. As if to make good for this, the residues are substantially harder to compute. For poles of order two one has

$$\operatorname{res}(f(z),u) = \lim_{u\to z} \frac{d}{du}\Big(f(u)(z-u)^2\Big);$$

The determination of the limit requires a triple application of de l'Hospital's rule. The results are

$$\operatorname{res}\left(\frac{\mathrm{e}^{u(\mathrm{i}\gamma+2)}}{\left(\mathrm{e}^{2u}+L_0^2\right)^2\left(\mathrm{e}^{2u}+L_c^2\right)^2}; \bar{u}_j^{(1)}\right) = -L_0^{\mathrm{i}\gamma}\,\frac{\mathrm{e}^{-(\pi\gamma/2)(2j+1)}}{2(L_0^2-L_c^2)} \tag{130}$$

for $\bar{u}_j^{(1)}$ and

$$\operatorname{res}\left(\frac{\mathrm{e}^{u(\mathrm{i}\gamma+2)}}{\left(\mathrm{e}^{2u}+L_0^2\right)^2\left(\mathrm{e}^{2u}+L_c^2\right)^2}; \bar{u}_j^{(2)}\right) = L_c^{\mathrm{i}\gamma}\frac{\mathrm{e}^{-(\pi\gamma/2)(2j+1)}}{2(L_0^2-L_c^2)} \tag{131}$$

for $\bar{u}_j^{(2)}$.
The two residues (130) and (131) must be summed up for $j = 0\cdots\infty$, which results in an alternating geometric series of the form $\sum_j (-1)^j q^j$. Such a series is easily determined to be

$$\sum_{j=0}^{\infty}(-1)^j q^j = \sum_{j=0}^{\infty} q^{2j} - \sum_{j=0}^{\infty} q^{2j+1} = \frac{1-q}{1-q^2} = \frac{1}{1+q}. \tag{132}$$

Using this to sum up (130) and (131), applying the residue theorem and inserting the resulting expression into (128) delivers

$$\bar{I}_1^{(L_z)} = -I\pi\Phi(\alpha,m')\frac{\sqrt{2}\,FL_c^2}{4K_{m'}(\alpha')(L_0^2-L_c^2)}\,\frac{L_0^{\mathrm{i}(\alpha-\alpha')}-L_c^{\mathrm{i}(\alpha-\alpha')}}{\sinh\big((\pi/2)(\alpha-\alpha')\big)}\,\mathrm{e}^{-\frac{\sigma^2}{4}(\alpha-\alpha')^2}. \tag{133}$$

Here, I have already performed the summation over $m$ (cf. Eq. 67). This is even more advisable in $\bar{I}_2^{w_1'}$, since the expressions are complicated enough even without keeping $m$ and $m'$. Note that (133) is regular at $\alpha = \alpha'$ despite the $\sinh\big(\pi(\alpha-\alpha')/2\big)$ in the denominator, because the $L_0^{\mathrm{i}(\alpha-\alpha')} - L_c^{\mathrm{i}(\alpha-\alpha')}$ in the numerator also has a zero of order 1 at $\alpha = \alpha'$.

### 4.4.2. Integration of $\bar{I}_2^{(w_1')}$, Part Without Sum

As I did in the self-consistent case, I split up the integration of $I_2^{(w_1')}$ into two parts. At first I consider the terms without the series. After again substituting $u = \ln(L_z)$ and writing $\gamma = \alpha - \alpha'$, one has to compute

$$\begin{aligned}\int_{-\infty}^{\infty} \frac{\mathrm{e}^{(\mathrm{i}\gamma+2)u}}{(m-\mathrm{e}^u\omega)(L_0^2+\mathrm{e}^{2u})^2(L_c^2+\mathrm{e}^{2u})^2}\Big(&mL_0^2L_c^2(1+\sigma^2) - \omega L_0^2L_c^2\mathrm{e}^u \\ &- m(\sigma^2-1)(L_0^2+L_c^2)\mathrm{e}^{2u} - \omega(L_0^2+L_c^2)\mathrm{e}^{3u} + m(1-3\sigma^2)\mathrm{e}^{4u} - \omega\mathrm{e}^{5u}\Big)\,du.\end{aligned} \tag{134}$$

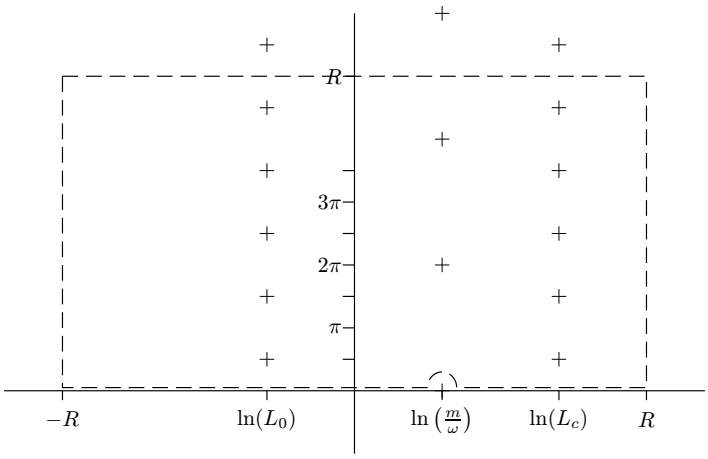


*Fig. 9: Integration path for the part without the sum in the integration the first part of $\bar{I}_2^{(w_1')}$ with $\gamma > 0$. The crosses mark the poles relevant for the integration.*

This problem is essentially solved when one knows the integral

$$\int_{-\infty}^{\infty} \frac{\mathrm{e}^{\mathrm{i}\gamma u}\mathrm{e}^{\lambda u}}{(m-\mathrm{e}^{u}\omega)(L_0^2+\mathrm{e}^{2u})^2(L_c^2+\mathrm{e}^{2u})^2}\,du \tag{135}$$

for $\lambda \in \{2,3,4,5,6,7\}$. This integrand has poles at $\bar{u}_j^{(1)}$ and $\bar{u}_j^{(2)}$, and, in addition to that, at

$$\bar{u}_j^{(3)} = 2\pi\mathrm{i}j + \ln(m/\omega), \tag{136}$$

where the poles at $\bar{u}_j^{(1,2)}$ are of order two, the poles at $\bar{u}_j^{(3)}$ are of order one. The situation in this case is sketched in Fig. 9.

At this point, the computations really get messy for Read's cut-out, and it seems wise to take recourse to computer algebra systems. In the appendix, I give the results from this and the following quadratures as exported by Maple. Apart from the sheer size of the expressions, the calculations can be carried out in close parallel to those in the case without the sum and those in the singular disk.

The result of having still rather clumsy expressions does not seem to warrant the effort of further cleaning up these formulae. As mentioned above, if goal is a cut-out disk with relatively compact expressions, I recommend using a cut-out of the type (122).

### 4.4.3. Integration of $\bar{I}_2^{(w_1')}$, Part With Sum

After the usual substitutions, the terms containing the $L_z$ integration of the part of $\bar{I}_2^{(w_1')}$ with the series can be computed evaluating

$$\begin{aligned}\int_0^{\infty} \mathrm{e}^{(\mathrm{i}\gamma+2)u} &\frac{2k\sin(k\ln\Lambda) - \mathrm{i}\sqrt{2}\cos(k\ln\Lambda)\big(m+\omega\mathrm{e}^{u}\big)}{\big((\omega\mathrm{e}^{u}-m)^2-2k^2\big)\big(\mathrm{e}^{2u}+L_0^2\big)^2\big(\mathrm{e}^{2u}+L_c^2\big)^2}\Big(mL_0^2L_c^2(1+\sigma^2) - \omega L_0^2L_c^2\mathrm{e}^{u} \\ &- m(\sigma^2-1)(L_0^2+L_c^2)\mathrm{e}^{2u} - \omega(L_0^2+L_c^2)\mathrm{e}^{3u} + m(1-3\sigma^2)\mathrm{e}^{4u} - \omega\mathrm{e}^{5u}\Big)\end{aligned} \tag{137}$$

Now the reduced problem is finding

$$\int_0^\infty \frac{\mathrm{e}^{(\mathrm{i}\gamma+\lambda)u}}{\left((\omega\mathrm{e}^u-m)^2-k^2\right)\left(L_0^2+\mathrm{e}^{2u}\right)^2\left(L_c^2+\mathrm{e}^{2u}\right)^2}\,du \tag{138}$$

for $\lambda \in \{2,3,4,5,6,7,8\}$. The zeroes the denominator of this integrand are at $\bar{u}_j^{(1)}$, $\bar{u}_j^{(2)}$, and

$$\begin{aligned} \bar{u}_j^{(4)} &= \ln\left(\frac{m-\sqrt{2}k}{\omega}\right)+2\pi\mathrm{i}j \\ \bar{u}_j^{(5)} &= \ln\left(\frac{m+\sqrt{2}k}{\omega}\right)+2\pi\mathrm{i}j \end{aligned}\quad . \tag{139}$$

The pole at $u_j^{(4)}$ plays the role of the pole at $u_j^{(3)}$ in the $I_2^{w_1'}$ integration in the self-consistent disk, i.e., when $\sqrt{2}m < k$ they are shifted vertically, and again a proper choice of the logarithm's branch cut allows the use of identical expressions regardless of the ratio between $m$ and $k$.

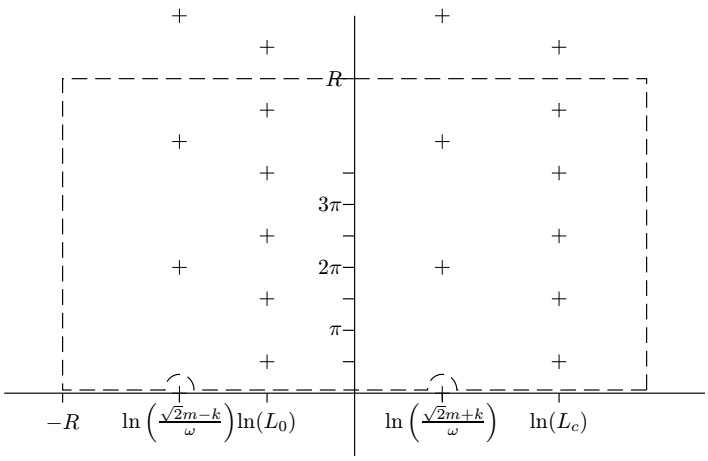


*Fig. 10: Integration path for the part with the sum in the integration of $\bar{I}_2^{(w_1')}$ with $\gamma > 0$ and $k < \sqrt{2}m$. The crosses mark the poles relevant for the integration.*

The situation found here is depicted in Fig. 10. Basically, the integral can be computed as the sum of four series over residues at poles of orders one ($u_j^{(3)}$, $u_j^{(4)}$) and two ($u_j^{(1)}$, $u_j^{(2)}$). But while the expressions for the residues at $u_j^{(3)}$ and $u_j^{(4)}$ are quite like those in the self-consistent disk with the denominator adapted, those for the residues at $u_j^{(1)}$ and $u_j^{(2)}$ are really messy, and I once more refer the reader to Appendix A.

Suffice it to say that the kernel of the integral equation for the cut-out disk is quite longish to write down but much easier to handle than the self-consistent disk's kernel: it is bounded at the diagonal $\alpha = \alpha'$ and it falls off rather quickly with increasing distance to the diagonal. So, the cut-out disk it is much more accessible to a numerical study of its behaviour.

## 4.5. Numerics

After the final integration over $L_z$ the integral equation for modes in the cut-out disk has the form

$$\begin{aligned} \Phi_{\alpha',m'} &= \int_{-\infty}^{\infty} \bar{\mathcal{K}}(\alpha,\alpha')\Phi_{\alpha,m'}\, d\alpha \qquad \text{with} \\ \bar{\mathcal{K}}(\alpha,\alpha') &= \left(\bar{I}_1^{(L_z)} + \bar{I}_2^{(L_z,1)} + \bar{I}_2^{(L_z,2)}\right) \end{aligned} \tag{140}$$

where $\bar{I}_1^{(L_z)}$ is given by (133) and $\bar{I}_2^{(L_z,1,2)}$ can be found in the appendix. Formally, this is a homogenous Fredholm integral equation of the second kind. However, due to the infinite integration interval, the operator induced by $\bar{\mathcal{K}}$ is not compact, and therefore the well-known results from the theory of integral equations (e.g., Pipkin 1991), and in particular the Fredholm Alternative, are not immediately applicable. Thanks to the exponential decay of the kernel, however, the operator is "compact for all practical purposes", meaning that as long the functions the operator is applied to do not diverge too quickly as $\alpha \to \infty$, the Fredholm Alternative still holds. Indeed, functions that do not vanish as $\alpha \to \infty$ can probably not be considered solutions to the given problem since they do not satisfy the condition that the perturbation of the surface density is much smaller than the surface density of the basic state unless they were finely crafted to do so.

This "almost-compactness" of $\bar{\mathcal{K}}$ was already noted by Zang, who simply cut off the integration region when increasing it did not change the solutions noticeably any more. I will adopt this scheme for purposes of the numerical investigation of the solutions. As for closed solutions, the integral equation (140) is far too complex to undertake an attempt to find them, even if there was any hope that a kernel that complex might have any.

The kernel of $\bar{\mathcal{K}}$ is quite easy to compute, since the series usually converges rather quickly and high-$k$ summands are small. However, the diagonal elements of the kernel are evaluated with poor accuracy, even diverging in the imaginary as $\alpha \to \alpha'$ at the limited accuracy provided by the C library or the numerical coprocessor. The problems surface when $|\alpha - \alpha'| \lesssim 0.05$ for IEEE double precision floats and parameters in the interesting range (say, $0.05 < \sigma < 0.5$ and $0.001 < \omega < 10$).

The reason for this behaviour is of course the presence of the $\sinh^{-1}$ term in (133) and the corresponding terms for $\bar{I}_2$. Although it is balanced by zeroes of order 1 in the numerators, rounding errors invalidate the results from the computation. To overcome this difficulty, one could rewrite the kernel isolating the zeroes in both numerator and denominator and compute them separately. With this approach the rounding errors are more confined, and indeed the GNU C library on iA86 and PPC architectures handles terms like $x/\sinh(x)$ quite well down to very small $x$. Another approach would be to use a suitable expansion of the kernel in the vicinity of the diagonal.

Both these approaches are unattractive because of the sheer size of the expressions. Therefore, I resorted to polynomial interpolation to compute the kernel for $\alpha \approx \alpha'$. When a kernel value $\bar{\mathcal{K}}(\alpha,\alpha')$ is requested with $|\alpha - \alpha'| < 0.05$, I compute the four points $\bar{\mathcal{K}}(\alpha' - 0.18 + 0.12\,j, \alpha')$, $j = 0 \cdots 3$ and determine $\bar{\mathcal{K}}(\alpha,\alpha')$ from the third-order polynomial fitting through these four points. For the values of $\omega$, $\sigma$, $L0$, and $L_c$ used in this work, the characteristic periods in the kernel are generally larger than 0.1, and thus this approach works very well.

Following Read and Zang, the integral equation itself is solved by re-writing it as an eigenvalue equation,

$$\lambda\Phi_{m'}(\alpha') = \int \bar{\mathcal{K}}(\alpha,\alpha')\Phi_{m'}(\alpha)\,d\alpha. \tag{141}$$

The complex numbers $\lambda$ for which a $\Phi_{\alpha,m}$ exists so that this equation can be satisfied are called mathematical (or artificial) eigenvalues. Although those eigenvalues have no physical significance in themselves, they will allow to judge on the solvability of the integral equation and have the advantage of being quite easily computed (see chapter 5.2). To find the $\Phi_{\alpha,m'}$ that really are modes, one has to look for parameters for which $\bar{\mathcal{K}}$ has an eigenvalue 1.

### 4.5.1. Quadrature

To compute the eigenvalues of $\bar{\mathcal{K}}$, I employ the method of Fredholm discretisation (also known as Nystöm method): Given a quadrature formula $\int f(x)\,dx = \sum_{i=1}^{N} w_i f(x_i)$ with equidistant grid points $x_i$ one can approximate the integral equation (141) with the system of linear equations

$$\lambda\Phi(\alpha_j,m') = \sum_{i=1}^{N} w_i\bar{\mathcal{K}}(\alpha_i,\alpha_j)\Phi(\alpha_i,m'). \tag{141}$$

Since the kernel oscillates rather quickly where it is large, a large number of grid points would be necessary to ensure useful accuracy of a simple quadrature formula without special adaption to the problem at hand. Thus, using an advanced quadrature formula is highly desirable.

In general applications of numerical integration, the most popular advanced quadrature formulae belong to the family of Gauss quadratures. These give quadratures exact for a weight function times a polynomial, but in general require an unevenly spaced grid. When solving integral equations, this feature makes them quite useless, since one has to derive a system of linear equations, and thus the discretisation has to be the same in $\alpha_i$ and $\alpha_j$. There are, however, adaptions of the Gauss quadrature on a grid (the most common of which is the Gauss-Legendre quadrature) and related methods to compute quadrature formulae with weight functions on an evenly spaced grid (e.g., Press et al 1992, p. 798).

Unfortunately, choosing a weight function for the present kernel is highly nontrivial, because the three periodic functions present in the kernel (with periods $2\pi/\omega$, $2\pi/L0$, and $2\pi/L_c$) are overlaid in a rather complicated way, and quasiperiodic terms further worsen the situation. I have tried implementing Press' prescription mentioned above with the dominant oscillation ($\omega^{\mathrm{i}(\alpha-\alpha')}$) as a weight function, which did not yield a very satisfying result. This did not really come as a surprise, since factoring out $\omega^{\mathrm{i}(\alpha-\alpha')}$ does not smoothen the kernel too significantly. Trying more complicated weight functions did not improve the situation.

A relatively proven tool to handle the discretisation of the integral equation at hand is the quadrature already used by Read (1997) and Zang (1976), which is based on an approximation of the kernel by Lagrangian polynomials. However, I found this scheme to be effective only when the kernel already is rather smooth. and it did not work too well for me. It is somewhat hard to understand why it worked that much better for Read, who only factored out the Kalnajs factor.

I finally settled for a quadrature based on local spline interpolation. In this scheme, one first determines the kernel on a grid of grid spacing $\Delta\alpha$, yielding $N^2$ numbers $\bar{\mathcal{K}}_{i,j}$. One then one puts a cubic spline $s(\alpha)$ through all the points $(\bar{\mathcal{K}}_{ij})_{i=1\cdots N}$, i.e. one row of the resulting matrix. This spline usually is a good representation of the true kernel unless the kernel is grossly undersampled. Hence an integral over this spline is a reasonable approximation to the integral $\int_{\alpha_1}^{\alpha_N} \bar{\mathcal{K}}(\alpha, \alpha_j)\, d\alpha$. This integral could in principle be computed analytically, but for convenience I evaluate in by the trapezoidal rule. Even with 30 abscissae per $\Delta\alpha$ interval, the computing time is still dominated by the evaluation of the kernel.

In terms of the matrix $\bar{\mathcal{K}}_{ij}$, this scheme invites setting $\bar{\mathcal{K}}_{ij} = \int_{\alpha_i - h/2}^{\alpha_i + h/2} s(\alpha)\, d\alpha$, where at $\alpha_1$ and $\alpha_N$ one only integrates from $\alpha_1$ and to $\alpha_N$, respectively. Strict numerics would tell one that this tapering with the first and last step does not mak much sense—in practice, it does. After this procedure, one transposes $\bar{\mathcal{K}}_{ij}$ and repeats it. Since the eigenvalues of a matrix and its transpose are identical, one does not need to undo the transposition.

### 4.5.2. Accuracy

The accuracy of the eigenvalues obtained by this discretisation depends on a number of parameters. Given that the purpose of my numerical calculations mainly is checking whether or not the approximations that lead the kernel in (140) deliver results comparable to those of Read, an accuracy of a few percent in the eigenvalues will suffice. What parameters are needed to attain this accuracy?

Firstly, the accuracy with which the kernel can be computed. Apart from the problems near the diagonal mentioned above, this is not a very serious issue. To check this, I have evaluated the expressions for the kernel in Maple with various settings of Maple's digits parameter and found that the expressions are not particularly prone to round-off errors. The values resulting from the C++ programme that delivered the results were in every case correct to at least five digits, in most cases correct to four digits less than machine accuracy.

Secondly, the numerical condition of matrix with respect to Schur's algorithm that was used to compute the eigenvalues. If this problem was ill-conditioned, one would expect slightly different discretisation sizes to lead to significantly different results. This is not the case; for example, computing the largest mathematical eigenvalue for a $m = 2$ perturbation with $\omega = 0.5$ in a $\sigma = 0.2$ disk, one finds that with $N = 250$, the eigenvalue is $0.8932459 - 1.253385\mathrm{i}$, whereas for $N = 251$, one finds $0.8932604 - 1.253254\mathrm{i}$.

Finally, the parameters of the discretisation, $N$ and $L$, influence the accuracy of the eigenvalues. For the $\omega = 0.5$, $\sigma = 0.2$ disk, one finds that the largest mathematical eigenvalues for an $m = 2$ perturbation are $0.892403 - 1.26264\mathrm{i}$ when $N = 150$ and $L = 30$, whereas for $N = 300$ and $L = 60$ it is $0.892419 - 1.26247\mathrm{i}$. So, for this moderately high $\sigma$, $L = 30$ would easily suffice for precision in the range of one per cent. As $\sigma$ decreases, however, the $L$ required to attain a given precision increases, and thus I use $L = 40$ in the calculations below unless otherwise stated.

The accuracy of the solution depends on $N$ through the grid point spacing $L/(N-1)$. Having $N = 200$ at $L = 30$, the largest mathematical eigenvalue is $0.89342 - 1.251445$, with $N = 300$, it is $0.89413 - 1.243457$, and with $N = 400$, it is $0.89437 - 1.240663$. It turns out that this

result is fairly generic, in that neither $\sigma$ nor $\omega$ significantly influence the dependence of the eigenvalues on $L/(N-1)$. Thus, with $L = 40$, $N = 250$ is a good choice.

# 5. The Classic Modes

The term "classic modes" here refers to the modes already well investigated by Read and, before her, Zang. The main purpose of this chapter is to show that in my approximation all the major features of the exact calculations show up, and that the quantitative results obtained from the two methods usually agree to within a few per cent.

## 5.1. Axisymmetric Stability

This chapter investigates the most fundamental stability property a disk can have, the stability against ring-like perturbations. In the potential basis (24), ring-like perturbations corresponds to setting $m = 0$. After this, $2\pi/\ln(\alpha)$ is the distance between two rings in the perturbation.

Axisymmetric stability is a fundamental stability property not only because it was the first to be closely investigated (Toomre 1964), but also because it is the equivalent of the Jeans instability in rotating disks. A long tradition of theoretical evidence and numerical experiments indicates that a disk susceptible to axisymmetric instabilities quickly fragmentates (e.g., Hockney and Hohl 1969).

To have a quick assessment of the stability of a disk, one frequently gives its Toomre-$Q$, defined as the ratio of its velocity dispersion to the velocity dispersion required for axisymmetric stability, $Q = \sigma/\sigma_{\min}$. The denominator in this definition is usually computed from the local analysis Toomre gave in 1964. As Zang showed, the local and global analyses are in excellent agreement for the Mestel disk. Whereas in real galactic disks $Q$ usually varies dramatically with the position within the disks, the self-consistent Mestel disk has one global $Q$.

### 5.1.1. Axisymmetric Stability of the Self-Consistent Disk

As Read remarks, $m = 0$ perturbations are not orientable and can therefore not rotate. Thus one may set $\omega = 0$ (or use a purely imaginary $\omega$ if one wants to investigate growing modes). However, in letting $m' = 0$ some care is required as once more, and one has to set $m = m' = 0$ in (78) and (86) to get the limit right—just setting $m' = 0$ in (110) leads to erroneous results. The two integrations over $L_z$ are as straightforward as in the general $\omega = 0$ case and yield

$$\mathcal{K}^{(m=0)} = \frac{\sqrt{1-2\sigma^2}^{1-1/\sigma^2}}{2\mathrm{e}\sigma^2} \frac{|\Gamma(1/4+\mathrm{i}\alpha'/2)|^2}{|\Gamma(3/4+\mathrm{i}\alpha'/2)|^2} \Big(1 - \mathrm{e}^{-\sigma^2\alpha'^2/2}\mathrm{I}_0(\sigma^2\alpha'^2/2)\Big). \tag{143}$$

To find modes, one has to look for $(\sigma, \alpha')$ pairs that solve $\mathcal{K}(\sigma, \alpha') = 1$. The special functions in (143) prevent an analytic solution of this problem, and so one has to take recourse to

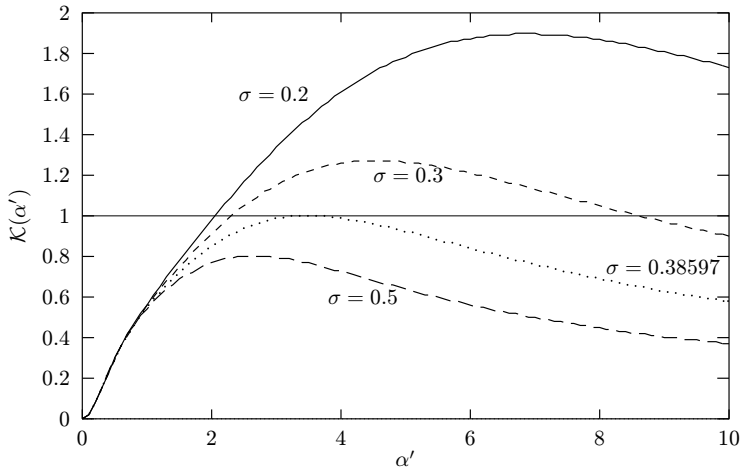


*Fig. 11: Plots of the kernel (143) governing $m = 0$ modes in the self-consistent Mestel disk for four values of $\sigma$.*

numerics. The result is shown in Fig. 11. For cool disks, $\mathcal{K}(\alpha')$ crosses unity twice, which means that there are two marginal modes in those disks. This will be of minor interest, since between them there are growing modes which will dominate those marginal modes. The axisymmetric modes set in at $\sigma = 0.3860$ with $\alpha_{\rm crit} = 3.51$. Below this threshold, the disks are stable against axisymmetric perturbations.

This result is in remarkable agreement with the findings of Read. She found that $\sigma = 0.3780$ was required to stabilise the disk, and the critical wavelength is $\alpha_{\rm crit} = 3.46$. The figures agree to within 2% in both $\sigma$ and $\alpha_{\rm crit}$, which in a way is surprising given that those disks are already quite hot, and thus a large number of stars will be on orbits for which the approximations in chapter 2.1 are very poor. On the other hand, this stability limit is fairly generic and is already given correctly in a local analysis without assuming a specific disk model. Therefore, while it is reassuring that it is reproduced, the agreement is not really an indicator for the quality of the approximation.

I will use $Q = \sigma/0.3860$ in the rest of the work for consistency, although it does not make much of a difference.

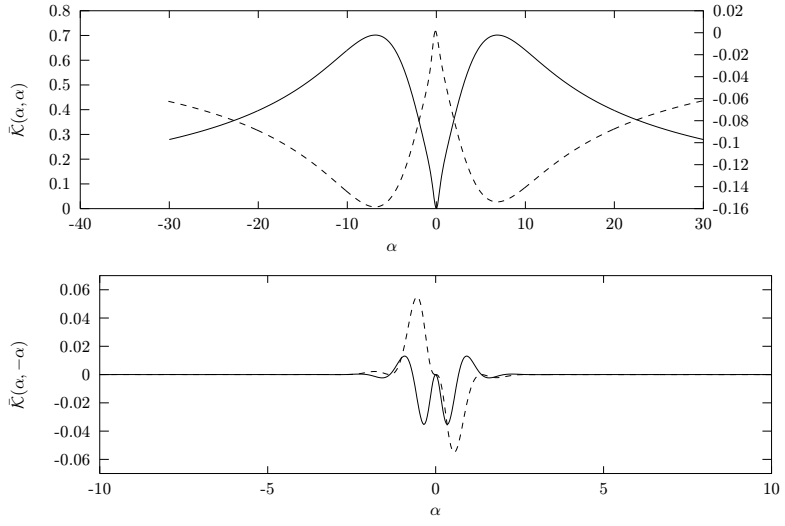


*Fig. 12: The kernel for axisymmetric perturbations of the cut-out disk ($\sigma = 0.2$). In the upper figure, the real (solid line) and the imaginary part (dotted, the right scale applies) along the diagonal is shown. In this case, the imaginary part is plotted a little bit off the diagonal since it vanishes exactly on the diagonal. In the lower plot, the real (solid line) and the imaginary part of the kernel are shown along the secondary axis.*

### 5.1.2. Axisymmetric stability of the Cut-Out Disk

For determining the axisymmetric stability of the cut-out disks, the kernel derived for the general case is again unsuitable since letting $m = 0$ in the finished expression for the kernel delivers incorrect results. Instead, one has to back up to perform the $L_z$ integration with $\omega = 0$ and $m = 0$. Again, this setting greatly simplifies the calculations that finally yields

$$\bar{\mathcal{K}}^{(m'=0)}(\alpha,\alpha') = \mathrm{i}\big(L_c^{\mathrm{i}(\alpha-\alpha')} - L_0^{\mathrm{i}(\alpha-\alpha')}\big)\frac{L_c^2\sqrt{1-2\sigma^2}^{1+1/\sigma^2}}{4\sigma^2(L_0^2-L_c^2)(\mathrm{e}^{-\pi(\alpha-\alpha')}-1)}\frac{\big|\Gamma\big((1+2\mathrm{i}\alpha')/4\big)\big|^2}{\big|\Gamma\big((3+2\mathrm{i}\alpha')/4\big)\big|^2}$$
$$\left(\mathrm{I}_0\big(\sigma^2\alpha\alpha'/2\big) - \mathrm{e}^{\sigma^2\alpha\alpha'/2}\right) \tag{144}$$

As Zang (1976) first noted (and one might suspect from the visual appearance of the cuts through the kernel in Fig. 12), the kernel of the integral equation governing axisymmetric perturbations of the Mestel disk can be brought to Hermitian form. The transformation that does this is identical to the one used by Zang. The basic observation is that (144) would be Hermitian but for the terms with the Gamma function. Looking back at (140), one sees that by writing the integral equation for a new function $\tilde{\Phi}_{\alpha,m} = \sqrt{K_m(\alpha)}\Phi_{\alpha,m}$, one attains Hermitian symmetry in the resulting kernel $\sqrt{K'_m(\alpha)/K'_m(\alpha')}\bar{\mathcal{K}}^{(m'=0)}(\alpha,\alpha')$. Now, if the kernel is equivalent to a Hermitian kernel, its eigenvalues will be real, and, as it turns out when using the machinery developed in chapter 4.5 on this kernel, this is indeed the case.

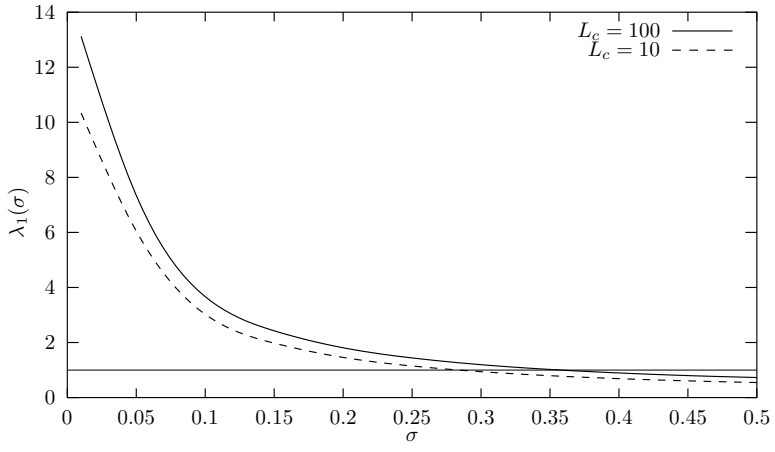


*Fig. 13: The largest mathematical eigenvalue of the $m = 0$ cut-out disk as a function of $\sigma$ for two values of the outer cut-out $L_c$.*

After that, finding the limit for marginal stability is just a matter of determining for which $\sigma$ the largest mathematical eigenvalue is unity. For the doubly cut-out disk with $L_c = 100$ (I deviate from my standard $L_c = 10$ following Read in this) one finds $\sigma_{\min} = 0.349$ or $Q = 0.904$, where Read has $\sigma_{\min} = 0.327$ or $Q = 0.866$. These figures agree to within about 5%, which is somewhat worse than the agreement in the self-similar disk. After the discussion at the end of the last subsection this does not come as a surprise. In the case of the cut-out disk the global structure of the disk plays a major role, and it is clear that at $\sigma \approx 0.35$ this global structure is already quite distorted by the approximations. Still, the qualitative result is that the cut-out slightly destabilises the disk, and also quantitatively the agreement is quite satisfactory.

On reducing $L_c$, the disks become more stable. For example, at $L_c = 10$, $\sigma_{\min} = 0.274$. This is easily explained by the reduced surface density of the disk.

## 5.2. One-Armed Modes

Both the works of Read and Zang found that the $m = 1$ modes are the most unstable in Mestel disks. This came as a surprise at least to Zang, since the classic picture of a spiral galaxy invariably involved a two-armed pattern. As a matter of fact, a marginally stable ($Q = 1$) cut-out disk admits *only* one-armed growing modes (at least with my choice of the index of the inner cut-out). In this chapter, I will show that the present formalism reproduces this result. The more exotic features of the $m = 1$ perturbation in the Mestel disk are also recovered.

### 5.2.1. Neutral Modes in the Self-Consistent Disk

The $m > 0$ cases are more complicated than the axisymmetric case was, since now one has to decide on the solvability of the full integral equation (111) with the kernel (118). Making this decision is quite involved indeed and requires techniques different from those applied when $\omega = 0$ or with a cut-out. Furthermore, neither Read nor Zang could solve this problem, but both were rather convinced from indirect arguments that growing modes should not exist in the self-consistent disk.

For these reasons, I postpone pondering this issue to chapter 6 and for now stick to the "classic modes" known to Read. In the self-consistent disk, those are the neutral modes, i.e. single logarithmic spirals with $\omega = 0$. Since a growth rate or a pattern speed would introduce time or length scales which the Mestel disk does not provide, those neutral modes are the only type of isolated modes that are possible in the self-consistent disk without breaking its self-similarity.

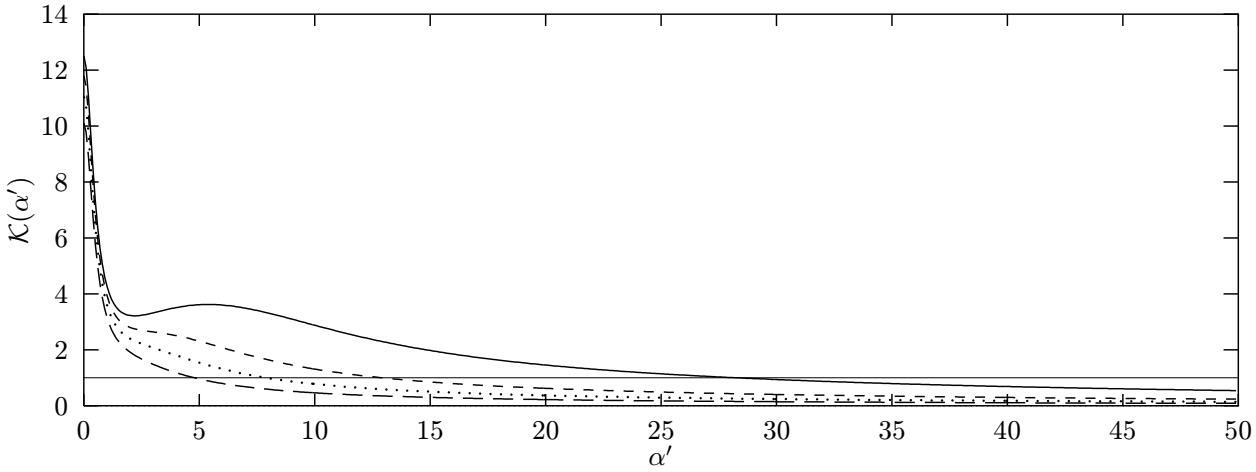


*Fig. 14: The kernel for neutral $m = 1$ modes. I show curves for (top to bottom) $\sigma = 0.2$, $\sigma = 0.3$, $\sigma = 0.38597$, and $\sigma = 0.5$.*

To find modes, one has to solve (121) for a given $\sigma$. Again, this can only be done numerically (or graphically). At least qualitatively, however, one can already say that as long as my approximations are valid, the self-consistent disk will admit neutral $m = 1$ modes at *any* temperature. Evaluating the kernel at $\alpha' = 0$, one sees that at least for $\sigma < 1/\sqrt{2}$, the kernel is larger than 1, whereas $\mathcal{K}$ tends to zero for $\alpha' \to \infty$. This latter asymptotics can be seen by recalling that $\mathrm{I}_\nu(z) \sim \mathrm{e}^z/\sqrt{2\pi z}$ for large $z$, which, combined with the factor $\exp(-\sigma^2\alpha'^2/2)$ and a $1/\alpha'$ form the Gamma functions gives the kernel an asymptotics of $\alpha'^{-3/2}$. Thus, for large $\alpha'$, the kernel vanishes, and because it is a continuous function of $\alpha'$, it must cross the $\mathcal{K} = 1$-line at some $\alpha'$. Indeed, as Fig. 14 indicates, this seems to be the case. As $\sigma$ increases, the wave number of the mode decreases.

Of course, it does not seem likely that a disk admits modes at any temperature form an astrophysical point of view. While one could maintain that at some point the linearised analysis will certainly no longer be applicable and higher contributions would suppress the modes, the behaviour found here is probably related to the fact that $m = 1$ perturbations can shift the centre of mass of the disk and that density cusps in the centres of galaxies tend to be unstable. This phenomenon is well known from numerical studies and was noticed as early as 1963 by von Hoerner as a nuisance and later re-discovered by Miller and Smith (1992) who investigated it on its own right. Recently, Taga (1999) reported his simulations lead him to believe that a black hole embedded in a dense stellar cluster would become unstable to to displacements when its mass was below about 10% of the mass of the cluster; for the Mestel disk, the central singularity is not associated with a compact object at all, and thus this 10%-rule would certainly make the cusp eligible for the displacement instability. In the formalism used here, the centre of mass is artificially kept fixed. Given these results, this is a serious forcing, and it appears entirely possible that the instability of the centre cusp—that is not dynamically present in the cut-out disk—resurfaces as the non-quenchable $m = 1$ instability. On the other hand, all this might as well be interpreatble along the lines of what I discuss in the context of the very similar behaviour is found for $m = 4$ in chapter 5.5. Possibly this issue might be decided by the appearence of the true marginal mode (as the limit of growing modes) arising from the equations laid out in chapter 6.1.

On a side note, the kernel (120) is symmetric in $\alpha'$. This means that in addition to "trailing" modes with positive $\alpha'$ (the disk stars enter the spiral arm from the convex side), there is also a "leading" one (the stars enter the arm from the concave side). This could have been anticipated since both modes are steady state solutions of a time-reversible physical system—both the Poisson and the Boltzmann equation are ignorant of the time arrow—, and thus the anti-spiral theorem (Lynden-Bell and Ostriker 1967) applies. The situation for the modes in the cut-out disk is different, since by application of Landau's rule in their construction they are limits of growing modes and thus not steady-state solutions even when their growth rate vanishes.

### 5.2.2. Modes in the Cut-Out Disk

In contrast to the self-consistent disk, the cut-out disk has a characteristic length scale ($L_0$, say), and $\omega$ is present in many terms in the kernel. Thus, discrete and growing modes should be possible. However, finding them is more difficult than in the axisymmetric case. The

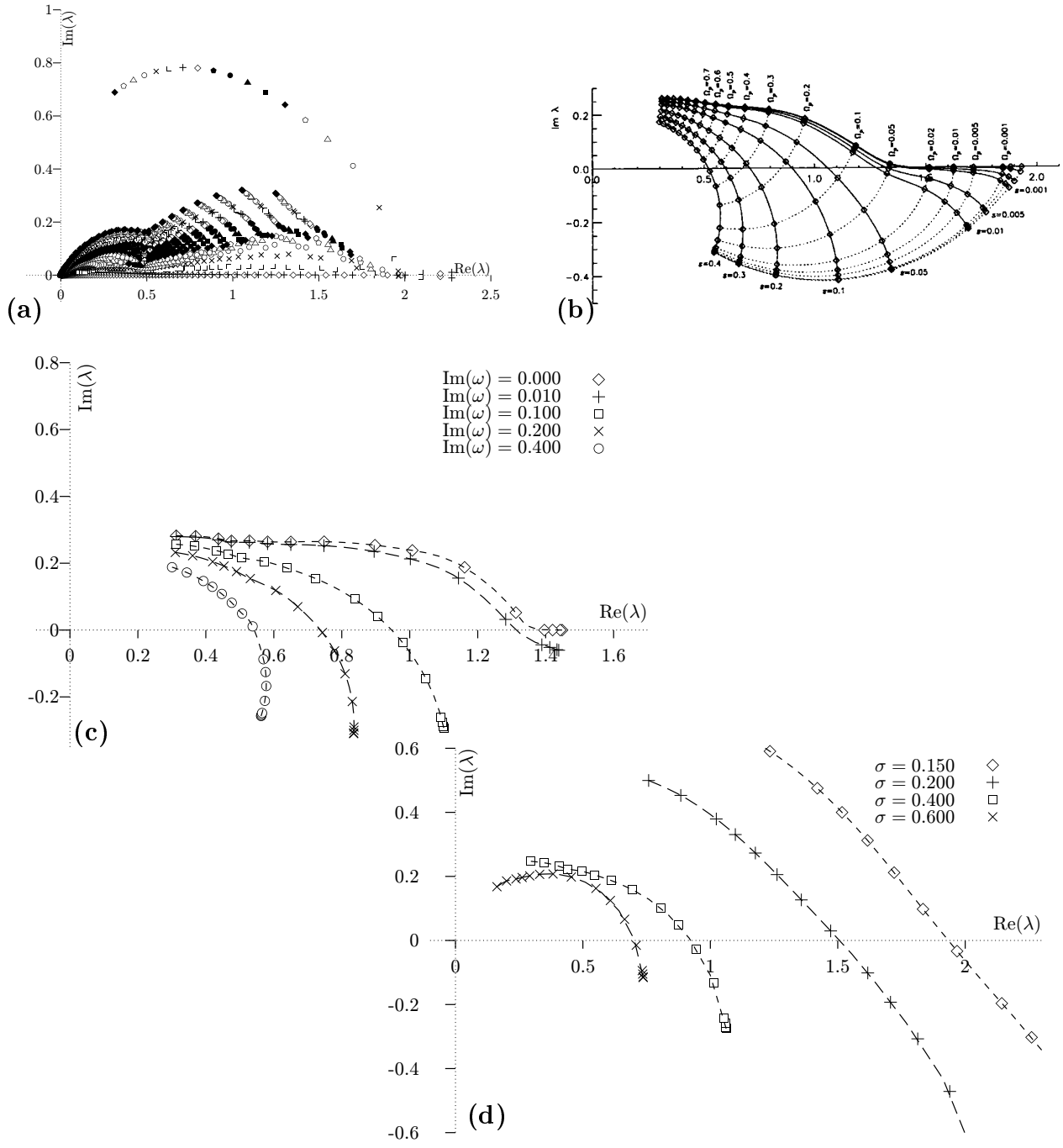


*Fig. 15: Eigenvalues of the cut-out $m = 1$ kernel. (a) shows spectra for kernels with $\omega = 0.001 \cdots 0.6$ in 20 steps, where each symbol corresponds to one value of $\omega$ (for most of them, actually two values, the symbols repeat after the filled circle); (b) is a plot of the largest mathematical eigenvalues of a $Q = 1$ disk versus the $Re(\omega)$ and growth rate $s = \mathrm{Im}(\omega)$ for Read's calculations for the inner cut-out disk, taken from Read (1997) with kind permission of the author; (c) is a plot of the eigenvalues with the largest real part form the approximated kernel versus* $\mathrm{Re}(\omega) = (0.0001, 0.001, 0.005, 0.01, 0.05, 0.1, 0.15, 0.2, 0.3, 0.4, 0.5, 0.6, 0.7, 0.8, 0.9, 1.0, 1.2)$ *and the indicated values of* $\mathrm{Im}(\omega)$*; (d) is the same plot for a fixed growth rate* $\mathrm{Im}(\omega) = 0.1$ *and the indicated values of the velocity dispersion* $\sigma$*.*

symmetry of the kernel that resulted in purely real eigenvalues is broken for nonzero $m$, and therefore the eigenvalues will in general be complex.

Pondering the kernel depicted in Fig. 17, one recognises the features discussed in chapter 3.6: A contribution reaching out to large $\alpha$ on the diagonal, quite pronounced in this case, and a spur along the secondary diagonal. The trailing bias discussed above is of course present here, too. As the $m = 1$ kernel of the self-consistent disk (Fig. 6b), the kernel, though still symmetric on the diagonal, quickly attains some distinctly antisymmetrical (w.r.t. the secondary diagonal) component, but has a roughly symmetrical appearance farther away from the diagonal.

Figure 15a shows the eigenvalue spectra of the $m = 1$ kernels for a few values of real $\omega$ (i.e., the plot only shows kernels describing marginal modes). The eye-catcher in this diagram is the arc that spans from about $0.3 + 0.7\mathrm{i}$ to $1.9 + 0\mathrm{i}$ far above the bulk of the eigenvalues. Those "rogue" eigenvalues do not show up for any azimuthal harmonic except $m = 1$.

Speculating for the moment, the physical significance of this feature can be expected to lie in one of the two features special to $m = 1$ modes, namely either the fact that the one-armed modes do not possess an inner Lindblad resonance, or that they can move the centre of gravity in violation of my assumptions. It seems hard to decide this matter handwavingly. Fortunately, this issue is not relevant for the basic stability properties of the disks because the eigenvalue with the largest real part will always be in the bulk part of the spectrum. However, in the plots of the largest eigenvalues I use the ones with the largest real part when $m = 1$, whereas for the other azimuthal harmonics I use the ones with the largest moduli.

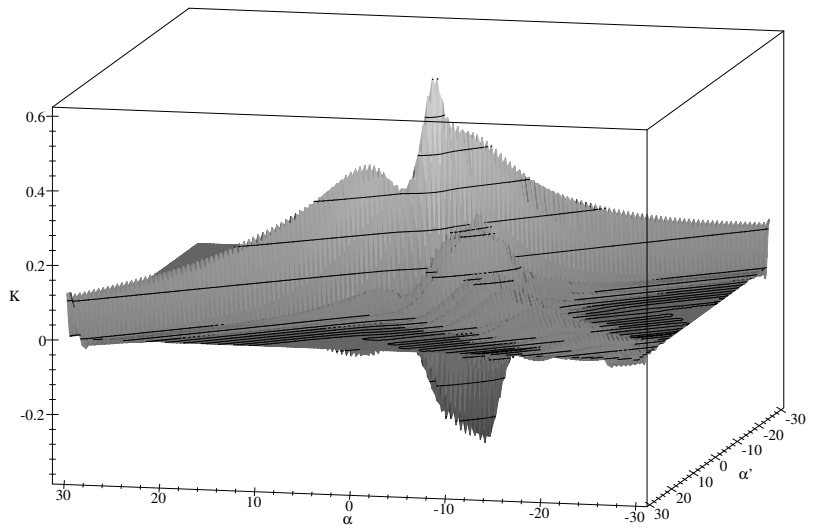


*Fig. 17: The real part of the kernel for $m = 1$ perturbations of the cut-out disk. This kernel is for a velocity dispersion $\sigma = 0.3$. The imaginary part is quite similar.*

This bulk part of the spectrum is quite simple: for each kernel, the eigenvalues are grouped along a dented curve from the origin to some point in the upper half plane, where this point lies the farther out the in the upper half plane the larger $\omega$ is. For very small $\omega$, the spectrum is almost aligned along the real axis. Apparently, no eigenvalues are located below the real axis as long as $\mathrm{Im}(\omega) = 0$, but the curves approach the real axis as $\omega$ decreases.

Most eigenvalues come in pairs, which, given the limited accuracy of the calculation, may well indicate that each pair actually corresponds to exactly one eigenvalue with a two-dimensional eigenspace. I will return to this issue when discussing the $m = 2$ modes.

Those eigenvalues as such are, however, only of limited interest, since all the physics is in the eigenvalue $\lambda = 1 + 0\mathrm{i}$; only the eigenvector(s) belonging to this eigenvalue correspond to modes in the disk described by the kernel under scrutiny. The obvious question now is whether these exist. Before plunging into the numerics, one should first approach the problem from a point of view of the theory of complex functions. Reformulating (141), one has

$$\lambda(\omega) = \frac{1}{\Phi_{m'}\big(\alpha'(\omega)\big)} \int \bar{\mathcal{K}}\big(\alpha, \alpha'(\omega)\big)\Phi_{m'}(\alpha)\, d\alpha. \tag{145}$$

Solutions $\Phi_{m'}(\alpha)$ that I am interested in will be depend at least continuously on $\omega$, and I require that they do not vanish except on countably many isolated points (with these assumptions, $\Phi_{m'}(\alpha)$ must even be an analytic function of $\omega$ because of its definition via an integral). Now (145) can be read as the definition of a function $\lambda(\omega)$, and since $\bar{\mathcal{K}}$ is an analytic function of $\omega$ in the sliced plane (taken as a complex number with a mode's growth rate in the imaginary part) and this property carries through the integration, $\lambda(\omega)$ is analytic as well. This means that one can exploit the rich theory of conformal mappings when exploring the mapping between $\omega$ and the mathematical eigenvalues.

Fig. 15c shows a part of this mapping by plotting the largest mathematical eigenvalues for various complex $\omega$ in the $(\mathrm{Re}\,\lambda, \mathrm{Im}\,\lambda)$ plane. Points of equal $\mathrm{Im}(\omega)$ are connected by spline-interpolated lines. The decisive point in this diagram is $\lambda = 1{+}0\mathrm{i}$, since when a line crosses the real axis there, the disk admits a mode with the corresponding growth rate. However, since $\lambda(\omega)$ is (as good as) analytic, it depends on $\omega$ continuously, i.e., when the line corresponding to a growth rate $\mathrm{Im}(\omega_1)$ crosses the real axis left of $1 + 0\mathrm{i}$ and the another of growth rate $\mathrm{Im}(\omega_2)$ right of it, the midpoint theorem states that there has to be a growth rate $\mathrm{Im}(\omega_0)$ in between that for some $\mathrm{Re}(\omega)$ has an eigenvalue $1 + 0\mathrm{i}$.

A similar reasoning works for $\sigma$ with the difference that of course the kernel is not an analytic function of $\omega + \mathrm{i}\sigma$. Still, using that $\lambda(\sigma)$ is continuous, one may again use the midpoint theorem to state that when the eigenvalue line corresponding to various $\mathrm{Re}(\omega)$ at a given growth rate $\mathrm{Im}(\omega)$ crosses the real axis right of unity and if for large velocity dispersions all eigenvalues are left of the $\mathrm{Re}(\lambda) = 1$ line, then there will be at least one $\sigma_0$ which allows a unity eigenvalue for at least one $\omega$ with the given growth rate as its imaginary part.

So, while the only point in the diagram relevant for the physics in the Figure 15b is $1 + 0\mathrm{i}$, the mappings $\lambda(\omega)$ and $\lambda(\sigma)$ do contain valuable information. The first thing to note is that at the velocity dispersion at which this plot was made ($\sigma = 0.3860$, corresponding to $Q = 1$), there should indeed be a growth rate for which the kernel has a unity eigenvalue, and thus, it does admit a growing mode.

This issue is much more difficult for the marginal ($\mathrm{Im}(\omega) = 0$) mode. From the graph, it is hard to tell whether or not it eventually reaches (or crosses) the real axis. In the above discussion of the spectrum of the kernel governing marginal modes (Fig. 15a), it was already pointed out that a very accurate calculation would probably show that all eigenvalues have positive imaginary parts. But even when using 800 discretisation points on a grid of $120 \times 120$ in $\alpha$ and $\alpha'$, the largest eigenvalue of a $Q = 1$ kernel is at $1.7485 - 4.053 \times 10^{-9}$—certainly attempting a decision on the positions of the true eigenvalues with respect to the real axis are very daring given the uncertainties involved with computing eigenvalues of matrices of that size.

A related question is whether the slow march of the $\omega = \epsilon + 0\mathrm{i}$ eigenvalue along the real axis as $\epsilon \to 0$ apparent in Fig. 15c continues or stops. It appears that it does stop at $\omega = 1.47$; at least going from $\omega = 10^{-6}$ to $\omega = 10^{-8}$ does not change the leading five figures of the eigenvalue $1.4753 - 7.4499 \times 10^{-7}$ when evaluating the kernel on a $N = 200$ grid.

Comparing Read's results in Fig. 15b (for an inner cut-out disks, so one has to expect her disks to be somewhat more stable) and my results in Fig. 15c, one immediately notices that although the curves roughly match, there are some differences in details. Read's curves approach the real axis somewhat faster, and they reach out to far larger values of $\mathrm{Re}(\lambda)$ as $\omega \to 0$. While the first disagreement is not very worrisome, particularly because for nonzero growth rate there is as good an agreement in the points where the $\lambda(\omega)$ curves cross the real axis as can be expected given that Read's disk only has an inner cut-out, the second one is serious since it will lead to different stability predictions in the limit of vanishing growth rate; while it appears uncertain if cut-out Mestel disks could ever be stabilised against $m = 1$ perturbations from Fig. 15b and indeed Read does not even attempt to find a $\sigma$ that would do this, Fig. 15c nourishes hope that the disks might eventually become stable as one raises the velocity dispersion.

In fact, this is a point in which the doubly cut-out disk behaves significantly different from the inner-cut out disk. Increasing the outer cut-out angular momentum $L_c$ to 100 raises the largest mathematical eigenvalue to 1.889 for $\omega = 0.0001$ and to 1.890 for $\omega = 0.00001$ when $Q = 1$. For $L_c = 1000$ the respective numbers are 1.926 and 1.928. Thus, the less important the outer cut-out becomes, the larger are the largest mathematical eigenvalues. Obviously, the infinite mass in the remote parts of the disk destabilises the inner parts with respect to $m = 1$ perturbations, and the behaviour of the doubly cut-out disk should be more applicable to real galaxies that do not have an infinite mass.

For an $L_c = 10$ doubly cut-out disk, one may attempt to determine a stability limit for the $m = 1$ perturbation. Evaluating the $m = 1$ kernel for $\omega = 10^{-8}$ on an $N = 200$ grid one finds that for $\sigma = 0.57$ the second-largest mathematical eigenvalue is unity within 0.001, and raising $\sigma$ further, it drops below unity. The value of this result might be somewhat debatable since $\sigma = 0.57$ is really a high velocity dispersion, at which not only my assumption that most stars are on almost circular orbits breaks down spectacularly but also the idea of a razor-thin disk becomes completely meaningless unless the approximate equipartition between radial and vertical degrees of freedom observed in spiral galaxies would be severely violated. Still, one can give a limit at which hypothetical disks would be stable against $m = 1$ perturbations.

The susceptibility of the cut-out disks to $m = 1$ modes might have been expected from a modal picture, since $m = 1$ modes do not possess an inner Lindblad resonance that could absorb density waves, which again means that as soon as some feedback loop is present, the instabilities will grow much easier than when an ILR is present that has to be hidden by some kind of $Q$-barrier. On a related note, Sellwood (1985) found in a series of simulations of various models of the Galaxy that without a halo, strong $m = 1$ perturbations develop on relatively short time scales. An outer cut-out effectively simulates such a halo and thus works to stabilise the disk.

I postpone the discussion of the solutions of the integral equation to the next chapter, in which I treat the aesthetically more satisfying two-armed spirals. Suffice it to say that the solutions do not look qualitatively different from the ones Read found.

## 5.3. Two-Armed Modes

The two-armed modes are of particular interest to investigations of spiral structure, mainly because it were the beautiful patterns of galaxies like M51 who inspired the first researchers to tackle the problem of the origin of this structure, and consequently, most of the early works on the subject were heavily biased towards two-armed patterns. Indeed, in the case of M51 and a few more of the classic galaxies, the $m = 2$ contribution dominates the decomposition of an image of the galaxy into angular harmonics in both the $V$- (supposed to trace gas and young stars) and $K$-band (which is thought to trace the bulk of the mass). In the case of M51, this was demonstrated quite convincingly by Rix and Rieke (1993).

However, the galaxies with the most impressive bisymmetric spiral structure almost invariably are part of a galaxy pair or group, and already the work of Toomre and Toomre (1972) had clearly shown that the interaction itself can form magnificent two-armed patterns even without self-gravity and thus instabilities in the disks themselves. Of course, the Toomre's own disclaimer cited in the introduction about the spiral structure that would have been there anyway cautions one not to overinterpret these findings.

Taking a less biased sample than the galaxies humans perceive as the most beautiful ones, the situation is far more complex (e.g., Naim et. al. 1995) with all kinds of azimuthal harmonics present in galaxies, including strong $m = 1$ components. So, maybe Zang's (1976) discomfort at finding that Mestel disks are quite stable against $m = 2$ perturbations was not so justified after all, even when Mestel disks are supposed to be more than a mere thought experiment.

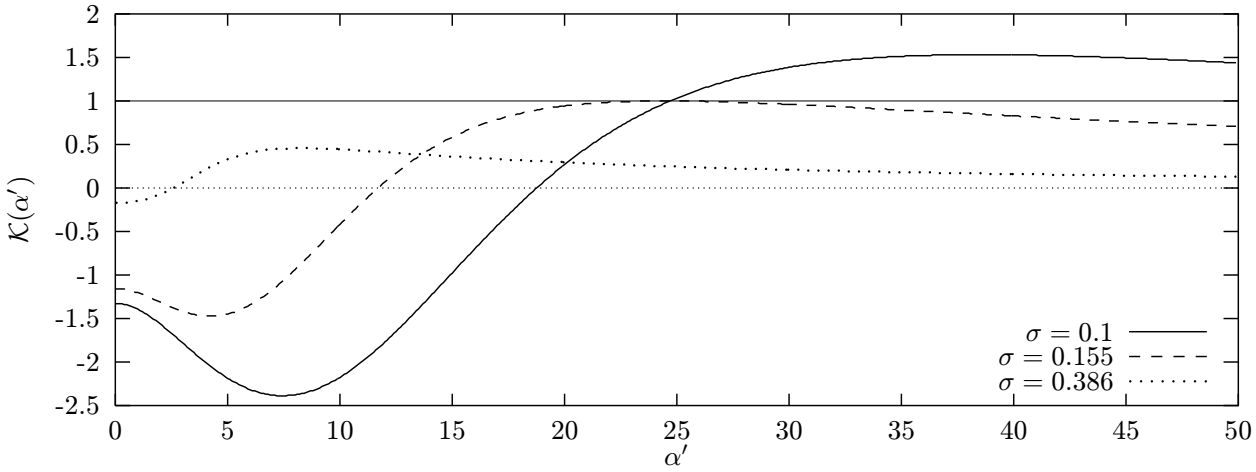


*Fig. 18: The kernel for neutral $m = 2$ perturbations in the self-consistent disk.*

### 5.3.1. Neutral Modes in the Self-Consistent Disk

Comparing Figure 18 with Figure 14, one first notices that the neutral $m = 2$ modes show a behaviour completely different from the neutral $m = 1$ modes. Their kernels start out below zero, decline a bit and then rise. After going through a maximum, they then settle down to zero for large $\alpha'$. The rise of the $Q = 1$ curve ($\sigma = 0.386$) is not nearly large enough to let it cross unity. Thus axisymmetrically stable disks do not admit neutral $m = 2$ modes.

The neutral $m = 2$ modes in the self-consistent disk set in at $\sigma = 0.155$ with $\alpha' = 25.18$. Read found that for her $\beta = -0.1$ disks, the modes set in at $\sigma = 0.156$ and for her $\beta = 0.1$ disks, at $\sigma = 0.149$ (Read 1999); unfortunately, she had no data available for the Mestel disk itself. Still, she expects that an interpolation would lead to a useful result (in her own words: *"In general, nothing special happened at $\beta = 0$. We wrote code specially for $\beta = 0$, using Zang's formulae, and the results always agreed with those from the general code with $\beta = \pm 0.001$ or something similarly small"*). It thus seems that here, again, my approximations deliver an excellent agreement with the more exact semi-analytic approach.

Beyond the limit of $\sigma = 0.155$, there are two branches of neutral modes since the kernel crosses the $\mathcal{K}(\alpha')$ line twice. Of course the remarks about the anti-spirality of the neutral modes apply here as well, so in total there are four branches of neutral $m = 2$ modes in the self-consistent Mestel disk.

### 5.3.2. Modes in the Cut-Out Disk

The kernel of the $m = 2$ modes in the cut-out disk (Fig. 21) has all the features familiar by now, set apart from the $m = 1$ kernel by its closer adherence to symmetry with respect to the secondary diagonal. Also, the diagonal appears less important in relation to the off-diagonal spur. Turning to the eigenvalue spectra in Fig. 19a now, one notices that in contrast to the $m = 1$ kernels, there usually are two branches of eigenvalues near the origin. Going towards eigenvalues of larger moduli, the branches merge to form a single arc of pairs of eigenvalues. In the superposition of the spectra shown in Fig. 19a, one sees that with decreasing $\omega$, the spectrum of a kernel is basically rotated clockwise and somewhat elongated. This leads to a series of arcs of eigenvalues. The most relevant of these arcs is the one with the largest moduli.

Those lines of eigenvalues of largest modulus are shown for three different values of the growth rate $\mathrm{Im}(\omega)$ in Fig. 19c. This figure can be be compared with Read's results in Fig. 19b, keeping in mind that these results are for a inner cut-out disk. While generally the approximated doubly cut-out disks are a little more more stable and the descent towards the real axis is a little steeper, the results match quite well (the match could be improved increasing $L_c$, thus lessening the impact of the outer cut-out).

Furthermore, with the outer cut-out an overtaking of eigenvalues occurs, i.e., the largest mathematical eigenvalue jumps from one family to a different one. This can be seen in the plot of the largest eigenvalues as a kink and is more clearly visible in the spectra of Fig. 19a. For high $\omega$, the largest eigenvalue belongs to the upper arc, whereas for lower $\omega$ it belongs the rightmost arc of pairs of eigenvalues.

The one most interesting number in the stability analysis is the velocity dispersion at which marginal modes set in; in the $M = N = 2$ cut-out disk, this happens at $\sigma = 0.214$ ($Q = 0.554$) with $\omega = 1.096$, corresponding to a pattern speed of $\Omega_p = 0.548$. Read's values (this time for the doubly cut-out disk) are $\sigma = 0.205$ ($Q = 0.542$) and $\omega = 1.164$, which translates into a discrepancy of 4% in both $\sigma$ and $\omega$; normalised onto the limit for axisymmetric stability, the difference in $Q$ is 2%. Given that the velocity dispersion in those disks is still quite high, this is a surprisingly good agreement.

The qualitative behaviour of the lines of largest eigenvalues as a function of $\sigma$ and $\omega$ for two-armed modes can be seen in Fig. 19d that can be compared to Read's Fig. 7.22 (where

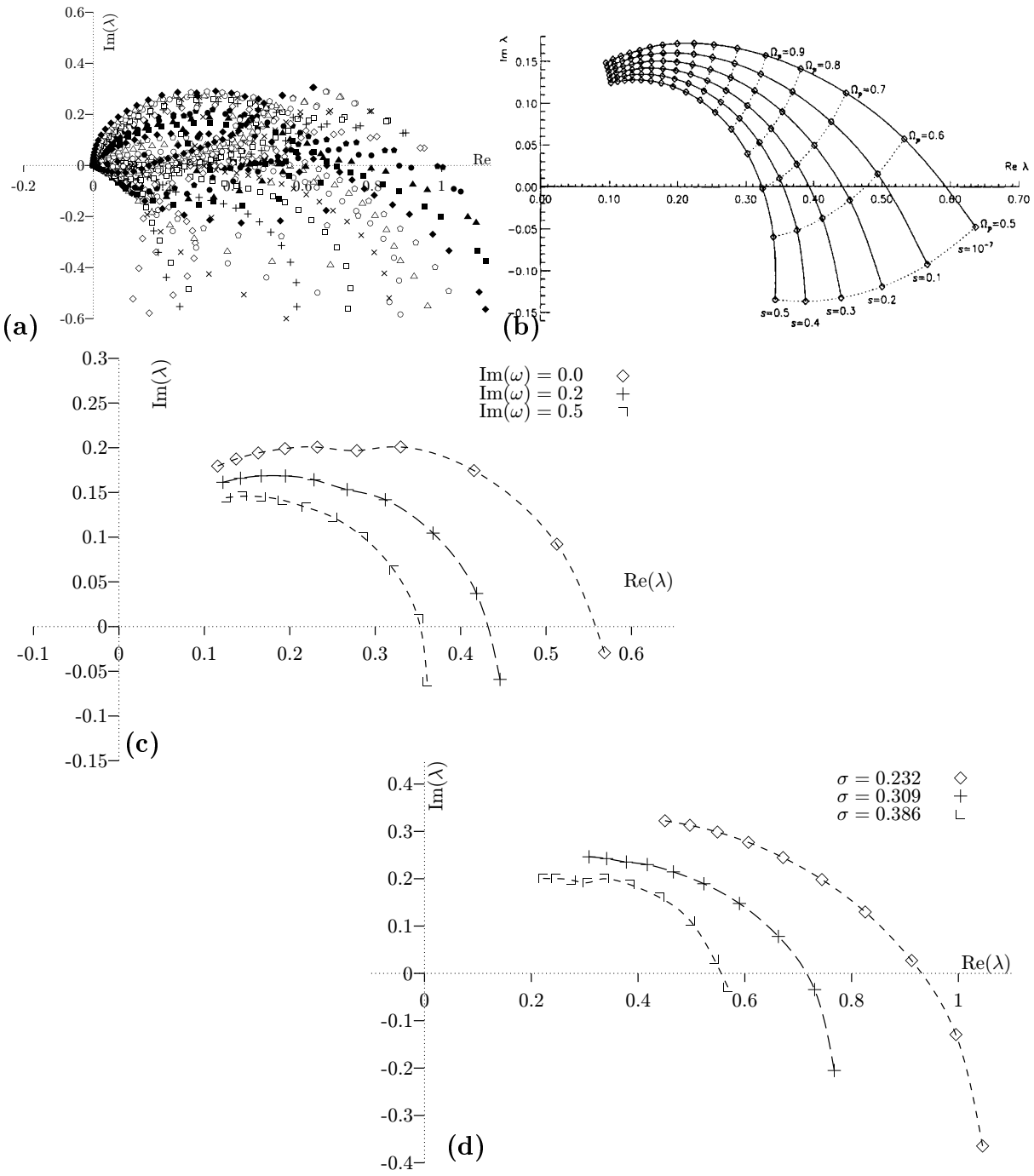


*Fig. 19: Eigenvalues of the cut-out $m = 2$ kernel. (a) shows the spectra for kernels from $\omega = 0.1 \cdots 1.2$ in 20 steps, the upmost points belonging to the $\omega = 1.2$ kernel; (b) is a plot of the largest mathematical eigenvalues of a $Q = 1$ disk versus $Re(\omega)$ and growth rate $s$ for Read's exact calculations, taken from Read (1997) with kind permission of the author; (c) is a plot of the largest mathematical eigenvalue versus the indicated values of the growth rate* $\mathrm{Im}(\omega)$ *and* $\mathrm{Re}(\omega) = 0.8 \cdots 2.2$ *in 5 steps; (d) is the same plot varying the velocity dispersion $\sigma$ instead.*

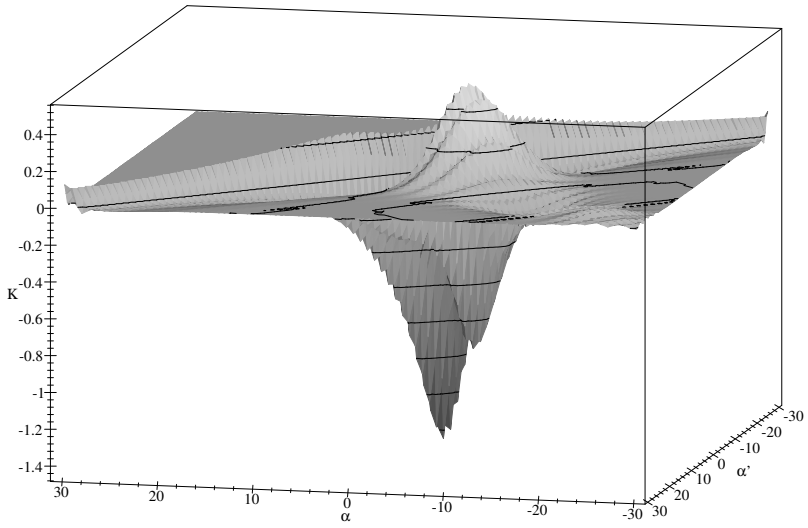


*Fig. 21: The real part of the kernel for $m = 2$ perturbations of the cut-out disk. To facilitate comparisons, as in the corresponding plot for $m = 1$ this kernel is for a velocity dispersion of $\sigma = 0.3$.*

the lines I computed are for $Q = 0.6$, $Q = 0.8$, and $Q = 1$), still bearing in mind that Read's disk has no outer cut-out. Again the approximation reproduces the previous results quite satisfactorily, with the doubly cut-out disk being a little more stable than its inner cut-out counterpart.

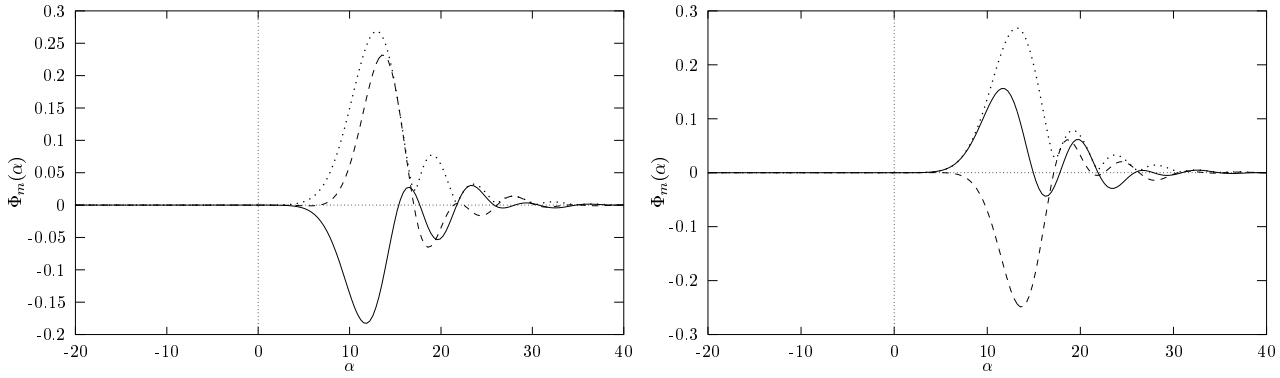


*Fig. 22: The eigenfunctions to the two largest eigenvalues of the kernel for $m = 2$ perturbations in the doubly cut-out disk. The solid line is the real part, the dashed line the imaginary part, and the dotted line is the absolute value.*

The marginal $m = 2$ mode is also a good example to discuss the general appearance of the modes. As in the $m = 1$ case, the eigenvalues come in pairs, with the difference that in the two-armed case this only is so after the two branches of the spectrum unite (cf. Fig. 19a). The obvious question is whether these pairs really are separate eigenvalues or rather a single eigenvalue with a two-dimensional eigenspace that are split up by numerical inaccuracies. While a thorough treatment of this issue would require some hard-core numerical mathematics, a "poor-man's approach" might yield at least an idea of what is going on.

An eigenvector $v_i$ to the eigenvalue $\lambda_i$ of a matrix $M$ certainly has $\delta_i := ||Mv_i - \lambda_i v_i||/||v_i|| = 0$. In the present case there is some numerical noise, but with $n = 300$ and $\lambda_1 = 1.00207 - 0.0012$ and $\lambda_2 = 0.9889 + 0.0024$, one has $\delta_1 = 2.3 \times 10^{-9}$ and $\delta_2 = 4.1 \times 10^{-9}$ for the marginal mode determined above, close enough to zero (I have used the Euclidean norm here).

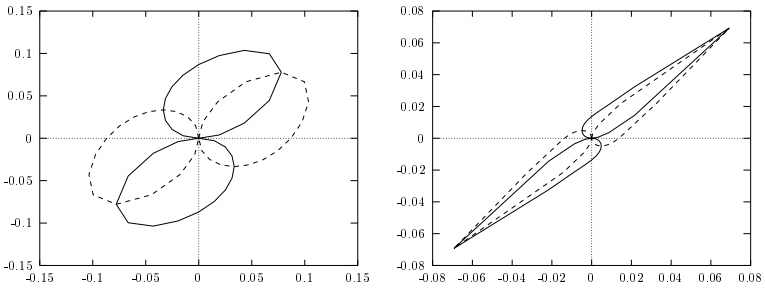


*Fig. 23: Parametric plots of $\bar{\delta}_1(\varphi)$ (solid line) and $\bar{\delta}_2(\varphi)$ (broken line). On the left, $n = 50$, on the right, $n = 300$. See text.*

If $\lambda_1 = \lambda_2$ (i.e., $\lambda_1$ is an eigenvalue f algebraic multiplicity $\geq 2$), clearly the eigenvectors of $\lambda_1$ would be the eigenvectors of $\lambda_2$ too, and indeed all linear combinations of these would be eigenvectors as well. If numerical errors have separated the eigenvalues, one would expect to see a remnant of this behaviour. Since ideally $\delta_i(v) := ||Mv - \lambda_j v||/||v||$ would vanish when $v$ is a linear combination of the eigenvectors of $\lambda_j$, one should see that $\bar{\delta}_{1,2}(\varphi) := \delta_{1,2}\big(\sin(\varphi)v_1 + \cos(\varphi)v_2\big)$ is "small", and it should furthermore not depend too heavily on $\varphi$, except where the linear combination suppresses one of the eigenvectors entirely. Given that the eigenvalues are different, the "small" in the last sentence will not mean $10^{-9}$, but it should be significantly smaller than the $\delta$ for an unrelated eigenvalue; for the eigenvector the the third largest eigenvalue one has, for example, $\delta_1(v_3) = 0.15$.

Referring to Fig. 23, one sees that the eigenvalues quite probably are distinct single eigenvalues, since with increasing numerical resolution the parametric plot of $\bar{\delta}(\varphi)$ becomes increasingly elongated, indicating that the mismatch of the sum of the eigenvectors is quite insensitive to the size of the grid. Note that this result most likely is not due to the fact that the two eigenvectors are "almost" linear dependent, $v_1 \approx -v_2$, which, when too severe, would make the numerics tricky – $\big\|v_1/\|v_1\| + v_2/\|v_2\|\big\|$ still is about 0.14, thus leaving enough headroom for numerics.

On the other hand, this issue is not too important for an assessment of the physics. The eigenvectors belonging to each of a pairs of eigenvalues will have about the same growth rate and will mix to some extent regardless if they really belong to a common eigenspace. And from Fig. 22 and Fig. 24 it is clear that these two modes are very similar anyway.

The basic features of these modes are quite as expected: There is no perturbation within the inner Lindblad resonance (ILR), the perturbation is quite strong between the ILR and the corotation (CR), and outside the CR the wave fades away, only barely reaching the outer Lindblad resonance. It is more or less coincidental that the position of the ILR quite nicely matches the inner edge of the spiral pattern, although it is tempting to specualte that the marginal mode occurs at that point in the $(\sigma, \omega)$ space right because the $Q$-barrier starts to shield the ILR. In general, though, one can move the $Q$-barrier out or the ILR in, so that there would be no waves that can reach the ILR in the first place.

Of course, this discussion is somewhat futile since a $M = N = 2$ cut-out disk will be badly instable when the $m = 2$ set in, and thus one would see everything but structures like those in Fig. 24.

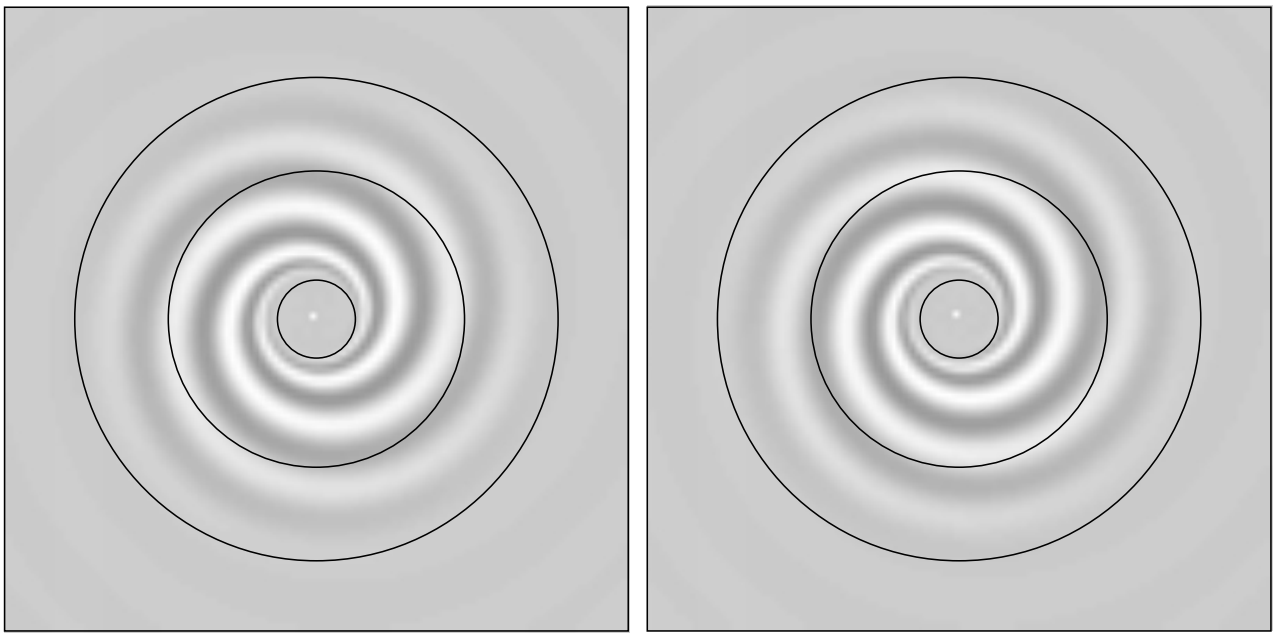

*Fig. 24: The modes belonging to the two eigenvalues close to one of the $m = 2$ kernel of the cut-out disk marginally stable against $m = 2$ perturbations. The circles mark the outer Lindblad resonance, the corotation, and the inner Lindblad resonance.*

## 5.4. Three-Armed Modes

Spiral galaxies with a pronounced three-armed pattern are not very common, and for some cases in which a galaxy shows one, Block and Wainscoat (1991) demonstrated that the stellar backbone of the galaxy still has a more or less bifold symmetry. Inspired by modal theory, Block et al (1994) suggested that the fact that the three-armed patterns are not found in the stellar backbone might indicate an ISM that is dynamically decoupled from the stellar backbone at least to some extent. On the other hand, it is as well conceivable that nonlinear coupling between modes of different $m$ could take place and destabilise an $m = 3$ mode that is stable by itself. Thus, although I will show that three-armed modes are yet more stable than $m = 2$ modes, there might be some merit in their examination in anticipation of a more complete theory taking into account nonlinear effects.

### 5.4.1. Neutral Modes in the Self-Consistent Disk

As shown in Fig. 25, the kernel for the neutral $m = 3$ modes starts out below zero for all $\sigma$ and finally levels out to zero, never approaching unity in the $\alpha$-range shown here. However, the curves for $\sigma = 0.05$ and $\sigma = 0.1$ are still rising at $\alpha = 70$, and it seems possible that they might eventually reach unity at some very large $\alpha$. However, even for a velocity dispersion as low as $\sigma = 0.05$, this is not the case; the $\sigma = 0.05$ curve, for example, reaches a wide maximum of 0.51 at $\alpha \approx 380$. An even cooler disk can be expected to admit neutral modes, but this is difficult to check because at large $\alpha$, the Gamma functions in the kernel (120) become really large, and although they could safely be replaced by their asymptotic expansions, it did not seem worth the effort to further pursue this issue. A $\sigma = 0.025$ kernel is still growing from 0.6 at $\alpha \approx 480$, and it seems likely that it will eventually cross the $\mathcal{K} = 1$ line.

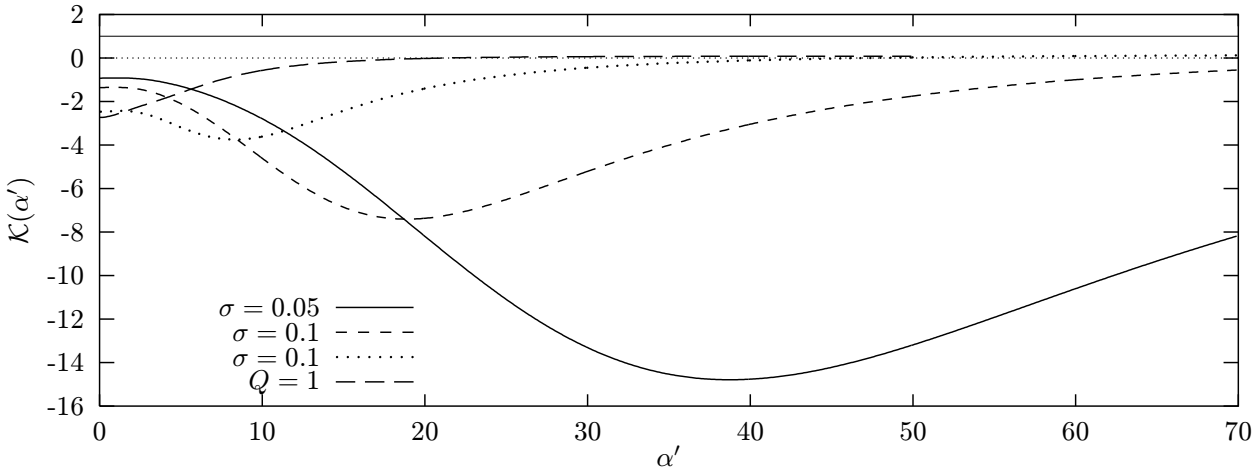


*Fig. 25: The kernel for neutral $m = 3$ perturbations in the self-consistent disk.*

This is exactly the behaviour Read found for her $\beta = 0$ disks.

### 5.4.2. Modes in the Cut-Out Disk

The $m = 3$ modes can be investigated quite analogously to the other non-axisymmetric modes. The kernel in Fig. 28 continues the pattern of off-diagonal contributions increasingly dominating over the diagonal as $m$ increases. Also, the width of the off-diagonal humps has further increased. Fig. 26a shows the spectra of some kernels. Again, increasing $\omega$ basically rotates a pattern counterclockwisely around the origin. The pattern itself is now a twofold arc with something like a tongue in between. It is striking that while the $m = 1$ spectra had one branch, the $m = 2$ spectra had two of them and the $m = 3$ spectra have three.

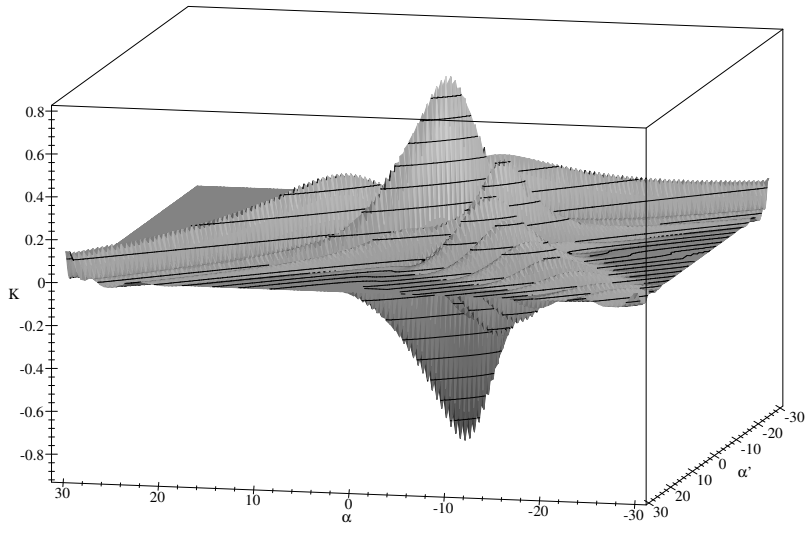


*Fig. 28: The real part of the kernel for $m = 3$ perturbations of the cut-out disk. As always for the kernel plots, $\sigma = 0.3$.*

The curves of largest eigenvalues versus $\sigma$ shows that cut out disks are more stable against $m = 3$ perturbations than they are against $m = 2$ perturbations. The $\sigma = 0.2$ disks near the margin of stability of the two-armed case are safely cross the real axis safely inside unity.

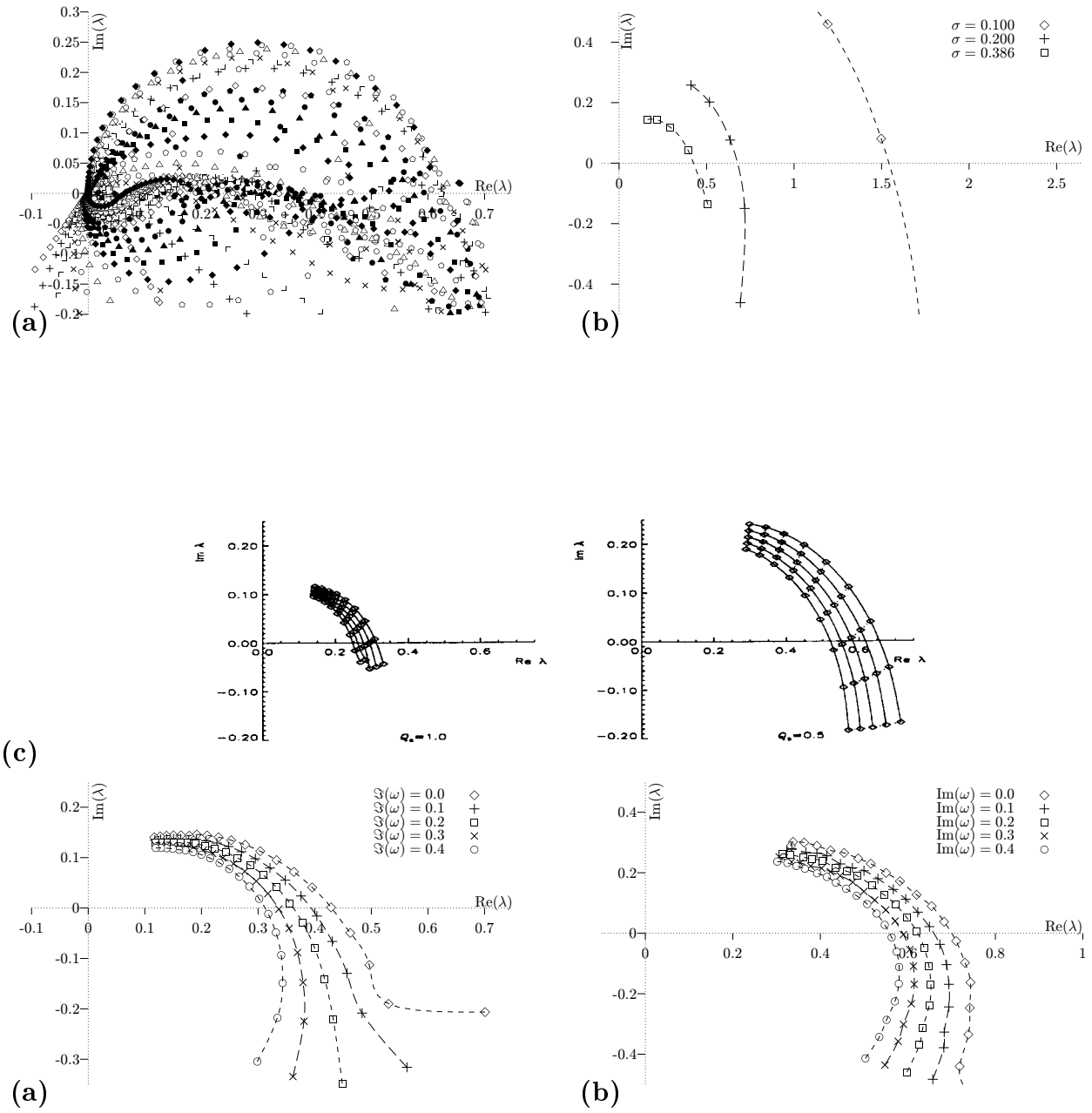


*Fig. 26: Eigenvalues of the cut-out $m = 3$ kernel. (a) shows the spectra for $\sigma = 0.205$ kernels from $\omega = 0.1 \cdots 2.0$ in 20 steps, the upmost points belonging to the $\omega = 2$ kernel; (b) is plot of the largest mathematical eigenvalue versus the indicated values of the velocity dispersion $\sigma$ and $\mathrm{Re}(\omega) = 0.8 \cdots 3.2$ in 5 steps; (c) are two plots of the largest mathematical eigenvalues of a $Q = 1$ (left) and a $Q = 0.5$ disk versus $Re(\omega) = 1.5 \cdots 3.9$ and growth rate $s = 0 \cdots 0.4$ for Read's exact calculations, taken from Read (1997) with kind permission of the author; (d) are two plots of the largest mathematical eigenvalue versus the indicated values of the growth rate $\mathrm{Im}(\omega)$ and $\mathrm{Re}(\omega) = 0.5 \cdots 3.9$ in 20 steps for a $Q = 1$ (left) and $Q = 0.5$ disk.*

The plots of largest mathematical eigenvalues versus $\omega$ at various growth rates show the familiar picture except that at very low $\omega$ the curve for the marginal mode bends towards large $\mathrm{Im}(\lambda)$. This is an artifact of too low numerical resolution, the corresponding kernels should be evaluated with a larger $L$.

Lowering the velocity dispersion further finally turns three-armed modes on at about $\sigma = 0.141$ with $\omega = 1.829$, corresponding to a pattern speed of $\Omega_p = 0.61$.

## 5.5. Four-Armed Modes

Generally speaking, the four-armed modes continue the pattern of the non-axisymmetric modes investigated so far in that Mestel disks are yet more stable against them than against their $m = 3$ cousins. However, the neutral modes do not fit into the picture drawn so far.

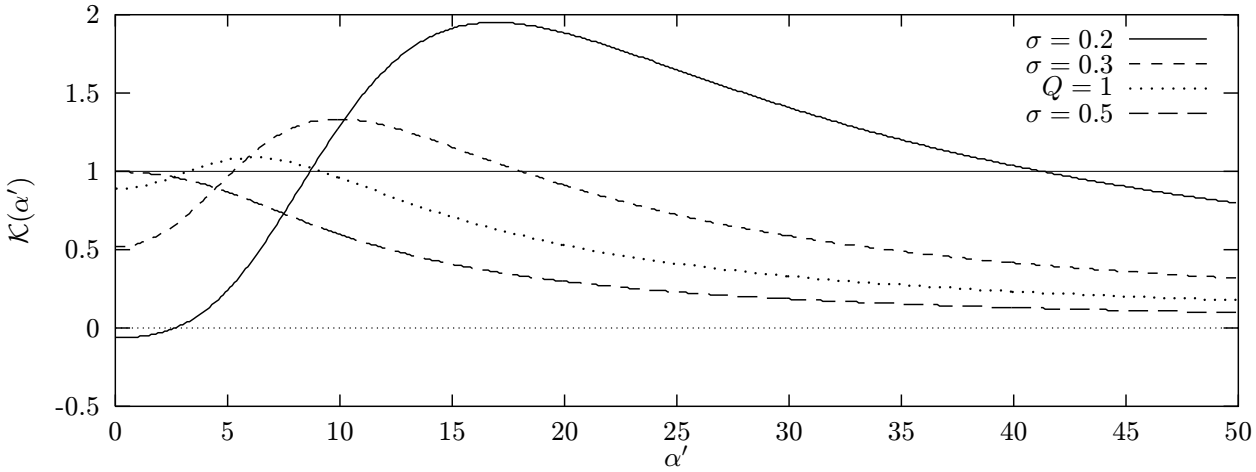


*Fig. 29: The kernel for neutral $m = 4$ perturbations in the self-consistent disk.*

### 5.5.1. Neutral Modes in the Self-Consistent Disk

In Fig. 29 one sees that the $m = 4$ neutral modes show a behaviour completely different from all previous cases. The cooler the disk, the lower the value of $\mathcal{K}(0)$, but also the greater the ascent afterwards. Even the $\sigma = 0.5$ disk can maintain a neutral mode. This reproduces what Read found out; in her more general perspective, the emergence of neutral modes at high temperatures seems to be linked to the existence or non-existence of closed orbits of $m$-fold symmetry in the case of three- and four-armed spirals, which, depending on the disk index $\beta$, may occur at $m = 3$ as well. Her hypothesis that stars on closed orbits "act as absorbers" and damp away the high-temperature modes, however, cannot be literally true. For one, neither for $m = 1$ nor for $m = 2$ do closed orbits of matching azimuthal symmetry exist, so high-temperature modes should exist, which, at least for $m = 2$, they do not. And secondly, in my disks no closed orbits of any azimuthal symmetry exist, since after the linearisation of $\Omega$ and $\kappa$ the two frequencies have the fixed ratio $\sqrt{2}$ and are thus strictly incommensurable.

Still, it seems likely that some kind of resonance does play a role here. Turning to (120), on sees that the contribution from the terms except the one with the sum is fairly independent

of $m$, whereas the sum does significantly change its value with $m$. The term to watch here is the $m'^2/(m'^2 - 2k^2)$. When $m' \approx \sqrt{2}k$, the corresponding summand is much larger than its neighbours since the ratio $I_k(x)$ and $I_{k+1}(x)$ basically is $k$ (plus some constant) and everything else does not depend on $k$; when $m$ is not too large, that "resonant" summand will dominate the value of the entire series. The sign of this resonant summand is determined by the side relative to the nearest $k$ on which $m' - \sqrt{2}k$ reaches its minimum—for the $m = 3$ series, the near-resonance is at $k = 2$ and thus one has a positive contribution with $m' - \sqrt{2}k = 0.17$ that enters into the kernel negatively (enhancing stability), whereas the resonance for the $m = 4$ occurs for $m' - \sqrt{2}k = -0.24$ and thus destabilises the disk. The next azimuthal harmonic that has an $m$ close to a $\sqrt{2}k$ is 7, and it is again negative; not surprisingly, the $m = 7$ harmonic is quite unstable as well.

Unfortunately, $k$ has no immediate meaning in physical terms, although it does have a loose connection to Read's radial harmonic number $l$. This latter quantity arises via a discrete Fourier transformation, whereas the source of the $k$ is (85) that can be viewed as a sort of modified discrete Fourier transform of some oscillatory function of the auxiliary angle $w_1'$. However, it is hard to attach a tangible meaning to $w_1'$ since it only enters the the distribution function through an integral, and the presence of the Bessel function in the sum does not exactly clarify the situation. But although $k$ is quite far from being anything like the index to a Fourier series of as $l$ is in Read's calculation, it seems that it should eventually end up imprinting itself as some kind of symmetry in the epicyclic variable $w_1$ of the perturbed distribution function (cf. Eq. 44).

If this is true, the interpretation of the above findings is quite obvious. Let us assume that $m$ is the azimuthal symmetry of the forcing and $k$ somehow dictates, say, the number of nodes in the $k$-th member of the series describing the response as a function of the epicyclic angle $w_1'$. The factor of $\sqrt{2}$ is simply the epicyclic frequency, so that the two frequencies in question are the frequency with which a body in the disk encounters a forcing, $m\Omega$, and the frequency with it would like to respond, $k\kappa$. If the forcing is near resonant with with the response times the epicyclic frequency but has a slightly higher angular symmetry, the response is damped, whereas in the reverse case it is amplified. This coincides nicely with the well-known fact that a harmonic oscillator responds out of phase when the forcing is slightly faster than its natural frequency (the epicyclic frequency times the angular symmetry), whereas it responds in phase in the reverse case. This situation is quite akin to a Lindblad resonance, with the difference that for one, the resonance is not exact (if it were, the series would evaluate to infinity), and, for second, it occurs on the entire disk.

All this does not really answer the question whether the bewildering stability behaviour is an artifact of the linearisation or not, although it does suggest that in general $m = 4$ modes in the self-consistent disk should be more unstable than their $m = 3$ counterparts. For rotating modes, on the other hand, this quasi-resonance should be broken for most part of the disk, since $m(\Omega + \Omega_p)$ and $k\kappa$ no longer have a constant ratio. Of course, for a perfectly self-similar disk, the phrase "most part of the disk" is quite meaningless, and thus there is little to keep rotating modes from showing a similar behaviour. Again, the unusual self-similarity of the Mestel disk makes for some quite bizarre features.

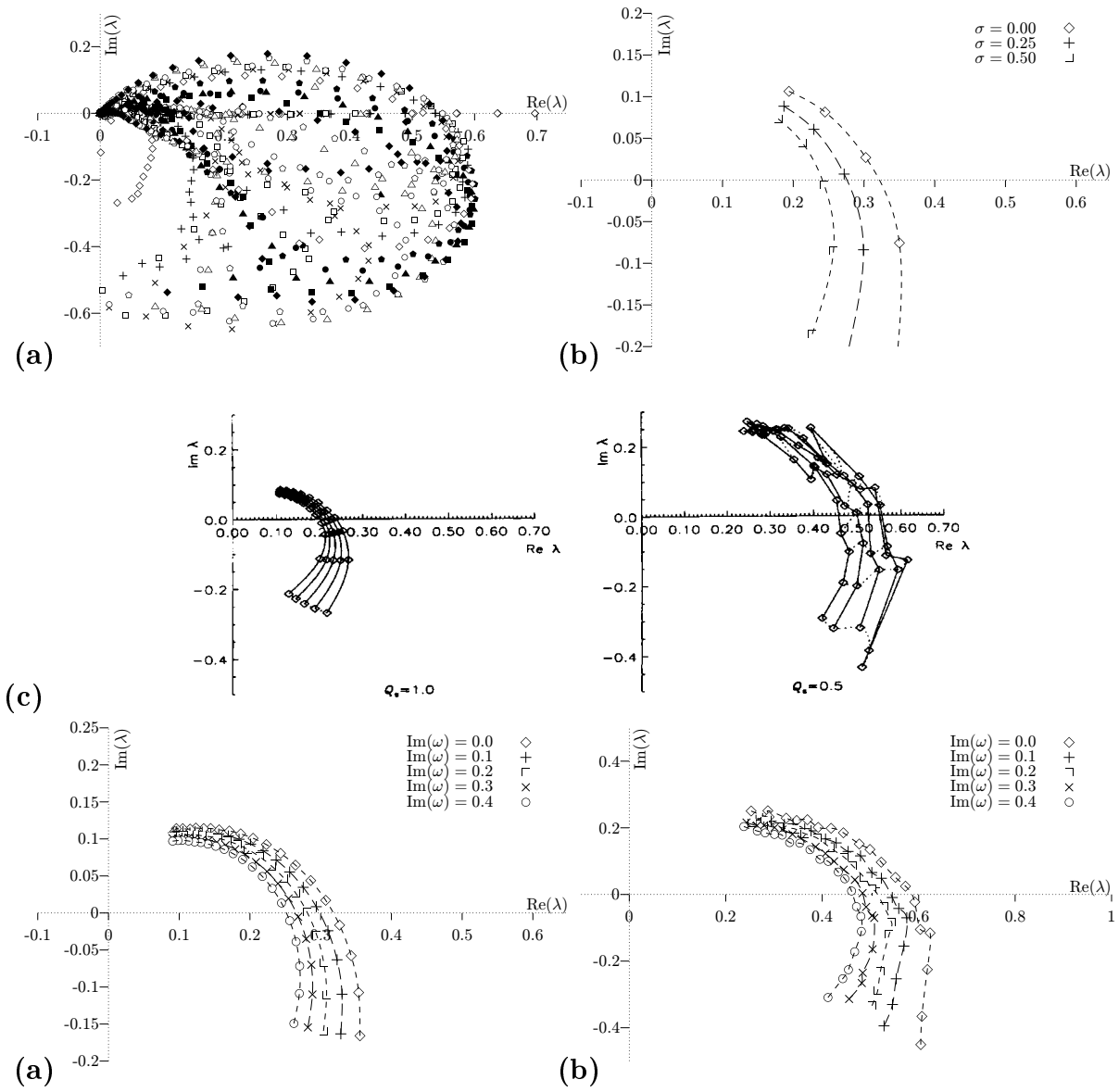


*Fig. 30: Eigenvalues of the cut-out $m = 4$ kernel. (a) shows the spectra for $\sigma = 0.205$ kernels from $\omega = 0.1 \cdots 2.0$ in 20 steps, the upmost points belonging to the $\omega = 2$ kernel; (b) is plot of the largest mathematical eigenvalue versus the indicated values of the velocity dispersion $\sigma$ and $\mathrm{Re}(\omega) = 0.8 \cdots 3.2$ in 5 steps; (c) are two plots of the largest mathematical eigenvalues of a $Q = 1$ (left) and a $Q = 0.5$ disk versus $Re(\omega) = 1.2 \cdots 5.2$ and growth rate $s = 0 \cdots 0.4$ for Read's exact calculations, taken from Read (1997) with kind permission of the author; (d) are two plots of the largest mathematical eigenvalue versus the indicated values of the growth rate $\mathrm{Im}(\omega)$ and $\mathrm{Re}(\omega) = 1 \cdots 5.2$ in 20 steps for a $Q = 1$ (left) and $Q = 0.5$ disk.*

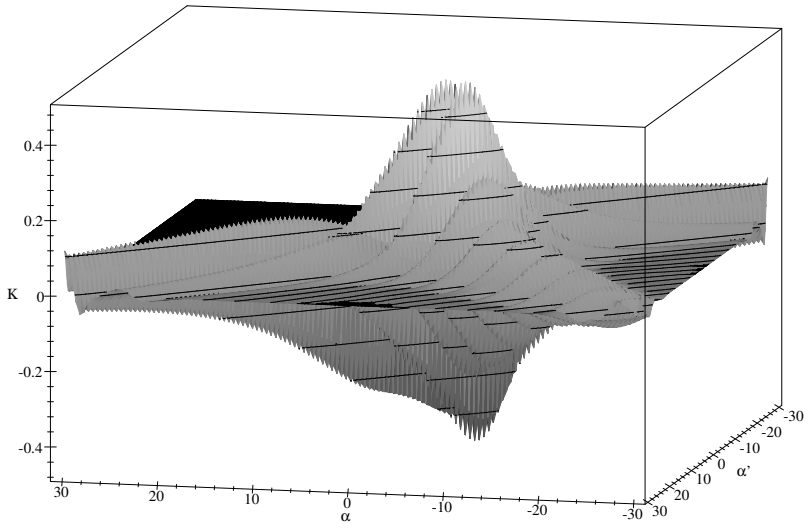


*Fig. 32: The real part of the kernel for $m = 4$ perturbations of the cut-out disk. As always, $\sigma = 0.3$.*

### 5.5.2. Modes in the Cut-Out Disk

In contrast to the neutral modes in the singular disk, almost nothing special happens in the cut-out disk. The kernel in Fig. 32 has yet wider and more dominant humps, and the spectra in Fig. 15a are still somewhat more complex than they were with $m = 3$, and the disk is yet a little more stable against $m = 4$ perturbations than it is against three-armed ones.

The quite complex spectra also show in the plots of the largest eigenvalues, particularly in the $Q = 0.5$ case where quite a few kinks in both Read's and my diagram witness that eigenvalues corresponding to different eigenvectors overtake one another rather frequently.

With this kind of stability behaviour, it is not surprising that $m = 4$ set in at even lower temperatures; the limit below which modes set in here is $\sigma = 0.124$ at $\omega = 2.35$, corresponding to a pattern speed of $\Omega_p = 0.588$.

The qualification "almost" with the above statement that nothing special happens in the cut-out disk was necessary nevertheless. Just as in Read's formalism, for very low $\omega$ the eigenvalues start to return through the third quadrant to the real axis, and given that for $N = 200$, $\sigma = 0.2$ and $\omega = 0.01$ the largest mathematical eigenvalue is $\lambda = 1 = 1.354 - 0.001$, one has to expect that modes will show up in this region. Clearly these modes feel the same resonance that caused the non-quenchable neutral modes, which had to be expected after the above discussion. Again it is hard to tell if these modes have much physical significance.

# 6. More Modes?

One major point that remained somewhat open in the works of both Zang and Read was the issue whether or not the self-consistent disk does indeed admit other modes than the rather exotic neutral modes investigated above. The behaviour in some limits in which the cut-out disk should approach the self-consistent disk (most notably, $\omega \to 0$) suggests that no such modes exist, but a conclusive answer could not be given due to the singular nature of the kernel. The main discomfort with the notion of modes in the singular disk is that in its governing equation $\omega$ factors out, so that without further devices a disk is either stable or becomes unstable at all growth rates and pattern speeds at once. This seemed weird enough to dismiss the possibility of such modes. On the other hand, this would imply that even a completely cold disk would be stable to all nonaxisymmetric perturbations, which again would be quite an exotic situation.

Quite recently, Goodman and Evans (1999) have tackled the problem from a different perspective, employing the Jeans equations to revisit the problem of modes in the self-consistent Mestel disk. The basic results of their work are that the Mestel disk's weirdness starts in its centre, and once one fixes boundary conditions there, the Mestel disk becomes quite tame. By the requirement that the centre does not absorb or emit energy, they curb down the two-dimensional continuum of solutions to a spectrum of one-dimensional continua, in which the ratio between growth rate and pattern speed is fixed and only the phase of $\omega$ remains unknown. Even this ambiguity can be removed by fixing the phase shift during the reflection of a wave at the disk's centre, thus reducing the spectrum to a countable set of discrete points; however, there currently are no good indications as to how this phase shift should fixed. Of course, this only raises new questions. A self-similar disk cannot just admit a single mode without also admitting its scaled brethren; so, somewhere Goodman and Evans must have broken the self-similarity simply by requiring a centre that conserves energy. How this happens is completely unknow at this point.

With a closed expression of the kernel of the Mestel disk, one is in a position to reconsider the stellar-dynamical equivalent of the Goodman and Evans' problem using the tools of the theory of singular integral equations: Does the integral equation (111) admit continuous solutions, and if, for what disk parameters?

## 6.1. The Singular Disk revisited

The kernel (118) of the equation governing the self-consistent disk has a singularity on the diagonal, and thus the familiar Fredholm theory does not apply to it since the operator $\int \mathcal{K}(\alpha, \alpha')\Phi(\alpha)\, d\alpha$ is not compact. The theory that replaces Fredholm theory in this case is developed in Muskhelishvili (1953) and Gakhov (1990), and is nicely summarised in the more modern work of Polyanin and Manzhirov (1998).

The integral equation (111) has the form

$$0 = a(\alpha')\Phi(\alpha') + \frac{1}{\mathrm{i}\pi}\int_L \frac{\hat{\mathcal{K}}(\alpha,\alpha')}{\alpha-\alpha'}\,\Phi(\alpha)d\alpha, \tag{146}$$

where $\hat{\mathcal{K}}$ is at least Hölder continuous, $L$ is the real axis (integration over the real axis is henceforth implied for integral signs not otherwise marked), I wrote $\Phi(\alpha')$ instead of $\Phi_{\alpha',m}$ to accentuate that $\Phi$ is a (complex) function of the real variable $\alpha'$, and, of course, the integral is to be understood as a Cauchy principal value. This equation is a homogenous equation of the second kind (or, in Pipkin's (1991) terminology, of the third kind). In my case, $a(\alpha') = \mathcal{F}(\alpha')-1$ and $\hat{\mathcal{K}} = (\alpha-\alpha')\mathcal{K}(\alpha,\alpha')/\mathrm{i}\pi$. The multiplication with $(\alpha-\alpha')$ ensures that the kernel is bounded on the diagonal, since the single zero in the denominator stemming from $\exp\bigl(2\pi(\alpha-\alpha')\bigr)-1$ now cancels out. The only part of the kernel that could jeopardise the condition of Hölder continuity is the square root, but since $\alpha'$ only enters squared in the arguments of the square roots, $\hat{\mathcal{K}}$ does indeed satisfy a Hölder condition.

It is convenient to rewrite (146) to the equivalent form

$$0 = a(\alpha')\Phi(\alpha') + \frac{1}{\mathrm{i}\pi}b(\alpha')\int \frac{\Phi(\alpha)}{\alpha-\alpha'}d\alpha + \frac{1}{\mathrm{i}\pi}\int \hat{\mathcal{K}}_r(\alpha,\alpha')\Phi(\alpha)d\alpha, \tag{147}$$

where

$$\begin{aligned} b(\alpha) &= \hat{\mathcal{K}}(\alpha',\alpha') \quad \text{and} \\ \hat{\mathcal{K}}_r(\alpha,\alpha') &= \frac{\hat{\mathcal{K}}(\alpha,\alpha')-\hat{\mathcal{K}}(\alpha',\alpha')}{\alpha-\alpha'}. \end{aligned} \tag{148}$$

It is quite easy to see that for the integral equation (111), $b(\alpha') = \mathcal{F}(\alpha')$. After this manipulation, $\hat{\mathcal{K}}_r$ is a compact operator, whereas

$$\mathbf{K}\Phi := a(\alpha')\Phi(\alpha') + \frac{1}{\mathrm{i}\pi}b(\alpha')\int \frac{\Phi(\alpha)}{\alpha-\alpha'}\,d\alpha = 0, \tag{149}$$

known as the dominant or characteristic part of the integral equation, decides if the integral equation has a nontrivial solution.

To find a solution of (149), let us introduce an auxiliary function

$$\Psi(z) = \frac{1}{2\pi\mathrm{i}}\int \frac{\Phi(\alpha)}{(\alpha-z)}\,d\alpha. \tag{150}$$

If $\Phi(\alpha)$ is continuous, this function is piecewise analytic in the upper and lower half planes but may be discontinuous across the real axis. The merit of this auxiliary function is that it allows to transform the problem of the solution of the integral equation (149) into a Riemann boundary value problem.

This can be done by applying the Sokhotski-Plemelj formulae, that, in their formulation for the real axis, state that when $\Phi$ and $\Psi$ are linked by (150),

$$\begin{aligned} \Psi^+(\alpha') + \Psi^-(\alpha') &= \frac{1}{\mathrm{i}\pi}\int \frac{\Phi(\alpha)}{\alpha-\alpha'}d\alpha \qquad \alpha' \in \mathbb{R} \\ \Psi^+(\alpha') - \Psi^-(\alpha') &= \Phi(\alpha') \end{aligned} \tag{151}$$

hold. Here, $\Psi^+(\alpha')$ and $\Psi^-(\alpha')$ are the limiting values of $\Psi(z)$ as $z \to \alpha'$ from above and below, respectively.

Inserting (151) into (149) and collecting the terms yields

$$\Psi^+(\alpha') = \frac{a(\alpha') - b(\alpha')}{a(\alpha') + b(\alpha')}\Psi^-(\alpha') =: D(\alpha')\Psi^-(\alpha'). \tag{152}$$

Going back to the integral equation for the singular disk, one has

$$D(\alpha') = -1/(2\mathcal{F}(\alpha') - 1).$$

This represents a Riemann boundary value problem, asking (in the special case used here) for two functions $\Psi^+$ and $\Psi^-$ that are analytic on the upper and lower half planes, respectively, and that satisfy $\Psi^+(\alpha') = D(\alpha')\Psi^-(\alpha')$ for all real $\alpha'$.

For reasons that will become clear below, I for the time being demand that $D$ has neither zeroes nor poles on the real axis. When will this be the case? To answer this question, consider the plots of $\mathcal{F}$ over $\alpha$ in Fig. 33 for $m = 1 \cdots 4$ and various values of the velocity dispersion $\sigma$ (as shown above, the axisymmetric case does not lead to a singular integral equation). The condition of a bounded and nonzero $D$ will be satisfied if $\mathcal{F}(\alpha) \neq 1/2$ ($\alpha \in \mathbb{R}$), where $\mathcal{F}(\alpha)$ clearly tends to zero for large $\alpha$.

For $m = 1$, $\mathcal{F}$ reaches the 0.5 line even for very large values of $\sigma$, although this might happen at very large $\alpha$ when $\sigma$ is small. In this case, $D$ would have two poles of order one over the entire range of $\sigma$ for which this analysis could even remotely be applicable. This nicely corresponds to the stability behaviour for neutral modes.

The bisymmetric case, on the other hand is "well-behaved" as long as $\sigma > 0.155$, showing four poles of order one below this threshold, reproducing the stability limit of the neutral modes. After this, it is probably not too surprising that since this stability limit was very low indeed in the three-armed case, $D$ is well-behaved for all but very low $\sigma$ for $m = 3$. At $m = 4$, the quite pathologic behaviour found for the neutral modes crops up again and leads to four poles of order one for all but ridiculously high $\sigma$.

Calling this suggestive probably is a gross understatement. On physical grounds, one would thus expect (111) to have no solution in the regular case of a bounded and nonzero $D$, and at least one marginal solution (given that the neutral modes have two or four branches, it would not be too surprising at least the trailing branches would show up here again) otherwise. With this concept mind, let us return to the analysis of the boundary value problem, still restricting the analysis to the regular case.

The $D(\alpha')$ treated here is the limiting value of an analytic function (in particular, according to my assumptions it has no poles on the real axis), and thus is guaranteed to be Hölder continuous. Furthermore, $D(\alpha')$ is a positive real function for real $\alpha'$. This ensures that its index, the increment of its argument over the integration contour,

$$\mathrm{Ind}(D) = \frac{1}{2\pi}\int d\arg D(\alpha)\, d\alpha, \tag{154}$$

is zero. This in turn implies that $\ln D$ is a well-defined (single-valued) function. Then one can take the logarithm of both sides of (152), to arrive at

$$\ln \Psi^+(\alpha') - \ln \Psi^-(\alpha') = \ln D(\alpha'). \tag{155}$$

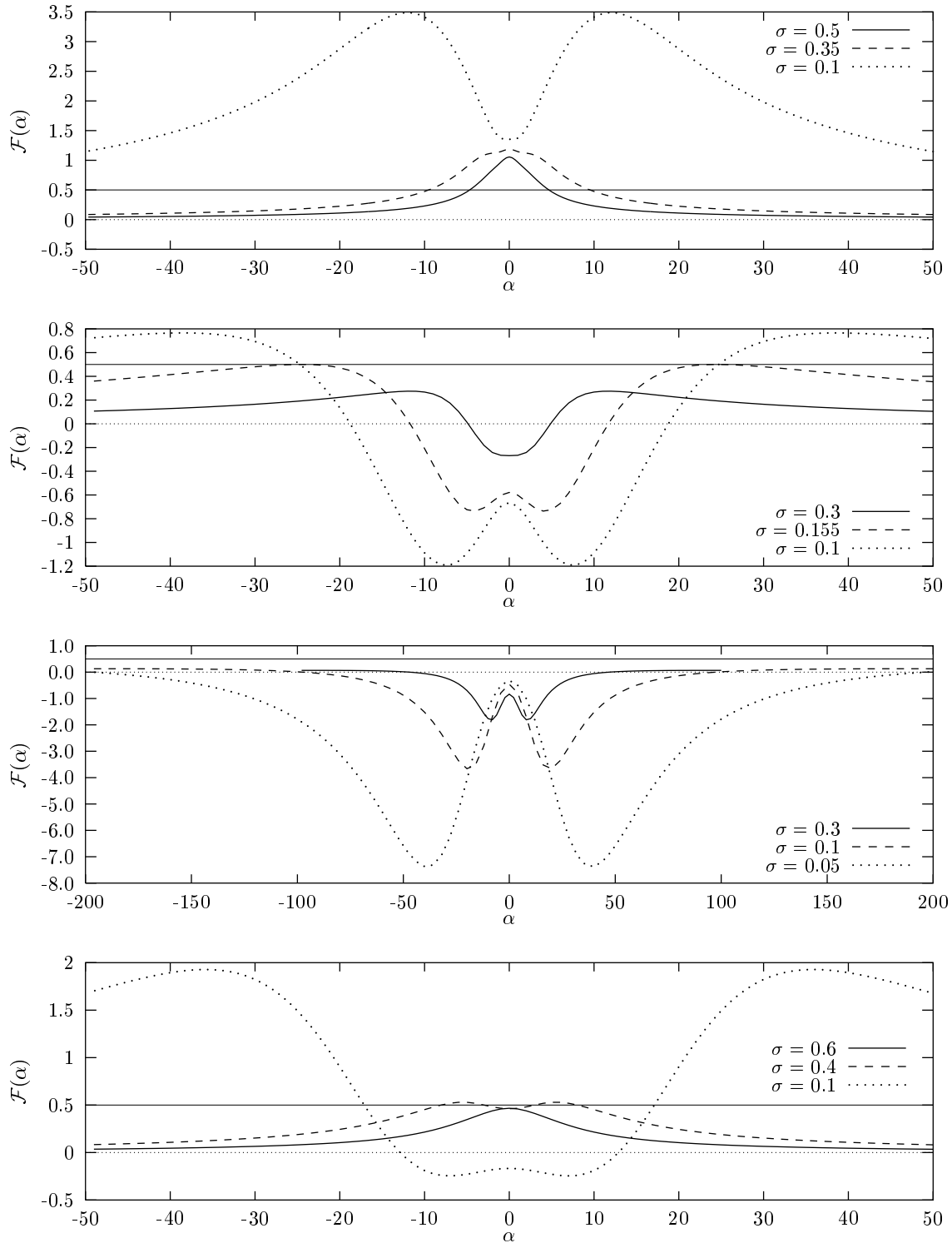


*Fig. 33: Plots of the function $\mathcal{F}(\alpha)$ for $m = 1, 2, 3, 4$ (from top to bottom) and the indicated values of $\sigma$. The solid horizontal line marks the $\mathcal{F}(\alpha) = 1/2$ line. When $\mathcal{F}$ crosses this line, $D$ will have singularities.*

Using the second of the Sokhotski-Plemelj formulae (151), it follows that with

$$G(z) = \frac{1}{2\pi \mathrm{i}} \int \frac{\ln D(\alpha)}{\alpha - z}\, d\alpha \tag{156}$$

one can write down a solution to the boundary value problem (152)

$$X^+(\alpha') = \mathrm{e}^{G^+(\alpha')} \qquad X^-(\alpha') = \mathrm{e}^{G^-(\alpha')}, \tag{157}$$

provided that the problem does have a solution.

Thus one has $D = X^+/X^-$, and the boundary value problem (152) can be written as

$$\frac{\Psi^+(\alpha')}{X^+(\alpha')} = \frac{\Psi^-(\alpha')}{X^-(\alpha')}. \tag{158}$$

Now, the functions $G^\pm$ by construction have no pole in their respective domains, and therefore $X^\pm$ has no zeroes. If $\Phi^\pm$ are defined via an integral as in (150), this implies that they are analytic in their respective half-planes, with the possible exception of $\infty$. Thus, the functions on the two sides of (158) are analytic in their respective half-planes, and they are identical on the real axis. By Morera's theorem this equation implies that the right-hand side and the left hand side represent the same analytic function, $S(z)$, say. Now, what are the properties of $S(z)$?

I already pointed out that $S(z)$ is analytic in the entire plane with the possible exception of the point at infinity, where $\Psi^\pm(\infty) = \pm\frac{1}{2}\Phi(\infty)$. Since I require any solution of the original integral equation (111) to vanish at infinity, one has $\Psi^\pm(\infty) = 0$ as well. Since $D \to 1$ for large $\alpha$, $G$ approaches 0 and $X^\pm$ tends to 1. This implies that $S$ vanishes at infinity. Since $S$ is an entire function, Liouville's theorem then states that $S$ must be identically zero. By the first Sokhotski-Plemelj formula one now has $\Phi(\alpha') = S(\alpha)(X^+ + X^-)$, and hence the homogenous integral equation has no nontrivial solution. This is a special case of the general result that is proven somewhat more rigorously in the literature cited above: A homogenous Cauchy integral equation with an index of zero is unsolvable.

Loosening the conditions on $D$, I now allow it to have "poles" at some points $\alpha_i$, which, for the sake of simplicity, are supposed to be poles of order one. The term "pole" has been put in quotes since it is not necessary that $D$ is analytic in $\mathbb{C} \setminus \{\alpha_i\}$, only that the $D(\alpha_i)$ behaves like $(\alpha' - \alpha_i)^{-1}$ at the exceptional points.

Writing

$$D(\alpha') = \frac{D'(\alpha')}{\prod_{i=1}^n (\alpha' - \alpha_i)}, \tag{159}$$

the boundary condition (152) takes the form

$$\Psi^+(\alpha') = \frac{D'(\alpha')}{\prod_{i=1}^n (\alpha' - \alpha_i)} \Psi^-(\alpha'), \tag{160}$$

where $D'$ now satisfies the conditions I required of the $D$ in (152). Solving the boundary value problem for this $D'$ and substituting the result back into (160), the equivalent of (158) now is

$$\frac{\Psi^+(\alpha')}{X^+(\alpha')} = \frac{\Psi^-(\alpha')}{X^-(\alpha') \prod_{i=1}^n (\alpha' - \alpha_i)}, \tag{161}$$

where this time $X = \mathrm{e}^G$ and $G(\alpha') = \frac{1}{2\pi\mathrm{i}} \int \ln D'(\alpha')/(\alpha - \alpha')\, d\alpha$. Let us again call the analytic function defined in the left and right sides of (161) $S(z)$.

By the right side of (161), $S$ now may have poles of order 1 at $\alpha_i$. By the generalzed Liouville theorem, a solution of the integral equation would then have the form

$$\Phi = \frac{1}{\prod c_i(\alpha' - \alpha_i)} \left( X^+ + X^- \prod (\alpha' - \alpha_i) \right). \tag{162}$$

Evidently, solutions of this type cannot be bounded at $\alpha_i$, since that would require the bracket to vanish at $\alpha_i$, implying $X^+(\alpha_i) = 0$ which is impossible due to the definition of $X$ via an exponential of a function bounded for finite arguments. Thus, no solutions exist even in the exceptional case.

Certainly, this is not what was to be expected after the above analysis. The reason for this surprise is of course the requirement of boundedness for $\Phi$ and thus for $\Psi^{\pm}$. Unfortunately, the requirement that $\Phi$ does not possess poles is necessary for (150) to be even defined. If $\Phi(\alpha)$ has as much as one singularity of order one, the integrad in (150) will have a singularity of order two at that point and will thus no longer be integrable. Indeed, the integral equation (147) itself cannot admit any $\Phi(\alpha)$ with a pole, since it would render the integral in the second summand undefined. It is still conceivable that $\Phi(\alpha)$ might have an integrable singularity of some kind, but then of course the basic assumption that any singularity $S$ might have is a pole breaks down and the entire theory does not work any more. Hence, for want of a theory for nonbounded solutions of Cauchy integral equations, once again the existence of solutions cannot be conclusively proven, although I can rule out bounded solutions.

Reviewing the solutions put forward by Goodman and Evans (1999), one finds that they do show singularities right at the exceptional points of (161), which is where one would expect singularities in the present analysis. This might be sufficient encouragement to actually try and *assume* solutions that may be found numerically. To do this, one has to solve the full equation (147). If both $\mathcal{F}$ and the solution were bounded, this would be quite an easy task, since dealing with the singularity in the kernel appears to be feasible. In preparatory experiments, the midpoint quadrature formula (constructed along the ideas laid down in Press et al, 1992)

$$\int_{-L}^{L} \frac{f(\alpha)}{(\alpha - \alpha')}\, d\alpha = \sum_{i=0}^{4n} \sum_{j=0}^{3} \chi_j(\alpha_{i+j}, \alpha') \Phi(\alpha_{i+j}), \tag{163}$$

where $\alpha_i = L(\frac{(1+2i)}{4n} - 1)$ and $\chi_i(\alpha, \alpha')$ is the (straightforward but lengthy) solution of

$$\int_{a-h/2}^{a+7/2h} \frac{f(\alpha)}{\alpha - \alpha'}\, d\alpha = f(a)\chi_0(a, \alpha') + f(a+h)\chi_1(a, \alpha') + f(a+2h)\chi_2(a, \alpha') + f(a+3h)\chi_3(a, \alpha'), \tag{164}$$

$f(x) = x^i, i = 0 \cdots 3$, with $h = L/(2n)$ worked quite well for the kernel and steers clear of evaluating the kernel on the diagonal. However, the only cases that can have solutions are those with a nonbounded $\mathcal{F}$ and a solution that will be in some way "bad" at the points where $\mathcal{F}$ diverges. Handling this appears to be at least difficult.

Once one had a solution, after the findings of Goodman and Evans one would certainly want to weed out solutions not satisfying some appropriate boundary conditions. This again does

not seem trivial in that it is hard to separate incoming and outgoing components in solutions like Fig. 22. All in all, the scope of such a project seems more like another thesis than a footnote to this one, and consequently I have little choice but to leave this issue open, although I strongly suspect that the neutral modes do indeed have families of rotating and growing modes behind them. Given that the stability of the neutral modes is governed by the fact that for them an approximate resonance between the frequency of the forcing and some harmonic of the epicyclic frequence stretches over the entire disk and for true rotating modes that is not the case, one can expect this procedure to lead to quite different stability limits for rotating modes. On the other hand, any pattern speed can be scaled to be arbitrarily small as long as the disk's self-similarity is not broken, and thus without "tricks" to introduce some scale into the disk the stability limits suggested here (if indeed the exceptional case admits modes) are valid. The most interesting case in an analysis employing such "tricks" should be the three-armed one. If the above analysis is correct, the inhibition of these modes by the resonance should pertain to rotating modes as well, and only when the self-similarity is broken in some way should one expect to see the stability limit rise.

# 7. Summary and Conclusions

In this work, I have investigated the modes admitted by Mestel disks. This problem has already been investigated by Zang (1976) and Read (1997), who chose a semianalytic approach that essentially relied on two approximations:

- The treatment of the disk as razor-thin.
- The linearisation of the Boltzmann equation (i.e., the perturbation amplitude is a small quantity)

While their results are as exact as one wishes them to be, their method does not deliver the kernel in a closed form—to compute it, some numerical integration is required. I traded in the exactness for (almost) closed expressions for the kernel by employing two further approximations:

- I approximate the orbits of bodies in the Mestel disk by epicyclic orbits, first deriving the two periods of the orbits by the method of harmonic balance, then linearising those simplified expressions.
- I (sort of) linearise the logarithmic spirals used as the potential basis

While the second of these approximations should not have much impact since slightly changing basis functions for an expansion is rather safe, the first one is quite serious, in particular because I still pretend that the coordinates I derive from these approximations are canonic action-angle coordinates, which, of course, they are only approximately. In particular the second linearisation of the expressions for the actions and angles can be expected to have a quite drastic impact on the results, basically reducing my approach to an epicyclic approximation of order 1.1, as it were. A strict first-order epicyclic approximation is unusable in the Mestel disk, since the resulting Hamiltonian does not contain the second integral of motion.

Following Zang, in addition to the self-consistent Mestel disk I also investigated a disk in which a part of the matter does not take part in the perturbation. While the main purpose of doing this is to remove some properties of the self-consistent disk that appear quite unphysical and also to introduce a $Q$-barrier, it is more than a pure mathematical device in that the cut-outs have real-world counterparts in dark haloes and bulges that influence the rotation curve of the disks without being dynamically active enough to take part in spiral perturbations. The cut-out function treated here is one of the cut-out functions investigated by Read in order to facilitate comparisons with her results. For further investigations, I suggest a different (one-parameter) cut-out that results in much more tractable expressions.

Despite the cautioning words above, in both the self-consistent disk and the cut-out disk the precision of the results is good enough to justify the approximations—the physics come out right to within 10% of the results of Read even in the more critical cases, and to within 2% when the problems are tame. Table 1 summarises the stability properties of the self-consistent and the cut-out disks with respect to the various azimuthal harmonics.

| | self-consistent | | cut-out | |
|---|---|---|---|---|
| $m$ | $\sigma_{\min}$ | $\alpha$ | $\sigma_{\min}$ | $\Omega_p$ |
| 0 | 0.386 | 3.51 | 0.349 | –[1] |
| 1 | –[2] | –[2] | 0.57[3] | 0.00[3] |
| 2 | 0.155 | 25.18 | 0.214 | 0.554 |
| 3 | $< 0.05$ | $> 600$ | 0.141 | 0.61 |
| 4 | –[4] | –[4] | 0.124 | 0.588 |

[1] $m = 0$ modes have no orientation and therefore no pattern speed.
[2] See the discussion in chapter 5.2.
[3] Even slightly rotating modes have more realistic stability properties. See chapter 5.2.
[4] See chapter 5.5.

*Table 1: A summary of the stability properties of the Mestel disk. "Cut-out" refers to the $M = N = 2$ cut-out disk (see chapter 4.1), self-consistent refers to the plain Mestel disk. The modes in the self-consistent disk become unstable for all $\Omega_p$ at the same time, at least as far as one can tell from my investigation. The parameter $\alpha$ is the logarithmic wave number of the neutral mode. The modes in the cut-out disks have contributions from a continuum of $\alpha$ but have a definite pattern speed $\Omega_p$.*

So, the picture of the Mestel disk is mainly like the one painted by Zang and Read: The axisymmetric stability is quite like predicted by the local theory. The disk readily admits growing $m = 1$ modes, whereas modes of higher azimuthal symmetry become unstable only when the disk already is axisymmetrically unstable and should thus not occur in disks sufficiently similar to a Mestel disk. The stability against neutral modes in the self-consistent disk in retrospect appears to be closely linked to the proximity of a harmonic of the epicyclic frequency $\kappa$ this the frequency of the forcing $m\Omega$. For $m = 2$, $m\Omega$ lies quite in between two harmonics of $\kappa$, and the disk becomes unstable at $\sigma = 0.155$; for $m = 3$, the driving is somewhat faster than than the closest $k\kappa$, inducing a response out of phase, so that the disk is remarkably stable; and for $m = 4$, the driving is somewhat slower, and the disk is very unstable. This becomes a global property of the disk for the (non-rotating) neutral modes because the frequency ratio between forcing and epicyclic frequency is constant over the disk, which for rotating modes it is not. Basically, the neutral modes can exhibit a near Lindblad resonance over the entire disk. The $m = 1$ case would fit into the $m = 4$ picture, although certain differences suggest that its instability might be linked to, e.g., an instability of the position of the cusp.

The most valuable asset this work adds to the body of knowledge piled up by Zang and Read is that it gives a closed form of the kernel. This may lead a way for further investigating Mestel disks or even more general disks, in particular with respect to their properties in the regime of mildly nonlinear perturbations. I did not follow those possible ways but restricted myself to a treatment of the issues raised by Zang and Read, where I shed some light on them from a slightly different perspective.

The main issue that remains to be solved to facilitate a completely analytic treatment of the problem is a closer investigation of the series involving Bessel functions in the kernels.

Although I have been unsuccessful in trying to find a way to find at least approximative analytic solutions, it is quite conceivable that the kernel is close enough to a degenerate one, so that the eigenvalues and eigenfunctions governing the problem might be writable in a closed form.

One point in which this work goes beyond Zang and Read is that the closed form of the kernel enabled me to explore the stability properties of the self-consistent disk with a broader set of tools. Although I can show that no modes with bounded Mellin transforms exist in the self-consistent disk, for velocity dispersions below the stability limit of the neutral modes this does not rule out the existence of rotating modes with some integrable singularities. Indeed, the structure of the problem strongly suggests that they should exist, even more so since the modes Goodman and Evans (1999) put forward from their gas-dynamical analysis show singularities right at the points where one would expect them to be from my analysis. However, without a solution theory for Cauchy integral equations on the space of functions with integrable singularities, their existence cannot be proven. Thus, once more the existence of $\omega \neq 0$-modes in the unmodified Mestel disk remains open.

**Acknowledgement**

A significant part of this work was done while the author was supported by a grant under the Landesgraduiertenförderungsgesetz des Landes Baden-Württemberg.

I want to express my gratitude to the students and the staff at the Astronomisches Rechen-Institut Heidelberg, in particular my supervisor Burkhard Fuchs, who not only provided advice and encouragement but also kindly arranged the defence while the author was not in Heidelberg, and to Holger Baumgart, Michael Biermann, Sabine Frink, and my office-mate Heiko Reffert, who provided a friendly environment.

Also, I want to thank Jenny Read for useful discussions, sending me a copy of her thesis, and the permission to reprint some figures from that work.

Furthermore, I want to acknowledge Guido von Rossum, the author of the wonderful Python language, Linus Thorvalds, the author of the Linux operating system, Donald E. Knuth, the author of the TEX typesetting system, Richard Stallman, spiritus rector of the GNU project, and countless other contributors to tools like Gnuplot, netpbm, NumPy, meschach and others that were instrumental to the present work.

Finally, I feel obliged to mention Klaus von Trotha, Peter Ulmer and Jürgen Siebke. Their unrelenting quest for the University of the Future provided endless distraction and entertainment.

# 8. Appendix

In chapter 4.4 I did not write down the results of the final quadrature over $L_z$ for the cut-out disk. In this appendix I give the results of their computation by means of computer algebra. These terms could be simplified to result in expressions about 1/4 the size of the expressions below, if one may extrapolate the behaviour of the analogous expressions for the simpler cut-out (122). However, even then the kernel would be extremely unwieldy, and thus I chose to simply dump the expressions actually used to compute the kernel in the C++ programme to a TEX-source.

Maple sometimes abbreviates common subexpressions with $\%n$. The definitions of the subexpressions can be found at the end of the formulae.

$$
\begin{aligned}
\bar{I}_2^{(L_z,1)} =& \frac{1}{4}\mathrm{i}\left( {L_0}^{(\mathrm{i}(\alpha-\alpha'))} - {L_c}^{(\mathrm{i}(\alpha-\alpha'))} \right) \%2 \left|\Gamma\left(\frac{1}{4}+\frac{1}{2}m+\frac{1}{2}\mathrm{i}\,\alpha'\right)\right|^2 {L_c}^2 \left(1-2\,\sigma^2\right)^{\left(1/2-1/2\,\frac{1}{\sigma^2}\right)} \mathrm{e}^{\left(1/2\,\frac{1}{\sigma^2}\right)} \\
& \mathrm{e}^{\left(-1/4\,\frac{2+\sigma^4\,\alpha^2-2\,\sigma^4\,\alpha\,\alpha'+\sigma^4\,\alpha'^2}{\sigma^2}\right)} \Bigg/ \Bigg( \left(-1+\mathrm{e}^{(-\pi\,(\alpha-\alpha'))}\right)\left(L_0+L_c\right)\left(L_0-L_c\right) \\
& \left|\Gamma\left(\frac{3}{4}+\frac{1}{2}m+\frac{1}{2}\mathrm{i}\,\alpha'\right)\right|^2 \mathrm{e}\,\sigma^2 \Bigg) - \frac{1}{2}\mathrm{i}\left(1-2\,\sigma^2\right)^{\left(1/2-1/2\,\frac{1}{\sigma^2}\right)} \mathrm{e}^{\left(1/2\,\frac{1}{\sigma^2}\right)} {L_c}^2 \\
& \left|\Gamma\left(\frac{1}{4}+\frac{1}{2}m+\frac{1}{2}\mathrm{i}\,\alpha'\right)\right|^2 \mathrm{e}^{\left(-1/4\,\frac{2+4\,\sigma^4\,m^2+\sigma^4\,\alpha'^2+\sigma^4\,\alpha^2}{\sigma^2}\right)} \\
& \mathrm{BesselI}\left(0,\frac{1}{2}\sqrt{\sigma^4\left(2\,m^2\,\alpha^2+2\,m^2\,\alpha'^2+\alpha^2\,\alpha'^2+4\,m^4\right)}\right) \Bigg( -\frac{1}{2}{L_0}^{(\mathrm{i}(\alpha-\alpha'))} \Big( \\
& -\%2\,{L_0}^4\,\omega^4 - 2\,\%2\,{L_0}^2\,\omega^2\,m^2 - \%2\,{L_0}^3\,\omega^3\,\sigma^2\,m\,(\alpha-\alpha') \\
& +\mathrm{i}\,\%2\,{L_0}^2\,\omega^2\,\sigma^2\,m^2\,(\alpha-\alpha') - \%2\,L_0\,\omega\,\sigma^2\,m^3\,(\alpha-\alpha') - \%2\,m^4 \\
& +\mathrm{i}\,\%2\,(\alpha-\alpha')\,m^4\,\sigma^2 - \%2\,\sigma^2\,m^2\,{L_0}^2\,\omega^2 + 2\,\mathrm{i}\,\%2\,\sigma^2\,m^3\,\omega\,L_0 + \%2\,\sigma^2\,m^4 \\
& -\%1\,{L_0}^4\,\omega^4 - 2\,\%1\,{L_0}^2\,\omega^2\,m^2 + \%1\,{L_0}^3\,\omega^3\,\sigma^2\,m\,(\alpha-\alpha') \\
& +\mathrm{i}\,\%1\,{L_0}^2\,\omega^2\,\sigma^2\,m^2\,(\alpha-\alpha') + \%1\,L_0\,\omega\,\sigma^2\,m^3\,(\alpha-\alpha') - \%1\,m^4 \\
& +\mathrm{i}\,\%1\,(\alpha-\alpha')\,m^4\,\sigma^2 - \%1\,\sigma^2\,m^2\,{L_0}^2\,\omega^2 - 2\,\mathrm{i}\,\%1\,\sigma^2\,m^3\,\omega\,L_0 + \%1\,\sigma^2\,m^4\Big) \Bigg/ \Bigg( \\
& \left(L_0+L_c\right)\left(L_0-L_c\right)\left(-1+\mathrm{e}^{(-2\,\pi\,(\alpha-\alpha'))}\right)\left(-{L_0}^2\,\omega^2-2\,\mathrm{i}\,m\,\omega\,L_0+m^2\right) \\
& \left(-{L_0}^2\,\omega^2+2\,\mathrm{i}\,m\,\omega\,L_0+m^2\right)\Bigg) + \frac{1}{2}{L_c}^{(\mathrm{i}(\alpha-\alpha'))}\Big( -\%2\,m^4 - 2\,\%2\,m^2\,{L_c}^2\,\omega^2 \\
& -\%2\,{L_c}^4\,\omega^4 + \%2\,\sigma^2\,m^4 + 2\,\mathrm{i}\,\%2\,\sigma^2\,m^3\,\omega\,L_c - \%2\,\sigma^2\,m^2\,{L_c}^2\,\omega^2
\end{aligned}
$$

$$
\begin{aligned}
&- \%2\, L_c\, \omega\, m^3\, \sigma^2\, (\,\alpha - \alpha'\,) + \mathrm{i}\, \%2\, {L_c}^2\, \omega^2\, m^2\, \sigma^2\, (\,\alpha - \alpha'\,) - \%2\, {L_c}^3\, \omega^3\, m\, \sigma^2\, (\,\alpha - \alpha'\,) \\
&+ \mathrm{i}\, \%2\, (\,\alpha - \alpha'\,)\, m^4\, \sigma^2 - \%1\, m^4 - 2\, \%1\, m^2\, {L_c}^2\, \omega^2 - \%1\, {L_c}^4\, \omega^4 + \%1\, \sigma^2\, m^4 \\
&- 2\, \mathrm{i}\, \%1\, \sigma^2\, m^3\, \omega\, L_c - \%1\, \sigma^2\, m^2\, {L_c}^2\, \omega^2 + \%1\, L_c\, \omega\, m^3\, \sigma^2\, (\,\alpha - \alpha'\,) \\
&+ \mathrm{i}\, \%1\, {L_c}^2\, \omega^2\, m^2\, \sigma^2\, (\,\alpha - \alpha'\,) + \%1\, Lc^3\, \omega^3\, m\, \sigma^2\, (\,\alpha - \alpha'\,) + \mathrm{i}\, \%1\, (\,\alpha - \alpha'\,)\, m^4\, \sigma^2 \Big) \Big/ \Big( \\
&(\,-1 + \mathrm{e}^{(\,-2\,\pi\,(\,\alpha - \alpha'\,)\,)}\,)\, (\,L_0 - L_c\,)\, (\,L_0 + L_c\,)\, \left(m^2 - 2\, \mathrm{i}\, m\, \omega\, L_c - Lc^2\, \omega^2\right) \\
&\left(m^2 + 2\, \mathrm{i}\, m\, \omega\, L_c - {L_c}^2\, \omega^2\right) \Big) \\
&+ \frac{\sigma^2\, m^2\, \omega^2\, \left(-\omega^4\, {L_0}^2\, {L_c}^2 + m^2\, {L_c}^2\, \omega^2 + \omega^2\, m^2\, {L_0}^2 + 3\, m^4\right)\, \left(\frac{\omega}{m}\right)^{(\,-\mathrm{i}\,(\,\alpha - \alpha'\,)\,)}}{\left({L_c}^2\, \omega^2 + m^2\right)^2\, \left(m^2 + {L_0}^2\, \omega^2\right)^2\, (\,-1 + \mathrm{e}^{(\,2\,\pi\,(\,\alpha - \alpha'\,)\,)}\,)} \Bigg) \Big/ \Big( \mathrm{e} \\
&\sigma^2\, \left| \Gamma\left(\frac{3}{4} + \frac{1}{2}\, m + \frac{1}{2}\, \mathrm{i}\, \alpha'\right) \right|^2 \Big) \\
&\%1 := \mathrm{e}^{(\,-3/2\,\pi\,(\,\alpha - \alpha'\,)\,)} \\
&\%2 := \mathrm{e}^{(\,-1/2\,\pi\,(\,\alpha - \alpha'\,)\,)}
\end{aligned}
$$

$$
\begin{aligned}
\bar{I}_2^{(L_z,2)} =& -\frac{1}{8}\mathrm{i}\, \left(1 - 2\, \sigma^2\right)^{\left(1/2 - 1/2\, \frac{1}{\sigma^2}\right)}\, \sqrt{2}\, \mathrm{e}^{\left(1/2\, \frac{1}{\sigma^2}\right)}\, {L_c}^2\, \left| \Gamma\left(\frac{1}{4} + \frac{1}{2}\, m + \frac{1}{2}\, \mathrm{i}\, \alpha'\right) \right|^2\, \mathrm{e}^{\left(-1/4\, \frac{2 + 4\, \sigma^4\, m^2 + \sigma^4\, \alpha'^2 + \sigma^4\, \alpha^2}{\sigma^2}\right)} \\
&\mathrm{BesselI}\left(k, \frac{1}{2}\, \sqrt{\sigma^4\, \left(2\, m^2 + \alpha'^2\right)\, \left(2\, m^2 + \alpha^2\right)}\right) \Big( - \sqrt{\%1}\, {L_0}^{(\,\mathrm{i}\,(\,\alpha - \alpha'\,)\,)}\, \pi\, \Big( \\
&- 4\, \sigma^2\, m^4\, \cos(\,\%2\,)\, \sqrt{2}\, \%1\, \xi 8^2 - \mathrm{i}\, L_0\, \sigma^2\, m\, \omega\, \sqrt{2}\, \cos(\,\%2\,)\, \xi 7^3 \\
&- 2\, m^2\, \cos(\,\%2\,)\, \sqrt{2}\, \%1\, \xi 8^2\, \xi 7 + 8\, \mathrm{i}\, L_0\, \sigma^2\, m\, \omega\, \sqrt{2}\, \cos(\,\%2\,)\, k^2\, \xi 7^2 \\
&- 2\, \mathrm{i}\, \sigma^2\, m\, k\, \sin(\,\%2\,)\, \xi 7^3 - 2\, \mathrm{i}\, \sigma^2\, m\, k\, \sin(\,\%2\,)\, \%1\, \xi 8^2\, \xi 7 \\
&+ 2\, \mathrm{i}\, \sigma^2\, m^2\, \cos(\,\%2\,)\, \sqrt{2}\, (\,\alpha - \alpha'\,)\, \%1\, \xi 8^2\, \xi 7 - 4\, L_0\, \omega\, k\, \sin(\,\%2\,)\, \%1\, \xi 8^2\, \xi 7 \\
&+ 2\, {L_0}^2\, \omega^2\, \sqrt{2}\, \cos(\,\%2\,)\, \%1\, \xi 8^2\, \xi 7 - \sigma^2\, m^2\, \cos(\,\%2\,)\, \sqrt{2}\, \xi 7^3 \\
&- 2\, \mathrm{i}\, \sigma^2\, m\, k\, \sin(\,\%2\,)\, \xi 8^3\, \%1 - 2\, m^2\, \cos(\,\%2\,)\, \sqrt{2}\, \xi 8\, \xi 7^2 \\
&+ 4\, L_0\, \omega\, k\, \sin(\,\%2\,)\, \xi 8\, \xi 7^2 - 8\, \mathrm{i}\, \sigma^2\, m^3\, k\, \sin(\,\%2\,)\, \xi 7^2 \\
&- 4\, \sigma^2\, m\, k\, \sin(\,\%2\,)\, (\,\alpha - \alpha'\,)\, \xi 8\, \xi 7^2 + 16\, \mathrm{i}\, \sigma^2\, m\, k^3\, \sin(\,\%2\,)\, \%1\, \xi 8^2 \\
&+ \mathrm{i}\, L_0\, \sigma^2\, m\, \omega\, \sqrt{2}\, \cos(\,\%2\,)\, \xi 8^3\, \%1 - 4\, \sigma^2\, m^4\, \cos(\,\%2\,)\, \sqrt{2}\, \xi 7^2 \\
&- \mathrm{i}\, L_0\, \sigma^2\, m\, \omega\, \sqrt{2}\, \cos(\,\%2\,)\, \%1\, \xi 8^2\, \xi 7 - 4\, \mathrm{i}\, L_0\, \omega\, \cos(\,\%2\,)\, \sqrt{2}\, m\, \xi 8\, \xi 7^2 \\
&+ 2\, L_0\, \sigma^2\, m\, \omega\, \sqrt{2}\, \cos(\,\%2\,)\, (\,\alpha - \alpha'\,)\, \%1\, \xi 8^2\, \xi 7 \\
&- 8\, \mathrm{i}\, L_0\, \sigma^2\, m\, \omega\, \sqrt{2}\, \cos(\,\%2\,)\, k^2\, \%1\, \xi 8^2 - \sigma^2\, m^2\, \cos(\,\%2\,)\, \sqrt{2}\, \%1\, \xi 8^2\, \xi 7 \\
&+ 8\, \sigma^2\, m^2\, \cos(\,\%2\,)\, \sqrt{2}\, k^2\, \%1\, \xi 8^2 - 2\, \mathrm{i}\, \sigma^2\, m\, k\, \sin(\,\%2\,)\, \xi 8\, \xi 7^2 \\
&- 4\, \mathrm{i}\, m\, k\, \sin(\,\%2\,)\, \xi 8\, \xi 7^2 - 8\, \mathrm{i}\, \sigma^2\, m^3\, k\, \sin(\,\%2\,)\, \%1\, \xi 8^2 \\
&+ 4\, \mathrm{i}\, L_0\, \omega\, \cos(\,\%2\,)\, \sqrt{2}\, m\, \%1\, \xi 8^2\, \xi 7 - 2\, L0\, \sigma^2\, m\, \omega\, \sqrt{2}\, \cos(\,\%2\,)\, (\,\alpha - \alpha'\,)\, \xi 8\, \xi 7^2 \\
&- \sigma^2\, m^2\, \cos(\,\%2\,)\, \sqrt{2}\, \xi 8\, \xi 7^2 + 2\, {L_0}^2\, \omega^2\, \sqrt{2}\, \cos(\,\%2\,)\, \xi 8\, \xi 7^2 \\
&+ 8\, \sigma^2\, m^2\, \cos(\,\%2\,)\, \sqrt{2}\, k^2\, \xi 7^2 + 16\, \mathrm{i}\, \sigma^2\, m\, k^3\, \sin(\,\%2\,)\, \xi 7^2
\end{aligned}
$$

$$
\begin{aligned}
&- 4\,\sigma^2\,m\,k\sin(\,\%2\,)\,(\,\alpha-\alpha'\,)\,\%1\,\xi8^2\,\xi7 + 2\,\mathrm{i}\,\sigma^2\,m^2\cos(\,\%2\,)\,\sqrt{2}\,(\,\alpha-\alpha'\,)\,\xi8\,\xi7^2\\
&+ \mathrm{i}\,L_0\,\sigma^2\,m\,\omega\,\sqrt{2}\cos(\,\%2\,)\,\xi8\,\xi7^2 + 4\,\mathrm{i}\,L_0\,\sigma^2\,m^3\,\omega\,\sqrt{2}\cos(\,\%2\,)\,\%1\,\xi8^2\\
&- 4\,\mathrm{i}\,m\,k\sin(\,\%2\,)\,\%1\,\xi8^2\,\xi7 - 4\,\mathrm{i}\,L_0\,\sigma^2\,m^3\,\omega\,\sqrt{2}\cos(\,\%2\,)\,\xi7^2\\
&- \sigma^2\,m^2\cos(\,\%2\,)\,\sqrt{2}\,\xi8^3\,\%1\Big)\Big/\Big(\xi7^2\,\xi8^2\,(\,\%1-1\,)\,(\,\%1+1\,)\,(\,L0-L_c\,)\,(\,L_0+L_c\,)\\
&\Big) + \sqrt{\%1}\,{L_c}^{(\,\mathrm{i}\,(\,\alpha-\alpha'\,)\,)}\,\pi\,\Big(\mathrm{i}\,m\,\sigma^2\,L_c\,\omega\,\sqrt{2}\cos(\,\%2\,)\,\xi10^3\,\%1\\
&+ \mathrm{i}\,m\,\sigma^2\,L_c\,\omega\,\sqrt{2}\cos(\,\%2\,)\,\xi9^2\,\xi10 + 4\,\mathrm{i}\,\omega\cos(\,\%2\,)\,\sqrt{2}\,m\,Lc\,\%1\,\xi9\,\xi10^2\\
&- 8\,\mathrm{i}\,m\,\sigma^2\,L_c\,\omega\,\sqrt{2}\cos(\,\%2\,)\,k^2\,\%1\,\xi10^2 + 8\,\mathrm{i}\,m\,\sigma^2\,L_c\,\omega\,\sqrt{2}\cos(\,\%2\,)\,k^2\,\xi9^2\\
&+ 4\,\mathrm{i}\,m^3\,\sigma^2\,L_c\,\omega\,\sqrt{2}\cos(\,\%2\,)\,\%1\,\xi10^2 - \mathrm{i}\,m\,\sigma^2\,L_c\,\omega\,\sqrt{2}\cos(\,\%2\,)\,\%1\,\xi9\,\xi10^2\\
&+ 2\,\mathrm{i}\,\sigma^2\,m^2\cos(\,\%2\,)\,\sqrt{2}\,\%1\,(\,\alpha-\alpha'\,)\,\xi9\,\xi10^2\\
&+ 2\,m\,\sigma^2\,L_c\,\omega\,\sqrt{2}\cos(\,\%2\,)\,\%1\,(\,\alpha-\alpha'\,)\,\xi9\,\xi10^2 - \mathrm{i}\,m\,\sigma^2\,L_c\,\omega\,\sqrt{2}\cos(\,\%2\,)\,\xi9^3\\
&- 2\,m^2\cos(\,\%2\,)\,\sqrt{2}\,\xi9^2\,\xi10 - 4\,\mathrm{i}\,\omega\cos(\,\%2\,)\,\sqrt{2}\,m\,L_c\,\xi9^2\,\xi10\\
&- 2\,\mathrm{i}\,\sigma^2\,m\,k\sin(\,\%2\,)\,\%1\,\xi9\,\xi10^2 + 2\,\mathrm{i}\,\sigma^2\,m^2\cos(\,\%2\,)\,\sqrt{2}\,(\,\alpha-\alpha'\,)\,\xi9^2\,\xi10\\
&- 4\,\mathrm{i}\,m^3\,\sigma^2\,L_c\,\omega\,\sqrt{2}\cos(\,\%2\,)\,\xi9^2 - 4\,\sigma^2\,m\,k\sin(\,\%2\,)\,\%1\,(\,\alpha-\alpha'\,)\,\xi9\,\xi10^2\\
&- \sigma^2\,m^2\cos(\,\%2\,)\,\sqrt{2}\,\xi9^3 - 4\,\sigma^2\,m^4\cos(\,\%2\,)\,\sqrt{2}\,\xi9^2\\
&- 4\,\mathrm{i}\,m\,k\sin(\,\%2\,)\,\%1\,\xi9\,\xi10^2 - 2\,m\,\sigma^2\,L_c\,\omega\,\sqrt{2}\cos(\,\%2\,)\,(\,\alpha-\alpha'\,)\,\xi9^2\,\xi10\\
&+ 8\,\sigma^2\,m^2\cos(\,\%2\,)\,\sqrt{2}\,\%1\,k^2\,\xi10^2 + 2\,{L_c}^2\,\omega^2\,\sqrt{2}\cos(\,\%2\,)\,\%1\,\xi9\,\xi10^2\\
&- 2\,\mathrm{i}\,\sigma^2\,m\,k\sin(\,\%2\,)\,\xi10^3\,\%1 + 16\,\mathrm{i}\,\sigma^2\,m\,k^3\sin(\,\%2\,)\,\%1\,\xi10^2\\
&- 4\,\omega\,k\sin(\,\%2\,)\,Lc\,\%1\,\xi9\,\xi10^2 - 2\,\mathrm{i}\,\sigma^2\,m\,k\sin(\,\%2\,)\,\xi9^2\,\xi10\\
&- \sigma^2\,m^2\cos(\,\%2\,)\,\sqrt{2}\,\%1\,\xi9\,\xi10^2 - 8\,\mathrm{i}\,\sigma^2\,m^3\,k\sin(\,\%2\,)\,\%1\,\xi10^2\\
&+ 2\,{L_c}^2\,\omega^2\,\sqrt{2}\cos(\,\%2\,)\,\xi9^2\,\xi10 - 4\,\sigma^2\,m\,k\sin(\,\%2\,)\,(\,\alpha-\alpha'\,)\,\xi9^2\,\xi10\\
&- \sigma^2\,m^2\cos(\,\%2\,)\,\sqrt{2}\,\xi9^2\,\xi10 - 8\,\mathrm{i}\,\sigma^2\,m^3\,k\sin(\,\%2\,)\,\xi9^2\\
&+ 8\,\sigma^2\,m^2\cos(\,\%2\,)\,\sqrt{2}\,k^2\,\xi9^2 - \sigma^2\,m^2\cos(\,\%2\,)\,\sqrt{2}\,\xi10^3\,\%1\\
&- 4\,\sigma^2\,m^4\cos(\,\%2\,)\,\sqrt{2}\,\%1\,\xi10^2 + 16\,\mathrm{i}\,\sigma^2\,m\,k^3\sin(\,\%2\,)\,\xi9^2\\
&- 2\,m^2\cos(\,\%2\,)\,\sqrt{2}\,\%1\,\xi9\,\xi10^2 + 4\,\omega\,k\sin(\,\%2\,)\,L_c\,\xi9^2\,\xi10\\
&- 2\,\mathrm{i}\,\sigma^2\,m\,k\sin(\,\%2\,)\,\xi9^3 - 4\,\mathrm{i}\,m\,k\sin(\,\%2\,)\,\xi9^2\,\xi10\Big)\Big/\Big(\xi10^2\,(\,\%1-1\,)\,(\,\%1+1\,)\\
&\xi9^2\,(\,L_0-L_c\,)\,(\,L_0+Lc\,)\Big) - 2\omega^6\,\pi\,\mathrm{e}^{\left(\mathrm{i}\ln\left(\frac{m-\sqrt{2}\,k}{\omega}\right)\,(\,\alpha-\alpha'\,)\right)}\,\Big(m-\sqrt{2}\,k\Big)\Big(-\frac{\left(m-\sqrt{2}\,k\right)^5}{\omega^4}\\
&+\frac{m\,\left(m-\sqrt{2}\,k\right)^4}{\omega^4} - \frac{{L_c}^2\,\left(m-\sqrt{2}\,k\right)^3}{\omega^2} - 3\,\frac{\sigma^2\,m\,\left(m-\sqrt{2}\,k\right)^4}{\omega^4} - {L_c}^2\,{L_0}^2\,\Big(m-\sqrt{2}\,k\Big)\\
&+\frac{{L_c}^2\,m\,\left(m-\sqrt{2}\,k\right)^2}{\omega^2} + \frac{{L_0}^2\,m\,\left(m-\sqrt{2}\,k\right)^2}{\omega^2} + {L_c}^2\,{L_0}^2\,m - \frac{{L_0}^2\,\sigma^2\,m\,\left(m-\sqrt{2}\,k\right)^2}{\omega^2}\\
&-\frac{m\,\sigma^2\,{L_c}^2\,\left(m-\sqrt{2}\,k\right)^2}{\omega^2} + m\,\sigma^2\,{L_0}^2\,{L_c}^2 - \frac{{L_0}^2\,\left(m-\sqrt{2}\,k\right)^3}{\omega^2}\Big)
\end{aligned}
$$

$$\left(\cos(\,\%2\,)\,m-\cos(\,\%2\,)\,\left(m-\sqrt{2}\,k\right)+\mathrm{i}\sin(\,\%2\,)\,\sqrt{2}\,k\right)\Big/\Big((\,\%1-1\,)\,(\,\%1+1\,)\,k$$
$$\left(2\,k^2-2\,\sqrt{2}\,k\,m+m^2+{L_0}^2\,\omega^2\right)^2\,\left(2\,k^2-2\,\sqrt{2}\,k\,m+m^2+{L_c}^2\,\omega^2\right)^2\Big)+2\omega^6\,\pi$$
$$\mathrm{e}^{\left(\mathrm{i}\ln\left(\frac{m+\sqrt{2}\,k}{\omega}\right)\,(\,\alpha-\alpha'\,)\right)}\,\left(m+\sqrt{2}\,k\right)\left({L_c}^2\,{L_0}^2\,m+m\,\sigma^2\,{L_0}^2\,{L_c}^2+\frac{{L_c}^2\,m\,\left(m+\sqrt{2}\,k\right)^2}{\omega^2}\right.$$
$$-\frac{{L_0}^2\,\left(m+\sqrt{2}\,k\right)^3}{\omega^2}-{L_c}^2\,{L_0}^2\,\left(m+\sqrt{2}\,k\right)-3\,\frac{\sigma^2\,m\,\left(m+\sqrt{2}\,k\right)^4}{\omega^4}-\frac{\left(m+\sqrt{2}\,k\right)^5}{\omega^4}$$
$$-\frac{m\,\sigma^2\,{L_c}^2\,\left(m+\sqrt{2}\,k\right)^2}{\omega^2}-\frac{{L_0}^2\,\sigma^2\,m\,\left(m+\sqrt{2}\,k\right)^2}{\omega^2}+\frac{m\,\left(m+\sqrt{2}\,k\right)^4}{\omega^4}$$
$$\left.-\frac{{L_c}^2\,\left(m+\sqrt{2}\,k\right)^3}{\omega^2}+\frac{{L_0}^2\,m\,\left(m+\sqrt{2}\,k\right)^2}{\omega^2}\right)$$
$$\left(\cos(\,\%2\,)\,m+\mathrm{i}\sin(\,\%2\,)\,\sqrt{2}\,k-\cos(\,\%2\,)\,\left(m+\sqrt{2}\,k\right)\right)\Big/\Big((\,\%1-1\,)\,(\,\%1+1\,)\,k$$
$$\left(2\,k^2+2\,\sqrt{2}\,k\,m+m^2+{L_0}^2\,\omega^2\right)^2\,\left(2\,k^2+2\,\sqrt{2}\,k\,m+m^2+{L_c}^2\,\omega^2\right)^2\Big)\Big)\Big/\Big(\pi\,\mathrm{e}\,\sigma^2$$
$$\left|\Gamma\left(\frac{3}{4}+\frac{1}{2}\,m+\frac{1}{2}\,\mathrm{i}\,\alpha'\right)\right|^2\Big)$$
$$\%1:=\mathrm{e}^{(\,\pi\,(\,\alpha-\alpha'\,)\,)}$$
$$\%2:=k\arctan\left(\frac{1}{2}\,\sigma^2\,\sqrt{2}\,m\,(\,\alpha-\alpha'\,),\frac{1}{2}\,\sigma^2\,\left({\alpha'}^2+2\,m^2+(\,\alpha-\alpha'\,)\,\alpha'\right)\right)$$

where

$$\xi7={L_0}^2\,\omega^2+2\,\mathrm{i}\,m\,\omega\,L_0-m^2+2\,k^2$$
$$\xi8={L_0}^2\,\omega^2-2\,\mathrm{i}\,m\,\omega\,L_0-m^2+2\,k^2$$
$$\xi9={L_c}^2\,\omega^2+2\,\mathrm{i}\,m\,\omega\,L_c-m^2+2\,k^2$$
$$\xi10={L_c}^2\,\omega^2-2\,\mathrm{i}\,m\,\omega\,L_c-m^2+2\,k^2$$

# 9. References

Abramowitz, M, and Stegun, I.A., 1968: Handbook of Mathematical Functions, New York: Dover Publishing [1968hmfw.book.....A]
Bertin, G., Lin, C. C., Lowe, S. A., Thurstans, R. P., 1989: ApJ **338**, 78 [1989ApJ...338...78B]
Bertin, G., and Lin, C.C., 1996: Spiral Structure in Galaxies: A Density Wave theory, Cambridge, Mass.: The MIT Press [1996ssgd.conf.....B]
Binney J., Tremaine S., 1987: Galactic Dynamics, Princeton: Princeton Univ. Press [1987gady.book.....B]
Biviano, A., Girardi, M., Giuricin, G., Mardirossian, F., and Mezzetti, M., 1991: ApJ **376**, 458 [1991ApJ...376..458B]
Block, D.L., and Wainscoat, R.J., 1991: Nature **353**, 48 [1991Natur.353...48B]
Block, D.L., Bertin, G., Stockton, A., Grosbøl, P., Moorwood, A.F.M., Peletier, R.F. 1994: A&A **288**, 365 [1994A&A...288B]
Bogoliubov N.N., Mitropolski Y.A., 1961: Asymptotic Methods in the Theory of Non-Linear Oscillations, New York: Gordon and Breach
Burton, W.B., 1971: A&A **10**, 76 [1971A&A....10...76B]
Clutton-Brock, 1972: Ap&SS **17**, 292 [1972Ap&SS..17..292C]
Evans, N.W., and Read, J.C.A., 1998a: MNRAS **300**, 83 [1998MNRAS.300...83E]
Evans, N.W., and Read, J.C.A., 1998b: MNRAS **300**, 106 [1998MNRAS.300..106E]
Goodman, J., and Evans, N.W., 1999: MNRAS, **309**, 599 [1999MNRAS.309..599G]
Fuchs, B, 1991: In: Sundelius, B. (ed.), Dynamics of Disc Galaxies, 359 [1991ddg..conf..359F]
Gakhov, F.D., 1990: Boundary value Problems, Mineola: Dover Publications (based on the the second Russian edition published in 1963)
Goldreich, P., and Lynden-Bell, D., 1965: MNRAS **130**, 125 [1965MNRAS.130..125G]
Gradshteyn, I.S., and Ryzhik, I.M., 1994: Table of Integrals, Series, and Products, New York: Academic Press [1994tisp.book.....G]
Hockney, R.W., and Hohl, F., 1969: ApJ **74**, 1102 [1969AJ.....74.1102H]
Jeans, J. H., 1919, Problems of Cosmology and Stellar Dynamics, Cambridge: Cambridge University Press [1919QB981.J35.....]
Julian, W.H., and Toomre, A., 1966: ApJ **146**, 810 [1966ApJ...146..810J]
Jungwiert, B., and Palouš, J., 1994: A&A **287**, 55 [1994A&A...287...55J]
Kalnajs, A.J., 1971: ApJ **166**, 275 [1971ApJ...166..275K]
Kalnajs, A.J., 1976a: ApJ **205**, 745 [1976ApJ...205..745K]
Kalnajs, A.J., 1976b: ApJ **205**, 751 [1976ApJ...205..751K]
Kalnajs, A.J., 1977: ApJ **212**, 637 [1977ApJ...212..637K]
Kuno, N, Tosaki, T, Nakai, N., and Nishiyama, K., 1997: PASJ **49**, 275 [1997PASJ...49..275K]

Kuypers F., 1990: Klassische Mechanik, Weinheim: VCH
Landau, L.D., 1946: J. Phys. USSR **10**, 25 [reprinted in: Ter Haar, D., 1969: Men of Physics: L.D. Landau II, Oxford: Pergamon Press]
Lemos, J.P.S., Kalnajs, A.J., and Lynden-Bell, D., 1991: ApJ **375**, 484 [1991ApJ...375..484L]
Lin, C.C., and Shu, F., 1964: ApJ **140**, 646 [1964ApJ...140..646L]
Lindblad, B, 1926: Uppsala Medd. No. 13 [1926MeUpp..13....1L]
Lindblad, B, 1940: ApJ **92**, 1 [1940ApJ....92....1L]
Lynden-Bell, D., and Ostriker, J.P., 1967: MNRAS **136**, 87P [1967MNRAS.136P..87L]
Lynden-Bell, D., and Kalnajs, A., 1972: MNRAS **157**, 1 [1972MNRAS.157....1L]
Mark, J. W.-K., 1976: ApJ **205**, 363 [1976ApJ...205..363M]
Mestel, L., 1963: MNRAS **126**, 553 [1963MNRAS.126..553M]
Miller, R.H., and Smith, B.F., 1992: ApJ **393**, 508 [1992ApJ...393..508M]
Muskhelishvili, N. I., 1953: Singular integral equations, Groningen: Noordhoff (based on the second Russian edition published in 1946)
Naim, A., Lahav, O., Sodre, L. jr., Storrie-Lombardi, M.C., 1995: MNRAS **275**, 567 [1995MNRAS.275..567N]
Persic, M. and Salucci, P., 1991: ApJ bf 368, 60 [1991ApJ...368...60P]
Pipkin, A.C., 1991: A course on integral equations, New York: Springer
Press, W.H, Teukolsky, S.A., Vetterling, W.T., and Flannery, B.P., 1992: Numerical Recipies in C, Cambridge, New York: Cambridge University Press [1992nrca.book.....P]
Polyanin, A.D., and Manzhirov, A.V., 1998: Handbook of integral equations. Boca Raton: CRC Press
Read, J.C.A., 1997: The Stability of Model Disk Galaxies, Ph.D. Thesis, University of Oxford
Read, J.C.A., 1999: private communication
Rix, H.-W., and Rieke, M.J., 1993: ApJ **418**, 123 [1993ApJ...418..123R]
Rohlfs, K., 1977: Lectures on Density Wave Theory, Berlin, Heidelberg, New York: Springer [1977ldwt.book.....R]
Rosse, William Parsons Earl of, 1852: Drawings to illustrate Recent Observations on Nebulæ, in: Parsons, Charles, 1926: The scientific Papers of William Parsons, Third Earl of Rosse 1800-1867, Bradford and London: Percy Lund, Humphreys&Co
Rots A.H., 1975: A&A **45**, 43 [1975A&A....45..43R]
Rubin, V.C., Thonnard, N., Ford, W.K., and Burstein, D., 1982: ApJ **261**, 439 [1982ApJ...261..439R]
Sellwood, J.A., and Carlberg, R.G., 1984: ApJ, **282**, 61 [1984ApJ...282...61S]
Sellwood, J.A., 1985: MNRAS **217**, 127 [1985MNRAS.217..127S]
Taga, M., 1998: In: ASP Conf. Ser. **182**, 71 [1998ASPC..182...71T]
Thornley, M.D., and Mundy, L.G., 1997: ApJ **490**, 682 [1997ApJ...490..682T]
Toomre, A., 1964: ApJ **139**, 1218 [1964ApJ...139.1218T]
Toomre, A., 1969: ApJ **158**, 899 [1969ApJ...158..899T]
Toomre, A., 1981: In: The structure and evolution of normal galaxies, Cambridge, UK, New York: Cambridge University Press, 111 [1981seng.proc..111T]
Toomre, A., and Toomre, J., 1972: ApJ **178**, 623 [1972ApJ...178..623T]
von Hoerner,S., 1963: Zs. f. Astrophysik **57**, 47 [1963ZA.....57...47V]

Wladimirow, W.S., 1972: Gleichungen der mathematischen Physik, Berlin: VEB Deutscher Verlag der Wissenschaften (Hochschulbücher für Mathematik, Band 74)
Zang, T.A., 1976: The Stability of a Model Galaxy, Ph.D. Thesis, Massachussetts Institute of Technology, Cambrigde, MA